Experimental and Numerical Study on the Spatial Distribution of Airflow and CO_2 in Photosynthetic Chamber and Greenhouse

(光合成チャンバーおよび農業用ハウスにおける気流と

CO_2の空間分布に関する実験的・数値的研究)

July, 2022

Doctor of Philosophy (Engineering)

Moliya Nurmalisa

モリヤヌルマリサ

Toyohashi University of Technology

Abstract

Carbon dioxide (CO_2) is one of the most importance factors that has high relation with photosynthesis process for plant growth. The optimal CO_2 concentration can provide better photosynthetic capacity and increasing crop productivity. However, analysis of detailed CO_2 distribution is rarely implemented and is still ongoing to date. Meanwhile, CO_2 is greatly affected by airflow. The fact of air movement affects the gas exchange between the plants and the ambient air, consequently affecting plant growth. Therefore, this study has purpose to reveal the detail of spatial distribution of airflow and CO_2 through numerical and experimental study in the photosynthesis chamber and greenhouse.

Measurement of air velocity was conducted to know the airflow distribution in the photosynthesis chamber, after that the numerical simulation by the Computational Fluid Dynamics (CFD) model was conducted for the validation of the model. The result of measurement and validation showed that the range of measured air velocities were 0.00 – 0.19 m s^{-1} and the simulation results followed within the range and also well reproduced the horizontal and vertical profiles of airflow in the chamber. Simulation and measurement of air velocity revealed uneven airflow distribution in the chamber.

Measurement of CO_2 concentration was conducted to understanding the CO_2 distribution in the photosynthesis chamber with tomato plant inside. The measured CO_2 concentration ranged 420-455 ppm inside of the chamber. The simulation results showed a good agreement with measured CO_2 concentration at the right side of the chamber. On the other hand, the simulation overestimated CO_2 concentration at the left and middle side of the chamber.

Carbon dioxide concentration data in a real greenhouse was used for the model validation. The measured CO_2 concentration were compared with the simulated CO_2 distribution inside the greenhouse. The simulation results may be reasonable to predict the CO_2 distribution considering CO_2 absorption due to photosynthesis of the plant.

For chamber simulation, to find the optimum method that makes airflow more even inside the chamber, the effect of different fan arrangement on airflow patterns and variability of air velocity were evaluated. The obtained results showed that a more even airflow distribution was observed in the middle and diagonally position of fans at the top of chamber with Coefficients of Variation (CV) for vertical velocity were 9.27% and 10.0%, respectively compared to default position (14.8%).

Multiple sizes of transparent plates were applied just below the top of the chamber to investigate the effect of the plates on airflow distribution. The simulation's results showed a diminishing stagnant area at the higher part of the plant, reaching a more even airflow distribution, with a CV for vertical velocity were 9.10% (full plate), 12.2% (half plate placed near the fans), 50.9% (without a plate), 45.5% (half plate placed on the opposite side of the fans), and 44.0% (small plate placed opposite with the fans). From simulation results, mounting a full-size transparent plate and a half-size one near the fans can significantly help to produce even air velocity distribution at the plant canopy.

A few simulations of greenhouse were conducted to know the effect of various environmental conditions on the CO_2 distribution inside of the greenhouse. The measurement of CO_2 concentration around the perforated tube was conducted. Simulation cases with open and closed side vents showed that closed side vents have slightly more even distribution of CO_2 concentration than those with open side vents (no outside wind case) inside the greenhouse. By contrast, the variability of CO_2 inside the plant, open (8.8%) and closed (8.7%) side vents, induced almost no significant improvement. Additionally, cases of a rainy- and sunny-day model showed that photosynthetically active radiation possibly compensated CO_2 through photosynthesis to be lower at low light (rainy day) and higher at high light (sunny day). Nonetheless, the variability of CO_2 concentration inside the plant between rainy and sunny days determined almost no significant difference. Different outside wind speed (0, 3, and 6 $m\ s^{-1}$) affected significantly CO_2 distribution inside the greenhouse. Focusing on the even distribution of CO_2 inside the plant, case of 3 $m\ s^{-1}$ and case of 6 $m\ s^{-1}$ of outside wind speed showed significant improvement to even the CO_2 distribution inside the plant canopy compared to case of 0 $m\ s^{-1}$ of outside wind speed. However, in the case of 6 $m\ s^{-1}$ outside wind speed showed CO_2 enrichment inside plant canopy was not effective to keep high CO_2 concentration since the high volume of outside CO_2 concentration (400 ppm) will dominate the CO_2 concentration inside the greenhouse.

Acknowledgments

Alhamdulillah, all praises to Allah for the strengths and blessing in completing my doctoral degree study. I would like to thank all those people who support and encourage me including my family, my friends, colleagues, and various institutions. First of all, my sincerest gratitude to my research supervisor, Dr. Takayuki Tokairin, Urban Thermal Environment and Atmospheric Environment Laboratory, Architecture and Civil Engineering Department, Toyohashi University of Technology, Japan. Under his guidance I successfully overcame many difficulties and learned a lot. This work would not have been possible without his guidance, support, and encouragement.

I am deeply indebted to Prof. Takanobu Inoue, Water Environment Engineering Laboratory, Architecture and Civil Engineering Department, Toyohashi University of Technology, Japan for his invaluable guidance, advice, and encouragement in my doctoral degree study. I am particularly grateful to Prof. Dr. Kotaro Takayama, Department of Mechanical Engineering, Toyohashi University of Technology, Japan. His invaluable advice encouraged me on my research work. My special thanks to Thesis Committee Chairman Prof. Dr. Shigeru Kato and Dr. Kuriko Yokota for their valuable guidance, careful reading, and constructive comments.

My unlimited grateful to my parents (Nurman Syafei and Erlistina Yazid) whose selfless sacrificial life, their great efforts, tears, and unceasing prayers have enabled me to reach the present position in life. I should not forget to acknowledge my husband (Indra Irawan) and my son (M. Kenzo Abrisam), sisters (Yunisca Nurmalisa and Aulia Nurmalisa) and my brother (M. Ilham Syah Putra) for their continuous love, support, understanding and good wishes whenever I needed.

Finally, I thank all those who have helped me directly or indirectly in the successful completion of my doctoral thesis. Anyone missed in this acknowledgement are also thanked. Again, I would like to thank everyone who supported and helped me during my study.

Moliya Nurmalisa

Table of Contents

List of Figures

List of Tables

List of Abbreviations

u_{out}	Air velocity at the exhaust fan boundary (m s^{-1})
Q	Outlet volumetric flow rate (m^3 s^{-1})
A_{out}	Outlet opening area (m^2)
ρ	Fluid density (kg m^{-3})
t	Time (s)
u	Air velocity components of x- directions
v	Air velocity components of y- directions
w	Air velocity components of z- directions
ϕ	Concentration of the transport variables, mass (air and CO_2 mass fraction), momentum and energy
Γ_ϕ	Diffusivity coefficient for ϕ
S_ϕ	Source term
LAD	Leaf area density (m^2 m^{-3})
LAI	Leaf area index (m^2 m^{-2})
P_{cg}	Canopy photosynthesis rate (g CO_2 h^{-1} m^{-2}ground area)
R'	Crop respiration (g h^{-1} m^{-2})
S_{CO_2}	Source or sink term
α_c	Initial light use efficiency of the plant canopy (or light utilization or photosynthetic efficiency) (g CO_2 J^{-1})
J_o	Incident light flux, photosynthetically active radiation at the top of canopy (W m^{-2})
τ_c	Conductance to CO_2 transfer (m s^{-1})
C'	Concentration of CO_2 in the air which calculated from the mass fraction of CO_2, Y_{CO2} (kg kg^{-1}) and the air density ρ (kg m^{-3})
C_D	Drag coefficient of the crop
h	Plant canopy's height (m)

Chapter 1 General Introduction

Some ways expect to increase agricultural productivity are by extending the farmland and by enhancing productivity inside the greenhouse. Enhancing productivity will be more important issue in the future, because of it, we need to improve the agriculture cultivation by empowering the technology including optimize the greenhouse function. Greenhouse microclimate can be controlled using environment control systems (water and nutrients support systems, intensity of light, temperature, and humidity) and CO_2 enrichment to control CO_2 concentration inside of the greenhouse.

Molina-Aiz et al. (2017) mentioned that greenhouse microclimate has four main factors that influence the crop development: solar radiation, air temperature, humidity, and CO_2 concentration. CO_2 is one of the most importance factors that has high relation with photosynthesis process for plant growth. The level of CO_2 concentration could be controlled artificially by CO_2 enrichment inside the greenhouse. The optimal CO_2 concentration can provide better photosynthetic capacity and increasing crop productivity. Meanwhile, although analysis of detailed CO_2 distribution is rarely implemented and is still ongoing to date, CO_2 enrichment has been widely used in various crops to gain the optimal productivity. A few methods of CO_2 enrichment have studied to know distribution of CO_2 to the plants. The importance reason of analyzing CO_2 distribution inside the greenhouse is to gain efficiency. For example, Zhang et al. (2020) showed that the efficiency of CO_2 distribution using CO_2 supplement/tube could save half of the fuel usage and achieve higher CO_2 concentration compared with a CO_2 generator.

Meanwhile, efficiency of crop production, obtaining high yields and converting atmospheric CO_2 to O_2 should be achieved with enhancing gas exchange in leaves and controlling environmental variables around the plants (Kitaya et al., 2003). The balance of heat and mass on leaf surfaces is strongly influenced by the convective exchange between leaves and the environment through the leaf boundary layer (Kimura et al., 2016). There are several factors that influences the thickness of boundary layer including leaf characteristics and air velocity near the leaf surface (Katsoulas et al., 2007). A thick boundary layer may reduce the transfer of CO_2 at the leaf then lead to impede photosynthesis. The fact of air movement affects the gas exchange between the plants and the ambient air, consequently affecting plant growth. Thus, for optimal plant growth, the air velocity in crop must be evaluated.

1.1 Air velocity

Many researchers have studied air velocity in the plant canopy to investigate its influence on plants for increasing and maintaining airflow uniformity in the plant canopy. Shibuya et al. (2006) experimentally clarified that upward and downward airflows enhanced the CO_2 exchange rate of the canopy and dry masses of the seedlings from 1.4–1.5 and 1.2–1.3 times, respectively, compared with a conventional horizontal airflow. Okayama et al. (2008) reported (that fans set on both sides of the space and opposed fans not set coaxially) could provide more uniform airflow distribution than the conventional airflow pattern (fans set on one side of the wall). It also enhanced the net photosynthetic rate more than that in the conventional airflow pattern with the same energy input. Kitaya et al. (2003) showed that the net photosynthetic rate and the transpiration rate increased significantly for sweet potato leaves as the air current speeds increased from 0.01 to 0.2 m s^{-1}. Furukawa (1975) showed the efficiency of airflow rate on photosynthesis was affected by air temperature around the leaf but was rather dramatically enhanced by increasing light intensity.

Basic data on adequate air circulation to enhance plant growth in a closed plant culture system (chamber) were obtained by investigating the effects of the current airspeed ranging from 0.01–1.0 m s^{-1}. Researchers also found that the plant canopy's net photosynthetic rate doubled with increased air current speed above the plant canopy (Kitaya et al., 2003). The net photosynthetic rate at an air velocity of 0.4 m s^{-1} was 1.3 more times than 0.1 m s^{-1} under CO_2 concentrations of 400-800 ppm (Kitaya et al., 2004).

1.2 Newly developed photosynthetic chamber

Chamber relatively has simple design and construction and mostly used in experiments to easily control the environment factors. Chamber is generally use for investigating the interaction of plants with environmental factors such as, CO_2 concentration, air velocity, temperature, light intensity, and photosynthesis.

There are many studies discussing photosynthesis measurement using a chamber for control plant growth and developing the model. Leadley and Drake (1993) monitored CO_2 concentrations using a mixing volume in the chamber's sampling line to reduce rapid variations in CO_2 concentration. Hamerlynck et al. (1997) estimated photosynthesis and stomatal conductance using portable infrared gas analyzer (LiCOR Li-6200) to assess leaf level photosynthetic gas exchange on a C4 grass, a perennial C3 forb, an C3 woody shrub in open top chambers. Dugas et al.(1997) measured CO_2 and H_2O concentration inside the canopy chamber using an infrared gas analyzer (Li-Cor 6262); using Bowen ratio/ energy balance, they calculated the CO_2 flux above the vegetation.

Burkart et al. (2007) determined the canopy gas exchange by comparing CO_2/H_2O molar fraction between the chamber's inlet and outlet air. Measurement of crop's net photosynthetic rate was conducted to determine the differences in CO_2 concentrations between the inlet and outlet of the assimilation chamber by the volumetric air exchange rate of the chamber and investigate the air velocity effects on photosynthesis (Kitaya et al., 2004; Shibuya et al., 2006; Shimomoto et al., 2020).

Shibuya et al., (2006) reported that a recently developed closed-type transplant production system could produce high-quality transplants, regardless of the weather. It was easier to design a ventilation system that provides the required air circulation in a closed-type system than in a greenhouse. A closed-type chamber with openings on both sidewalls through which air flew inside is discussed in the literature (Kitaya et al., 2003; Kitaya et al., 2004; Shibuya et al., 2006). The chamber's length and width were greater than its height.

In this study, we focused on a newly developed bottom opened chamber with exhaust fans on top of the chamber. The newly developed photosynthetic chamber is a semi-closed hanging type chamber covering a whole plant and monitoring real-time photosynthetic rate. The chamber's shape is vertical because the new chamber is designed to cover the entire plant, such as a tomato. Shimomoto et al. (2020) using a similar chamber, successfully traced the time courses of the net photosynthetic rate, transpiration rate, and total conductance of tomato plants inside the monitoring system. However, since measurement was only conducted for photosynthetic rate and its related environmental factors, airflow and the uniformity in the chamber is not well known even though the fact that air movement affects the gas exchange between the plants and the ambient air, consequently affecting plant growth.

1.3 Greenhouse

Nowadays, greenhouse is globally used in agriculture. Many researchers have studied microclimate phenomena of greenhouses because of the increasing demand for value-added agricultural products and the efficacy area of the greenhouse (Zhang et al., 2016; Benni et al., 2016; Santolini et al., 2018). A smart agriculture system with real time information for crop environment monitoring and management was developed for small scale greenhouse farming (Rubanga et al., 2019). Product quality of the vegetables can be affected by changing the climate condition in the greenhouse (Gruda, 2005). Environment control inside the greenhouse possible to manage the growth of the plants to produce high quality products.

1.4 Carbon dioxide (CO_2) distribution

Carbon dioxide enrichment is one of methods that used to increase and distribute the CO_2 concentration near to the plant. This method is conducted by controlling and maintain CO_2 concentration inside the greenhouse. Previous studies focused on the relationship between climatic factors that affect crop development (Roy et al., 2002; Kim et al., 2017; Kichah et al., 2012; Fang et al., 2020). By contrast, only a few studies have investigated CO_2 distribution (Roy et al., 2014; Molina-Aiz et al., 2017; Niam et al., 2019; Zhang et al., 2020).

It is challenging to maintain optimal CO_2 concentration inside a greenhouse due to CO_2 being condemned with temperature, humidity, and light intensity, leading the ambient CO_2 concentration to be often suboptimal or excessive (Li et al., 2018). For example, Kuroyanagi et al. (2014) discussed the amount of CO_2 that leaks from an unventilated greenhouse enriched with CO_2 on short-term (hourly) and medium-term investigation. For short-term during daylight of 4 days, CO_2 efficiency by crop uptake was 57.3% on average. For the medium term, more than 27 days, the efficiency of CO_2 enrichment was 45.5% on average. It revealed that the lowest solar radiation or strongest outside wind did not only cause the efficiency at the lowest. In comparison, higher efficiency was achieved by higher solar radiation and weaker external wind.

Since CO_2 could not be homogeneously spread far from the CO_2 tube (CO_2 source), CO_2 distribution depends on air circulation inside the greenhouse. Thus, the delivery system (air circulation and ventilation) must be designed to ensure an even distribution throughout the greenhouse. Additionally, Kim et al. (2013) showed that unequal distribution of CO_2 depends on temperature and location. A comparison showed that temperature is inversely proportional to the change in CO_2 distribution. As mentioned above, CO_2 enrichment plays a significant role in stable crop yield. Nevertheless, the detailed spatiotemporal distribution of CO_2 in foliage remains unknown.

1.5 Computational fluid dynamics (CFD)

Computational fluid dynamics (CFD) has been applied in various research areas to predict and simulate a similar process close to the actual condition. CFD can simulate various simulation cases and build several experimental conditions on a computer easily.

Many researchers have analyzed greenhouse designs, airflow, temperature, and radiation distribution in the agricultural field using CFD (Campen, 2005; Wang et al., 2013; Boulard et al., 2017; Kuroyanagi, 2017a; Kim et al., 2017; Hong et al., 2017; Saberian dan Sajadiye, 2019). CFD has often been used to evaluate and predict airflow and temperature distribution in various types of greenhouses and chambers (Papakonstantinou et al., 2000; Wang et al., 2013; Ali et al., 2018;

Boulard et al., 2017; Hong et al., 2017; Kim et al., 2017; Kuroyanagi, 2017; Santolini et al., 2018; Saberian and Sajadiye, 2019).

CFD is a powerful tool for describing not only greenhouse microclimate, but also plant behavior (Ali et al., 2018), and photosynthesis. Molina-Aiz et al. (2017) reported that photosynthesis could be simulated accurately using CFD in each cell of the domain corresponding to the crop. In their study, photosynthesis was computed as a function of the CO_2 concentration estimated by the CFD . The CFD model made it possible to reveal airflow details above and within the canopy, effects of the different structures on water irrigation, and predicted crop transpiration (Boulard and Wang, 2002; Majdoubi et al., 2009; Zhang et al., 2021). The validity of the CFD results has been a perennial problem. However, the continuous development of computer and numerical methods enhances the accuracy of the simulation prediction and shows outstanding potential for analyzing complex airflow in a greenhouse (Hong et al., 2017). Although the photosynthesis has been just considered in a recent CFD model, analysis of CO_2 distribution by CO_2 enrichment and emitted by CO_2 supplement/tube is insufficient. Since this research is rarely conducted, this study focuses on finding detailed CO_2 distribution concerning the increased efficiency of photosynthesis.

1.6 Objects of research

The objects of this study were:

1. To reveal the detailed of airflow inside the photosynthesis chamber experimentally and numerically to optimize the CO_2 distribution related to photosynthesis.
2. To clarify the CO_2 distribution using a CFD model considering photosynthesis in the chamber.
3. To identify CO_2 distribution with CO_2 enrichment (CO_2 supplement/tube) using the CFD model considering photosynthesis in the greenhouse.

To accomplish those objectives, several steps were performed:

1. To validate the model performance for air velocity through the comparison of numerical simulation and observation inside the chamber.
2. To reveal the detailed of airflow numerically inside the chamber.
3. To find the optimum method that makes airflow more even inside the chamber with several simulation cases.

   3-1. To numerically investigate airflow distribution in the chamber under different fan arrangements.

   3-2. To evaluate the effect of the transparent plates on the airflow distribution in the chamber.

4. To evaluate the model performance by comparing numerical simulations and measurement of CO_2 concentration in the chamber. The photosynthesis model is considered in the chamber simulation to perform CO_2 absorption by photosynthesis.
5. To validate the CFD model applied to the greenhouse to determine the detailed CO_2 distribution with CO_2 enrichment.
6. To simulate the effect of various environmental conditions such as side vent (open/close), weather (sunny/rainy) , different outside wind speed conditions on the CO_2 distribution inside of the greenhouse.

1.7 Organization of the thesis

The thesis consists of seven chapters that presented the research entitled “Experimental and Numerical Study on the Spatial Distribution of Airflow and CO_2 in Photosynthetic Chamber and Greenhouse”.

Chapter 1: Provides the subject of investigation, purposes, and general introduction of the study. Summarizing the previous literature studies to review and show how the present study is distinguished from other related studies.

Chapter 2: Describes the two types of chambers (chamber 1 and chamber 2) and the greenhouse, including the measurement setting and results of airflow and CO_2 concentration inside the chamber and the greenhouse.

Chapter 3: Description of CFD model, such as governing and continuity equations, source term, turbulence model, photosynthesis model. Presents the model validation for airflow in chamber1, model validation for CO_2 distribution in chamber 2 and greenhouse.

Chapter 4: Discuss the effect of different arrangement position of fans on airflow pattern in chamber 1.

Chapter 5: Presents the effect of different size of the transparent plate on airflow pattern in chamber 1.

Chapter 6: Detail distribution of CO_2 on various environmental conditions in greenhouse, such as open and closed side ventilations, sunny and rainy day, and different outside wind speed at side ventilation.

Chapter 7: Concludes the important findings and directions for future work. The appendices and references are attached at the end.

Chapter 2 Measurement of Airflow and CO_2 in the Chamber and Greenhouse

2.1 Airflow measurement in the chamber 1

2.1.1 Description of the chamber 1

The chamber was made of transparent film (Vinyl sheet: SUS. Co., Ltd., Japan, provided by PLANT DATA Co., Ltd.) and the size was 1.05 m in length, 0.52 m in width, and 1.88 m in height. (Note that although the actual chamber height was 2.15 m, 0.27 m of the bottom sheet of the chamber was folding up (therefore, the chamber height was 1.88 m, Figure 2.1). The chamber's bottom [area: 0.55 m^2 (1.05 m long × 0.52 m wide)] is fully opened for outside air inflow. Three exhaust fans (MB 630-B, 0.36 m^3 min^{-1}, Orix AC FAN, Oriental Motor Co., LTD, Tokyo, Japan) were placed on one side (with the distance between the two neighboring fans set at 5.3 cm and 29.4 cm, Figure 2.2) on the ceiling of the chamber, as indicated by short thick line shown in Figure 2.1.

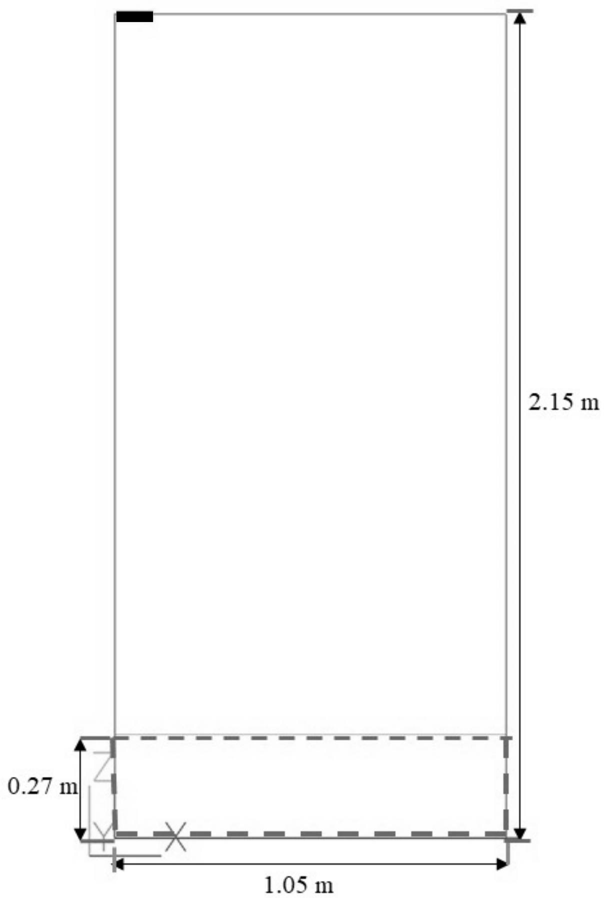

Figure 2.1 Chamber layout, the dotted square represents opening. Fans are placed at the top left side of the chamber (▬).

Figure 2.2 Fan position inside the chamber, circles (○) represent the fans.

2.1.2 Measurement settings

Measurement of air velocity in the empty chamber was conducted to obtain air velocity data for model validation (Figure 2.3). A hot-wire anemometer (Climomaster Model 6501-B0, range 0.01-30 m s^{-1}, accuracy: ± 2%, Kanomax, Japan, Figure 2.4) was used to measure the airflow rate of the fans and horizontal and vertical air velocities at 90 different points in the chamber (Figure 2.5 and 2.6). These are the data to be used for CFD model validation. At each point, the air velocity was measured with an anemometer fixed on a stand and recorded manually to a sheet when the value displayed on the anemometer was stable. The average measurements of air velocity of fans were 7.45 m s^{-1} (fan near to cross section A), 6.83 m s^{-1}(fan between cross section A and B), and 7.03 m s^{-1} (fan near to cross section C, see Figure 2.6), that used to calculate the airflow rate. On the basis of the fan's volumetric flow rate, the average airflow rate obtained by measuring the three fans was approximately 0.009 m^3 s^{-1}, as represented below in Equation 1 (Zhang et al., 2016), which is also used in the simulation.

$$Q = u_{out} \times A_{out} \tag{1}$$

where u_{out} is the air velocity at the exhaust fan boundary (m s^{-1}), Q is the outlet volumetric flow rate (m^3 s^{-1}), and A_{out} is the outlet opening area (m^2).

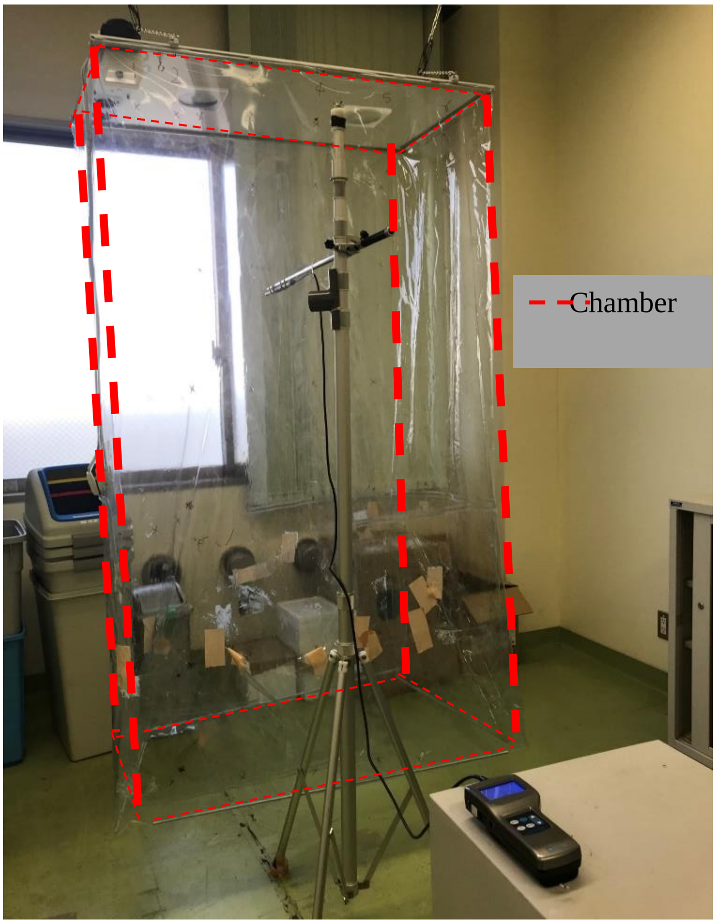

Figure 2.3 Empty chamber for air velocity measurement.

Figure 2.4 A hot-wire anemometer (Climomaster Model 6501-B0).

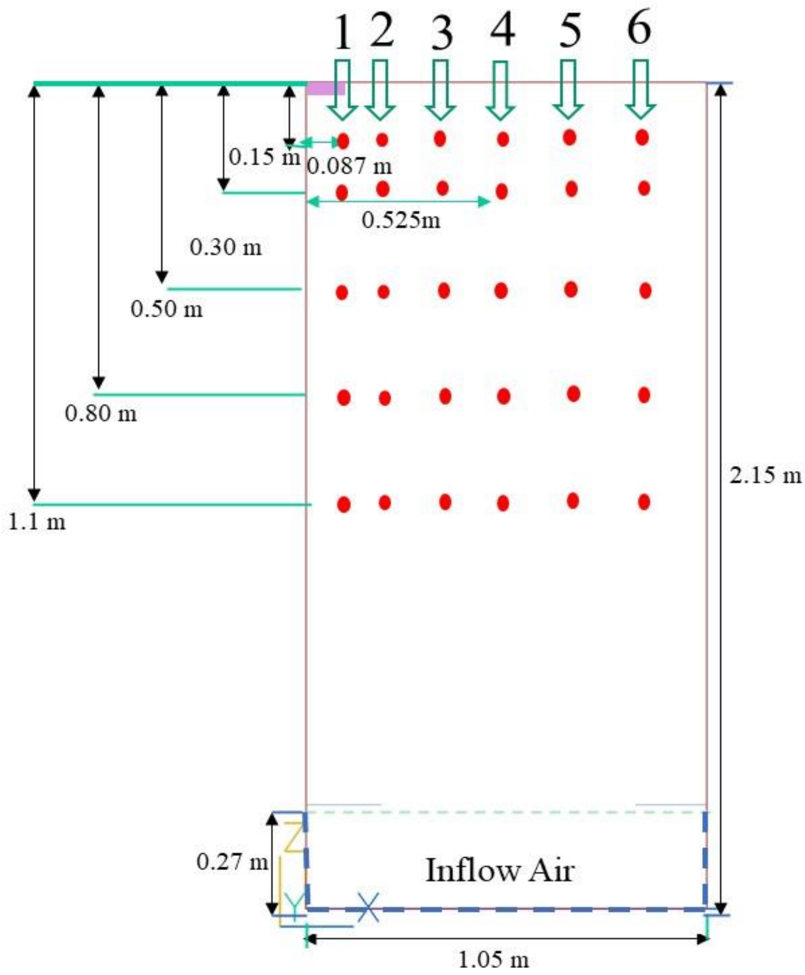

Figure 2.5 Vertical measurement point no.1─6, points 2─6 are 0.175 m apart (Front-view).

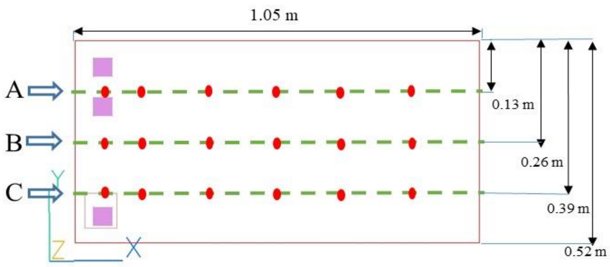

Figure 2.6 Horizontal measurement points A, B, C (Top - view).

2.1.3 Results of the chamber 1 measurement

X-velocity (horizontal velocity) and z-velocity (vertical velocity) measurement was conducted in the chamber without plant with the total measurement data were 162 values of air velocity (x-velocity was 81 values of air velocity and z-velocity was 81 values of air velocity) as shown in the Table 2.1. The measurement points for the comparison start from 1A, B, and C cross section, close to the left wall of the chamber, until 6A, B, and C cross section, close to the right wall of the chamber.

Table 2.1 Air speed measurement values from vertical (z) – direction and horizontal (x) direction.

Distance from top chamber (m)	y- cross sections	Air speed measurement cross sections (m s^{-1})											
		1		2		3		4		5		6	
		Z	X	Z	X	Z	X	Z	X	Z	X	Z	X
0.15	A	0.19	0.09	0.15	0.17	0.08	0.07	0.03	0.03	0.03	0.01	0.02	0.01
	B	0.13	0.08	0.05	0.10	0.03	0.04	0.02	0.02	0.02	0.01	0.02	0.01
	C	0.13	0.05	0.05	0.14	0.02	0.02	0.01	0.01	0.01	0.01	0.02	0.01
0.30	A	0.17	0.03	0.16	0.04	0.07	0.05	0.03	0.01	0.03	0.01	0.02	0.01
	B	0.10	0.02	0.05	0.02	0.03	0.03	0.02	0.02	0.02	0.01	0.02	0.01
	C	0.13	0.02	0.04	0.01	0.02	0.02	0.01	0.01	0.02	0.01	0.02	0.01
0.50	A	0.13	0.03	0.12	0.01	0.05	0.01	0.02	<0.01	0.03	<0.01	0.03	<0.01
	B	0.06	0.03	0.02	0.01	0.02	0.01	0.02	0.02	0.02	<0.01	0.01	<0.01
	C	0.07	0.02	0.02	<0.01	0.02	0.02	0.01	0.02	0.01	0.01	0.01	<0.01
0.80	A	0.05	0.01	0.02	<0.01	0.01	0.01	0.02	0.02	0.02	0.01	0.02	0.01
	B	0.03	0.01	0.02	0.01	0.02	<0.01	0.03	<0.01	0.03	0.01	0.02	0.01
	C	0.03	<0.01	0.01	<0.01	0.02	<0.01	0.01	0.02	0.02	0.01	<0.01	0.01
1.10	A	0.01	<0.01	0.02	<0.01					0.02	0.01		
	B	0.01	<0.01	0.02	<0.01					0.01	0.01		
	C	0.01	<0.01	0.02	<0.01					0.02	<0.01		

2.2 Carbon dioxide measurement in the chamber 2

2.2.1 Description of the chamber 2

The experiment was conducted in a chamber inside the greenhouse (Figure 2.7) with a CO_2 concentration of approximately 420 ppm. The study was focusing on the movement of air particularly how CO_2 distribute inside the chamber with the plant that considering the photosynthesis.

The chamber is a semi closed hanging type that is 1 m in length, 0.52 m in width, 1.64 m in height, and an air opening at the bottom side with dimension area: 0.52 m^2 (1 m in length × 0.52 m in width). The air inside the chamber flows out through an exhaust fan (9BMB24P2H01, Sanyo Denki, Philippines) at the left ceiling of the chamber. The air velocity of the fan is 18.7 m s^{-1}.

Two whole-grown tomatoes were placed inside the chamber in the substrate with a drip nutrient and irrigation system. The tomatoes had a height of 1.63 and 1.40 m, respectively, from the chamber's bottom; leaf area index (LAI) of 4.00 m^2 m^{-2}; and leaf area density (LAD) of 2.67 m^2 m^{-3}. Later, in the chamber model validation, the average height of 1.5 m was used to represent the height of the plant.

Figure 2.7 Chamber inside the greenhouse.

2.2.2 Measurement settings

Carbon dioxide concentrations were measured using a handheld CO_2 meter (GM70, Vaisala, Finland). The measurements of CO_2 concentration without CO_2 enrichment were conducted in three positions: top (0.15 m from the chamber ceiling), middle (0.815 m from the chamber ceiling), and bottom (at the bottom opening of the chamber) to obtain CO_2 distribution data for model validation. Each position was measured in three horizontal points (left, middle, and right) in the exact distance between the point is 0.25 cm. However, the top positions were measured at the left and right because of difficulty reaching the middle point while avoiding human breath exhaling CO_2. Also, air velocities were measured at the bottom of the chamber (0.83 m from the ground) and 0.2, 0.4, and 0.815 m from the ceiling of the chamber, respectively, using a hot wire anemometer (WGT 10, Hario, Japan) to determine the airflow and CO_2 distribution (Figure 2.8).

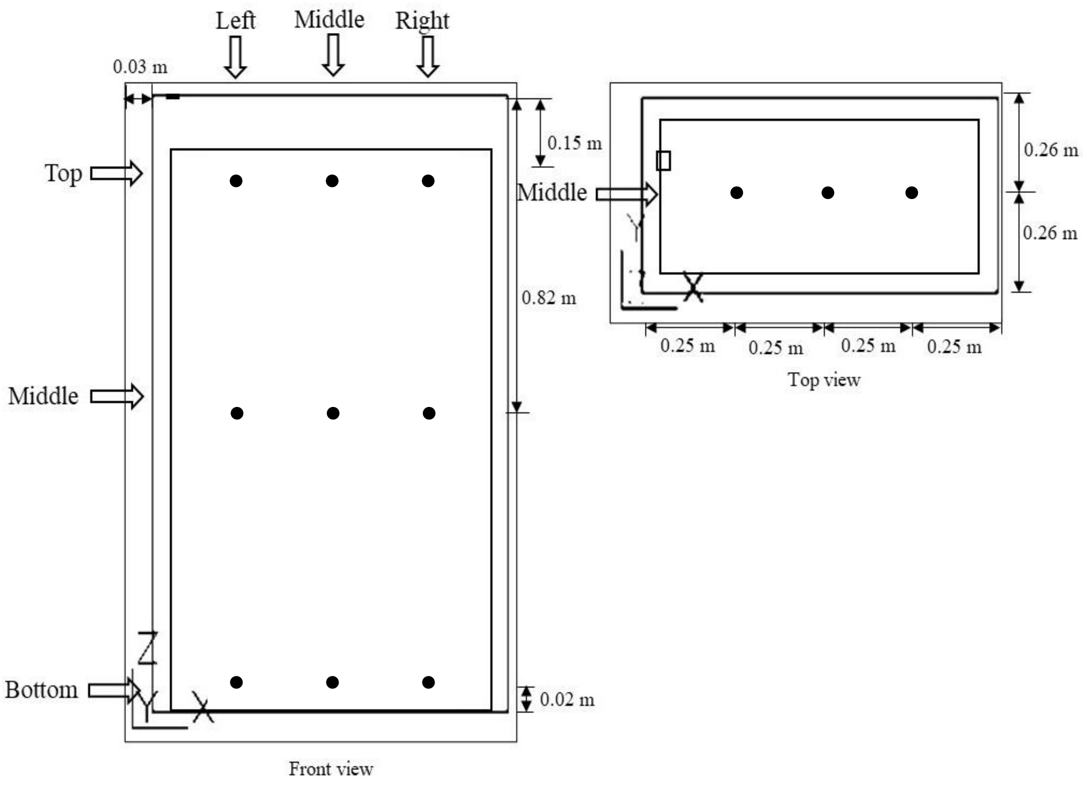

Figure 2.8 CO_2 measurement points (•) at front and top – view.

This study conducted a chamber simulation, compared the measurement data, and analyzed the CO_2 concentration in three chamber positions. The model validation calculated three positions of CO_2 concentration in the middle of the chamber (Figure 2.8): (i) above the plant and near the fan, (ii) in the middle of the plant, (iii) at the bottom of the chamber near the area of inflow air from the outer chamber. Those positions were chosen to be representative of the characteristics of airflow in the whole chamber, including plants with photosynthesis process. A validated chamber model will be applied to simulate the actual greenhouse.

2.2.3 Results of the chamber 2 measurement

Carbon dioxide concentration measurement was conducted in the chamber with plant with the total measurement data were 9 values of CO_2 concentration as shown in the Table 2.2. The measurement points for the comparison start from bottom (left, middle, and right cross section near to the bottom opening of the chamber) until top (left, middle, and right cross section at the top of canopy).

Table 2.2 CO_2 measurement values base on canopy layer in chamber 2.

Canopy layer	**Measured (ppm)**		
	Left	**Middle**	**Right**
Top	420	–	440
Middle	440	420	440
Bottom	450	455	450

2.3 Carbon dioxide measurement in a real greenhouse

2.3.1 Description of the greenhouse

The research conducted in a vinyl greenhouse of 120 m^2 (length: 12 m; width: 10 m; height: 6.03 m) located at Toyohashi University of Technology, Japan (Figure 2.9). The greenhouse was equipped with air conditioning, air circulators, roof and side vents, water and nutrient solution drip-irrigation system, and a perforated plastic tube of airflow system placed above the bed of plants shelves (Figure 2.10). Additionally, the greenhouse's roof and side vents were covered with insect-proof nets. Tomatoes were grown on four shelves inside the greenhouse: tomato seedlings (Solanum lycopersicum), cv. 'Momotaro hope', was planted on November 4th, 2020, in greenhouse. Tomatoes grow in the cultivated bed (0.23 m in width and 8 m in length), mounting 0.83 m from the ground floor. The water and nutrient solution supply are controlled using monitoring instruments (Aqua beat, Inochio, Japan). The solar radiation data were acquired from the NEDO database (New Energy and Industrial Technology Development Organization, Japan) to calculate Photosynthetically Active Radiation (PAR).

Figure 2.9 Greenhouse in Toyohashi University of Technology.

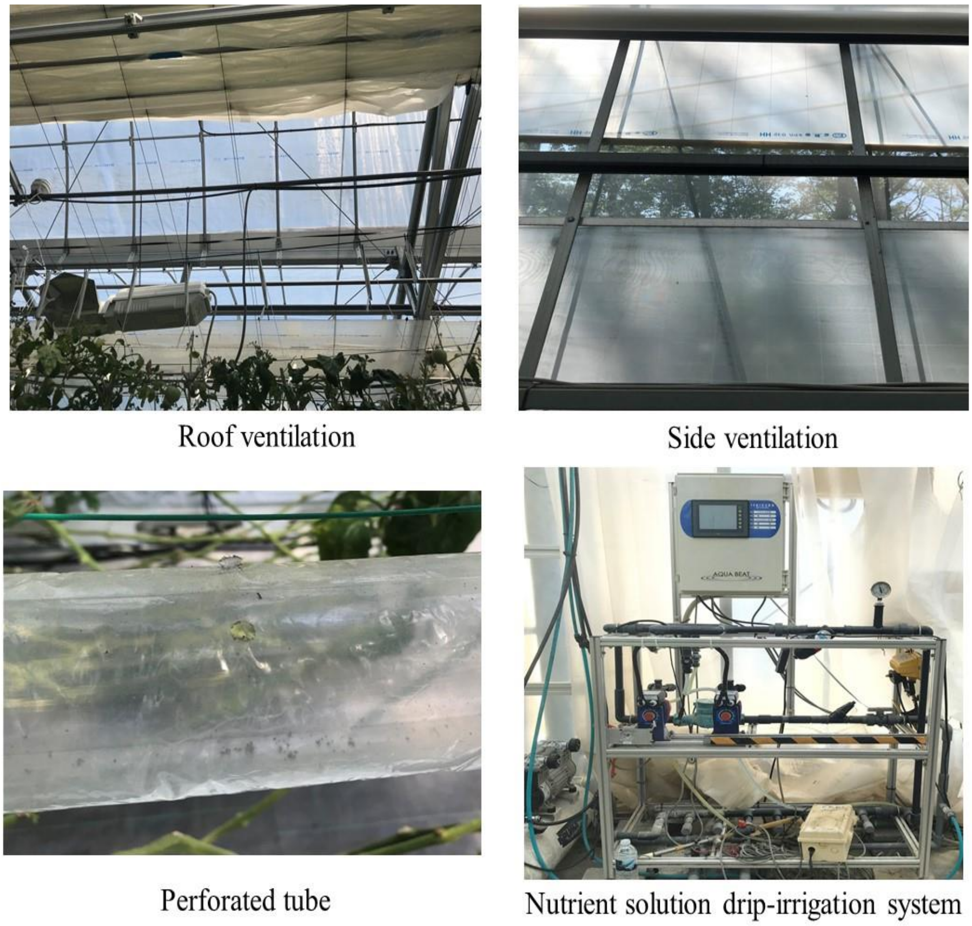

Figure 2.10 The greenhouse equipment.

2.3.2 Measurement settings

2.3.2.1 Carbon dioxide enrichment with different position of CO_2 supply in a greenhouse

Kumazaki et al. (2021) studied influential positions of CO_2 supply in tomato plants inside the greenhouse in this study. The tomato plants have LAI 1.1 $m^2\ m^{-2}$. The CO_2 was supplied in two positions: (i) at the base of the canopy plant (0.6 m above the ground) and (ii) the middle canopy (1.2 m above the ground). CO_2 supply started when the CO_2 concentration average was below 400 ppm and stopped when it achieved 450 ppm. CO_2 concentrations were measured at 3.4 m from north and south wall (Figure 2.11A) and 0.6, 1.2, 1.8, 2.4, and 4.2 m above the ground (Figure 2.11B). Because CO_2 distribution in the entire greenhouse remains unclear, this study conducted a numerical simulation to predict the CO_2 distribution by CO_2 concentration measurement data, especially for CO_2 supply in the middle canopy (1.2 m above the ground).

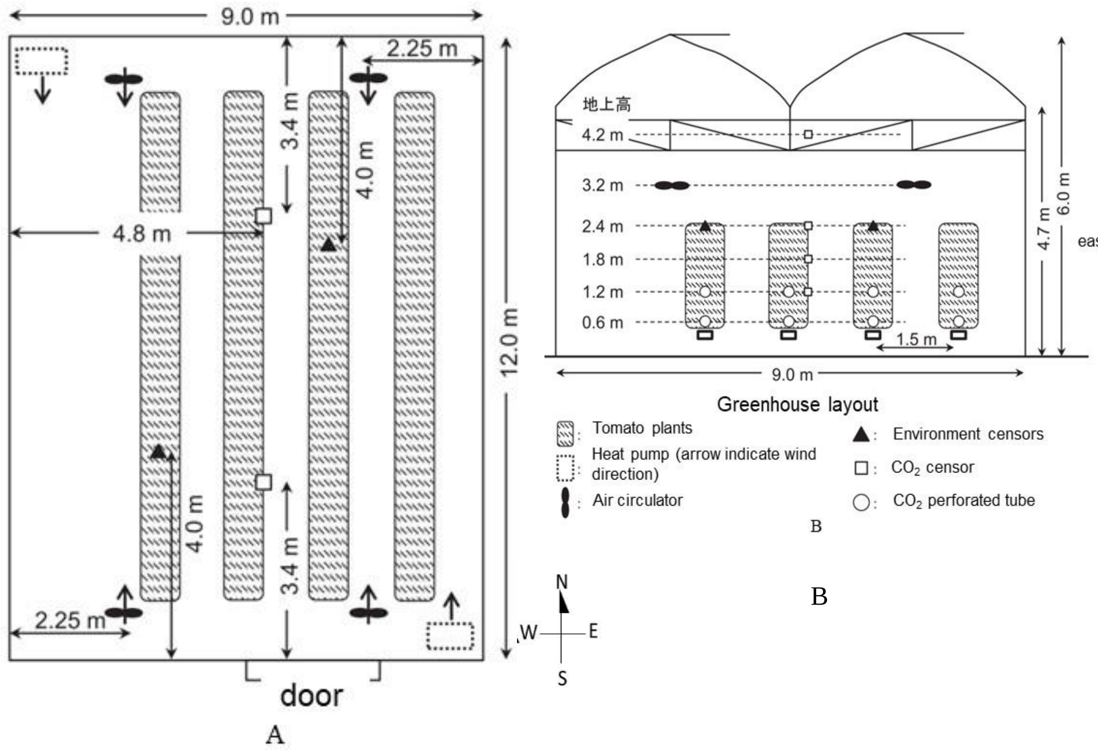

Figure 2.11 Greenhouse measurement layout: A. Top view and B. Front view.

2.3.2.2. Carbon dioxide enrichment measurement

Carbon dioxide enrichment was conducted during the daytime on a sunny day (on August 30th, 2021, at 1.30 PM). The initial CO_2 concentration injection was 1160 ppm. Pure CO_2 gas was supplied through a perforated plastic tube airflow system placed in the middle of a bed of plants for each shelf. The perforated tube has a length of 8 m, a diameter of 0.10 m, and 16 holes with a diameter of 0.006 m, and the distance between the hole is 0.52 m. The average air velocity of the outlet perforated plastic tube airflow system was 6.21 m s^{-1}. CO_2 gas was flowing from north to south in the perforated tube. CO_2 gas from the perforated tube hole was measured after less than 5 min of injection of CO_2 gas. CO_2 concentrations were measured using a handheld CO_2 meter (GM70, Vaisala, Finland) within a 30-s average.

2.3.3. Results of the greenhouse measurement

Carbon dioxide concentration measurement was conducted in the greenhouse with plant with the total measurement data points were 8 points of CO_2 concentration as shown in the Table 2.3. The measurement points for the comparison start from (1.2 m, 1.8 m, 2.4 m, and 4.2 m from the ground).

Table 2.3 CO_2 measurement values base on canopy layer in greenhouse.

Height (m)	Measured (ppm)	
	North	South
4.2	391	418
2.4	411	439
1.8	418	431
1.2	432	443

Chapter 3 Model Validation

Simulated air velocities and CO_2 concentration were compared to measured ones at the predetermined measurement points in the chamber. The accuracy of the simulation model was evaluated by the root mean square error (RMSE) and Mean Absolute Percentage Error (MAPE). The greenhouse simulation was conducted and compared with the measurement data of CO_2 enrichment. Model validation calculated CO_2 distribution from CO_2 perforated tubes in the whole greenhouse and took the represent cross image result 3.4 m from the south wall of greenhouse The accuracy of the simulation model was evaluated by RMSE and MAPE.

3.1 Description of numerical model

3.1.1 Computational Fluid Dynamics (CFD) model

3.1.1.1 Governing Equations

CFD simulations were conducted using a commercial CFD software (PHOENICS, v.2020, CHAM Ltd., England). The software solves the steady-state three-dimensional simulations using the finite volume method. Benni, et al. (2016) explained that the finite volume method reduces the governing partial differential equations to a set of algebraic equations, resulting in algebraic equations for the dependent variable at nodes on every element. PHOENICS solves a finite volume formulation of the balance equation, which is unsolved in differential form (Spalding, and Markatos, 1982). The numerical simulation imposed the boundary conditions at the calculation domain to conduct airflow, CO_2 distribution, and photosynthesis processes. Equations with boundary conditions were solved using CFD with the flow management simulation as show in APPENDIX, page A.1.

3.1.1.2 Continuity Equation

The continuity equations model (eq. 2), momentum equations (eq. 3, 4, and 5), and the energy equation applied to calculate airflow and heat transfer in this research are shown below:

$$\frac{\partial \rho}{\partial t} + \frac{\partial (\rho u)}{\partial x} + \frac{\partial (\rho v)}{\partial y} + \frac{\partial (\rho w)}{\partial z} = 0 \quad (2)$$

where ρ is the fluid density (kg m^{-3}); t is time (s); and u, v, and w are air velocity components of x, y, and z directions. In the case where the flow is incompressible, ρ is constant.

3.1.1.3 General equation for transport of physical quantities

X-direction;

$$\frac{\partial(\rho u)}{\partial t} + \mathrm{div}(\rho \boldsymbol{u}\, u) = \mathrm{div}(\rho\eta \text{ grad } u) - \text{grad } p_x + B_x \tag{3}$$

Y-direction;

$$\frac{\partial(\rho v)}{\partial t} + \mathrm{div}(\rho \boldsymbol{u}\, v) = \mathrm{div}(\rho\eta \text{ grad } v) - \text{grad } p_y + B_y \tag{4}$$

Z-direction;

$$\frac{\partial(\rho w)}{\partial t} + div(\rho \boldsymbol{u}\, w) = div(\rho\eta \; grad \; w) - grad \; p_z + B_z \tag{5}$$

where $\eta = {}^{\mu}/_{\rho}$ is the kinematic viscosity (m s^{-2}); p is the pressure (N m^{-2}), and B is the body force (gravity) (N m^{-3}).

The transport equation (eq. 6), where represents the concentration of the transport variables, mass (air and CO_2 mass fraction), momentum, and energy (Stathopoulou, O. I. and Assimakopoulos, V.D. 2008).

$$\frac{\partial}{\partial t}(\rho\phi) + \mathrm{div}(\rho\boldsymbol{u}\phi) = \mathrm{div}\big(\acute{\Gamma}_{\phi}\mathrm{grad}\phi\big) + S_{\phi} \tag{6}$$

where ρ is density, u is the component of directional air velocity, $\acute{\Gamma}_{\phi}$ is the diffusivity coefficient for ϕ, and S_{ϕ} is the source term.

3.1.1.4 Source term

3.1.1.4.1 Source term for airflow

The deceleration is often represented as momentum sink (eq. 7) in source term of eq. (8):

$$S_{\phi} = -C_D LAD|\boldsymbol{u}|^2 \tag{7}$$

where C_D is a drag coefficient of the crop (0.3) and LAD (m^2 m^{-3}) is obtained from LAI (eq.7):

$$LAD = {}^{LAI}/_{h} \tag{8}$$

where h is the plant canopy's height.

3.1.1.4.2 Source term for CO_2 concentration

Carbon dioxide absorption by plants photosynthesis is represented as the formula of net photosynthesis (kg s^{-1} $m^{-3}{}_{row}$) (eq. 9) (Molina-Aiz et al., 2017):

$$S_{CO_2} = -\,P_{cCFD} = \frac{LAD}{LAI \cdot 1000 \cdot 3600}\left(R' - P_{cg}\right) \tag{9}$$

where *LAD* is the leaf area density (m^2 m^{-3}), *LAI* is the leaf area index (m^2 m^{-2}), P_{cg} is canopy photosynthesis rate (g CO_2 h^{-1} $m^{-2}{}_{\text{ground area}}$), R' is the crop respiration (g CO_2 h^{-1} m^{-2}), and S_{CO_2} is the source or sink term.

3.1.2 Turbulence Model

3.1.2.1 Study for CO_2 distribution in chamber and greenhouse were using turbulence model: the standard $k-\varepsilon$ model.

A turbulence model can be described as a set of relations and equations needed to determine the unknown turbulent correlations that have arisen from the averaging process. In this research two-equation models (The Chen-Kim $k-\varepsilon$ model and the standard $k-\varepsilon$ turbulence model) used as perform of turbulence model, where k represents the turbulent kinetic energy (kg m^2 s^{-2}), ε represents the rate of dissipation of turbulent kinetic energy (kg m^2 s^{-3}t), and P_k represents the volumetric production rate of k.

The standard $k-\varepsilon$ turbulence model was applied in the greenhouse simulation. The standard high reform of the $k-\varepsilon$ model employs the following turbulence transport equations (10) and (11):

$$\frac{\partial \boldsymbol{k}}{\partial t} + \overline{u_J}\frac{\partial \boldsymbol{k}}{\partial x_j} = P_k - \varepsilon + \frac{\partial}{\partial x_j}\left\{\left(\frac{v_t}{\sigma_{\boldsymbol{k}}} + v\right)\frac{\partial \boldsymbol{k}}{\partial x_j}\right\} \tag{10}$$

$$\frac{\partial \varepsilon}{\partial t} + \overline{u_J}\frac{\partial \varepsilon}{\partial x_j} = \left(C_{\varepsilon 1}P_k - C_{\varepsilon 2}\varepsilon\right)\frac{\varepsilon}{k} + \frac{\partial}{\partial x_j}\left\{\left(\frac{v_t}{\sigma_\varepsilon} + v\right)\frac{\partial \varepsilon}{\partial x_j}\right\} \tag{11}$$

The kinematic turbulent viscosity and the length scale, L_s are given by eq. (12):

$$v_t = C_\mu \frac{k^2}{\varepsilon} \tag{12}$$

The model constants are:

$$C_\mu = 0.09;\; \sigma_{\boldsymbol{k}} = 1.0; \sigma_\varepsilon = 1.314;$$

$$C_{\varepsilon 1} = 1.44;\; C_{\varepsilon 2} = 1.92$$

The $k - \varepsilon$ model is known to be too dissipative – the turbulent viscosity in recirculation tends to be too high, thus damping out vortices. TURMOD (KERNG) select the RNG $k - \varepsilon$ model. This attempt to correct this deficiency by using slightly different constants, and by adding the following volumetric source term (eq. 13 and 14) to the ε equation 15:

$$S_\varepsilon = \frac{-\rho\alpha\varepsilon^2}{k} \quad (13)$$

where, $$\alpha = C_{\mu d}\eta^3 \frac{1-\frac{\eta}{\eta_0}}{1+\beta\eta^3} \quad (14)$$

$$\beta = 0.012;\ \eta_0 = 4.38;$$

$$\eta = \frac{k}{\varepsilon}\left(\frac{\rho P_k}{\mu^t}\right)^{1/2} \quad (15)$$

The changes to the model constants are $C_{\varepsilon 1} = 1.42$; $C_{\varepsilon 2} = 1.68$; $C_{\mu d}$ = 0.0845. Although very good for separation and reattachment, its predictions for jets and plumes are inferior to the standard model.

3.1.2.2 Study for airflow was using turbulence model : the Chen – Kim $k - \varepsilon$ model

To calculate air velocity in the chamber, TURMOD (KECHEN) selected as the modified $k - \varepsilon$ model of Chen and KIM, which is another attempt to cure the over-dissipative nature of the $k - \varepsilon$ model. The variant of the $k - \varepsilon$ model uses slightly different constants and introduces an additional source term into the equation (16), (Phoenics user manual):

$$S_\varepsilon = \frac{-\rho C_4 P_k^2}{\boldsymbol{k}} \quad (16)$$

where, C_4 = 0.25. The changes to the model constants are $\sigma_{\boldsymbol{k}}$ = 0.75; σ_ε= 1.15.

3.1.3 Photosynthesis Model

Canopy photosynthesis rate and net photosynthesis equations were using in chamber and greenhouse simulation to consider photosynthesis process.

3.1.3.1 Canopy photosynthesis rate

Canopy photosynthesis rate of Acock's model modified by Nederhoff and Vegter (1994a) (eq. 17):

$$P_{cg} = \frac{\alpha_c j_o \tau_c C' \cdot 3600}{\alpha_c j_{o+} \tau_c C'} \tag{17}$$

where α_c is the initial light use efficiency of the plant canopy (or light utilization or photosynthetic efficiency) (g CO_2 J^{-1}), $j_o$is the incident light flux, PAR at the top of the canopy (W m^{-2}), τ_c conductance to CO_2 transfer (m s^{-1}), C' is the concentration of CO_2 in the air which is calculated from the mass fraction of CO_2, Y_{CO2} (kg kg^{-1}), and the air density ρ (kg m^{-3}) (Molina-Aiz et al., 2017).

3.1.3.2 The net photosynthesis rate

PHOENICS automatically computes the mass fractions of CO_2 in the air. The net photosynthesis was calculated using the equation below as the difference between canopy photosynthesis and crop respiration. The formula of net photosynthesis (kg s^{-1} $m^{-3}{}_{row}$) was given as follows (Molina-Aiz et al., 2017) same the equation (9).

3.2 Model Validation for Airflow (Chamber 1)

Model validation conducted by comparing measurement and simulation data to know the airflow distribution without a plant inside the chamber.

3.2.1 Model Settings

3.2.1.1 Computational domain

Figure 3.1 shows the meshing of the modeled chamber. The number of meshes for model validation, where a finer mesh was applied near the fans and walls. The meshing characters are shown in Table 3.1.

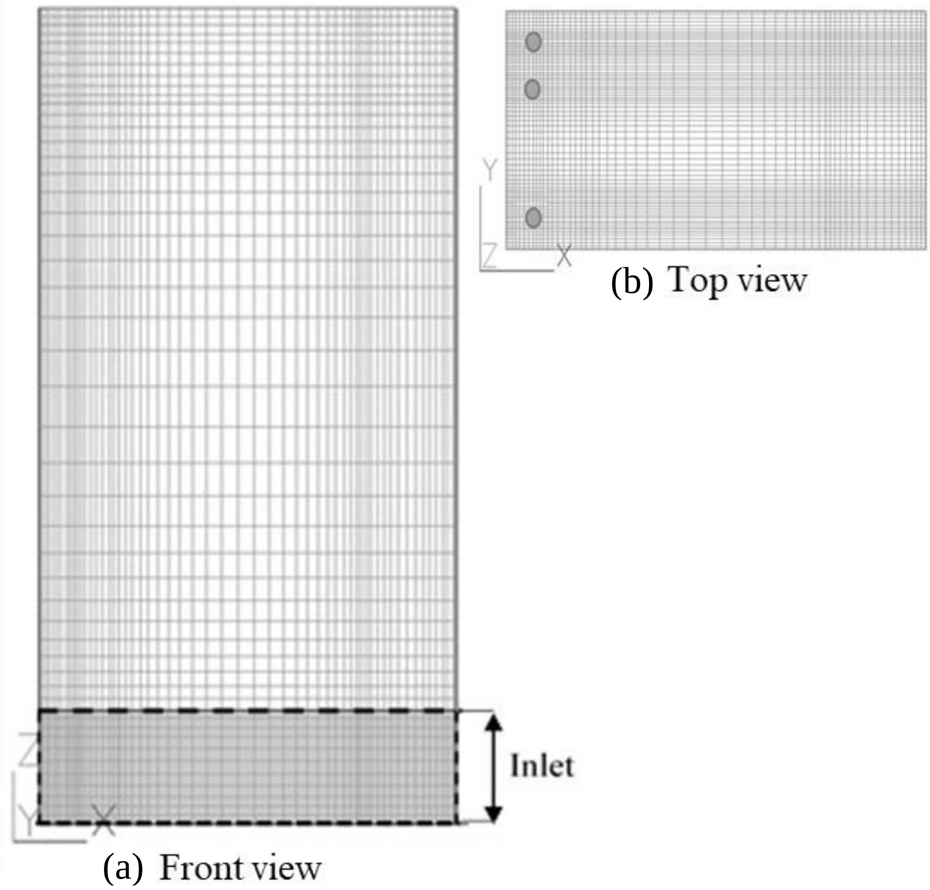

Figure 3.1 Meshing of computational domain. ● represents fans.

Table 3.1 Meshing of computational domain for chamber 1.

Mesh	Properties
Number	110,880
Coordinate Type	Cartesian

3.2.1.2 Initial and boundary conditions

The Chen-Kim turbulence model developed by modifying the two-equation eddy-viscosity k-ε turbulence model was employed in the modeled chamber 1. The Chen-Kim model proposed a modification that improves the dynamic response of the ε equation by introducing an additional time scale (k-ε) (PHOENICS user manual). The k-ε-based turbulence model including the realizable k-ε model has been well used to improve airflow uniformity for the design of air circulation system in a single cultivation shelf (Zhang et al., 2016). This model has been also used in studies related to ecological agriculture (Niam et al., 2019) and airflow in greenhouses (Molina-Aiz et al., 2017).

The average of airflow rate from the three fans was approximately 0.009 $m^3 s^{-1}$, which was used in the simulation (Table 3.2).

Table 3.2 Boundary conditions for model validation chamber 1.

Parameter	Conditions
Air volume rate of the fans	0.009 $m^3 s^{-1}$
Bottom opening	Pressured fixed
Wall	No slip

3.2.2 Comparison of airflow between measurement and simulation data

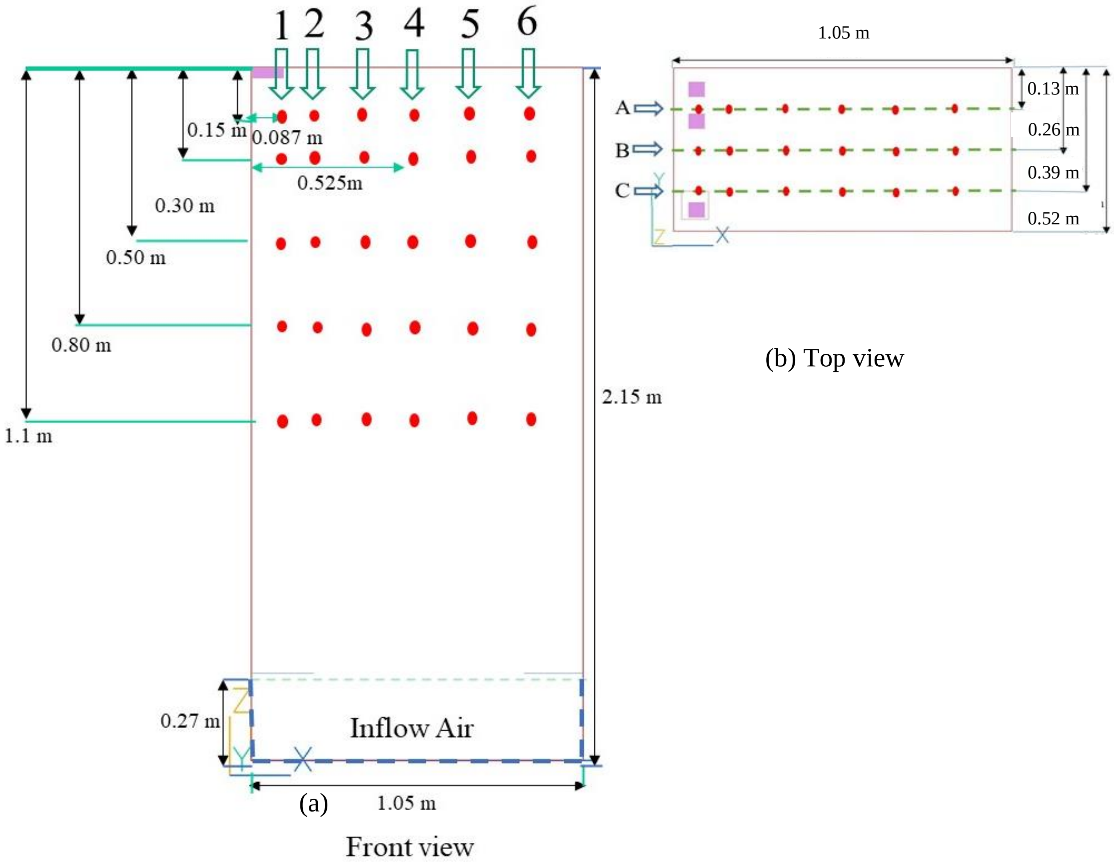

Figure 3.2 Points of air velocity measurement for model validation: x-direction consist of 3 sections (A, B, and C) and y-direction consist of 6 sections (1-6).

Figures 3.2 shows cross section from 1 A, B, C to 6 A, B, and C compare the horizontal airspeed between measurement and simulation. Air velocity measurements of x-velocity in cross section 1A, B, C and 2 A, B, C showed increasing of air velocity near to the fans (2.12 m height). In the middle of chamber, 3 A, B, C; 4 A, B, C; and 5 A, B, C showed the air velocities were almost constant with the height except 3A, 3B and 4A showed higher air velocity near to the fan. In the cross section 6 A, B, and C showed the air velocities were constant.

The simulation results of x-velocity were plotted in cross-section from 1 A, B, C to 6 A, B, and C to compare between the measurement data and simulated airflow inside the bottom opened chamber (Figure 3.3). The simulation results, near the fan (1 A, B, C; 2 A, B, and C) could reproduce the measurement results. In the middle of chamber, 3 A, B, C; 4 A, B, C; and 5 A, B, C showed a good agreement between the measurement data and simulated airflow, whereas the simulation results for 3C, 4B, and 4C from 1.85 m to 2.15 of the chamber height were slightly overestimated. The simulation results from near to the right wall (6 A, B, and C) showed good agreement with the measurement results. The simulation of airflow distribution inside the chamber based on height show in Figure 3.4.

Figures 3.5 shows cross section from 1 A, B, C to 6 A, B, and C compare the vertical airspeed between measurement and simulation. Air velocity measurement of z-velocity in cross section 1A, B, C, and 2 A, B, C show that the observed air velocity rapidly decreased by increasing the distance from the fans (2.12 m height). In the middle of chamber, 3 A, B, C; 4 A, B, C; and 5 A, B, C show the air velocities were almost constant with the height except 3A observed higher air velocity near to the fans. In the cross section 6 A, B, and C showed almost stagnant condition where the air velocities were constant.

The simulation results of z-velocity were plotted in cross-section from 1 A, B, C to 6 A, B, and C to compare between the measurement data and simulated airflow. The simulation results, near the fan (1 A, B, and C) showed good agreement with the measurement results, whereas the simulation results under 1.5 m of the chamber height were slightly overestimated. In cross section 2 A, B, C; 3 A, B, and C showed simulation results may be reasonable because the tendency of vertical profiles of air velocity between measurement and simulation was similar, even though the simulation results from 1.65 m to 2.15 of the chamber height were slightly underestimated. The simulation results from the middle of chamber (4 A, B, C; 5 A, B, and C) and near to the right wall (6 A, B, and C) showed good agreement with the measurement results, although 4 A and 4 B were slightly overestimate. The simulation of airflow distribution inside the chamber based on z-direction (A, B, and C cross section) show in Figure 3.6.

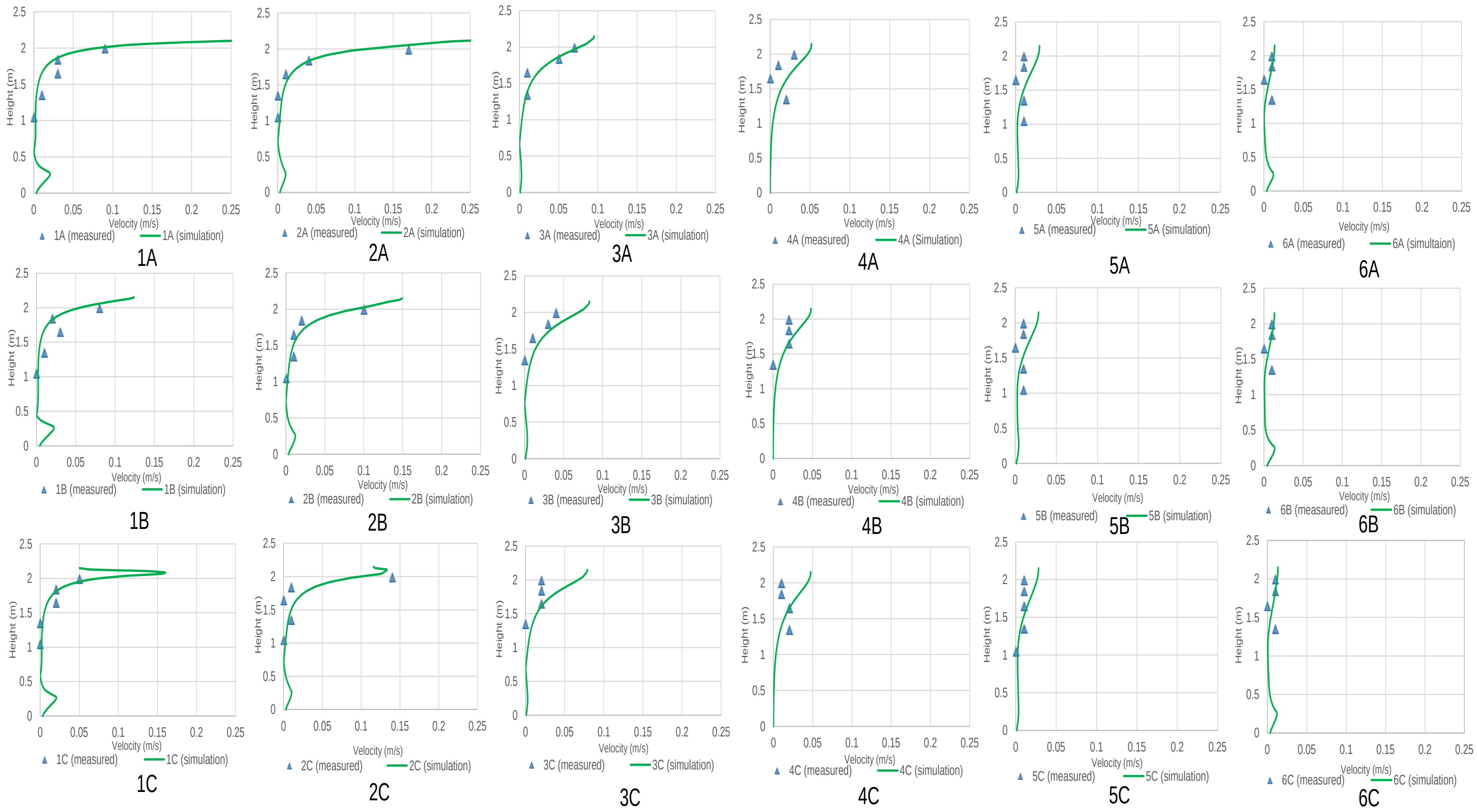

Figure 3.3 Simulated and measured air velocity for x-velocity.

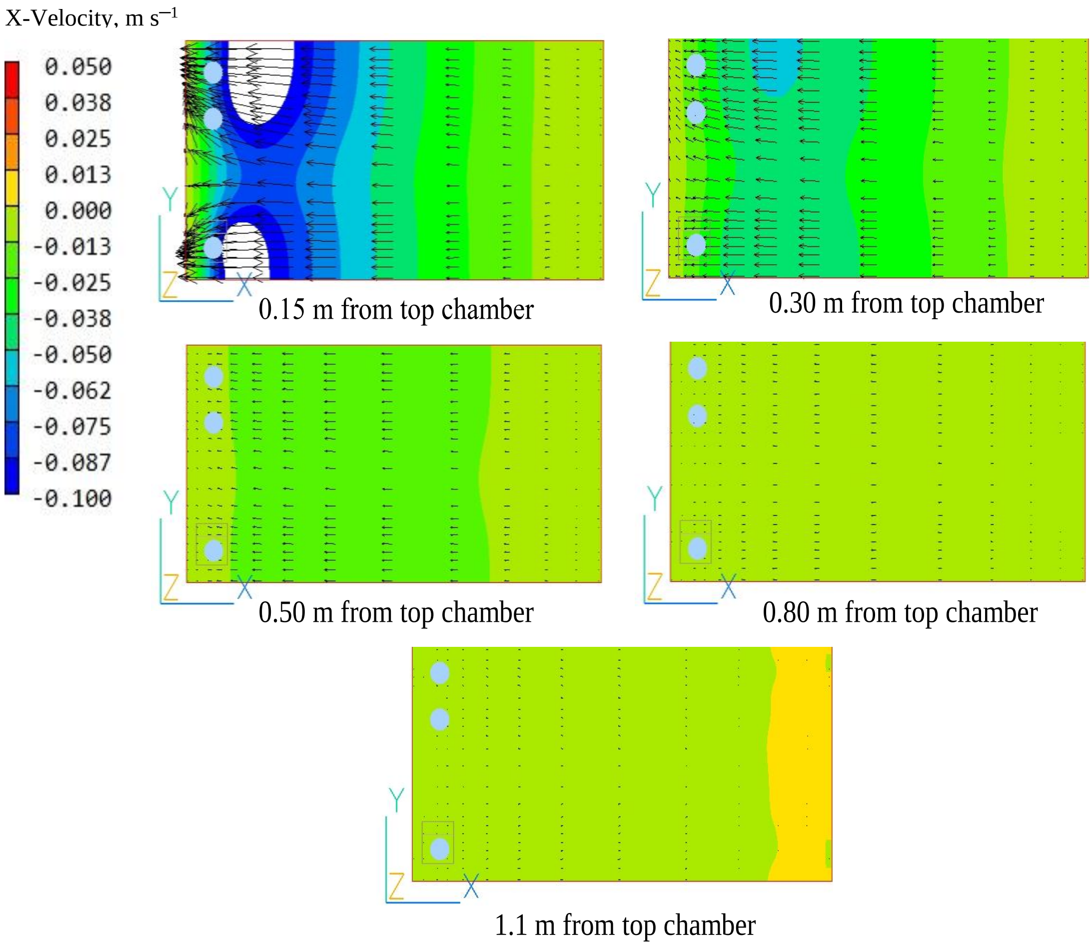

Figure 3.4 Airflow distribution simulation from different height of the chamber for x-velocity.

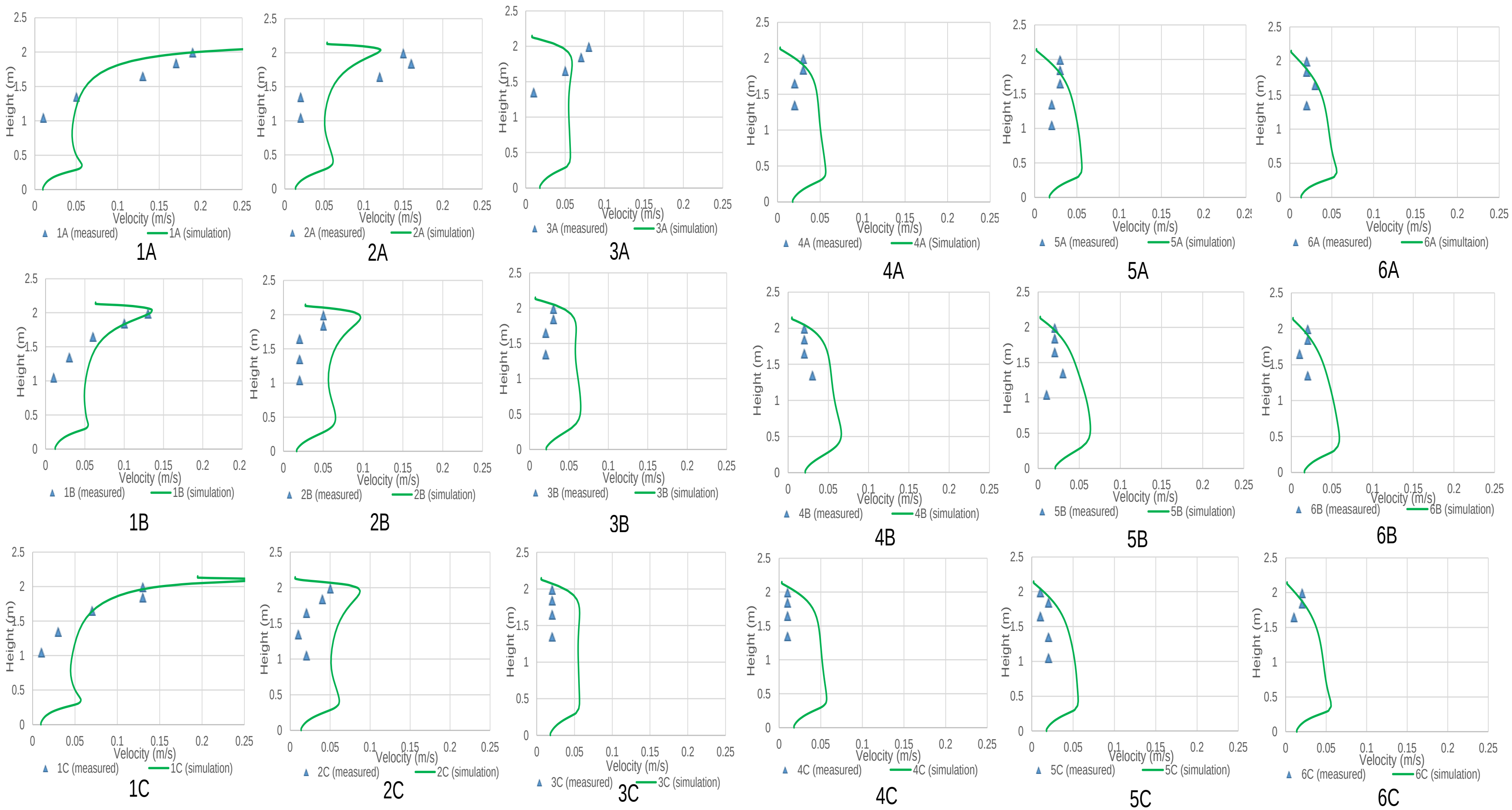

Figure 3.5 Simulated and measured air velocity for z-velocity.

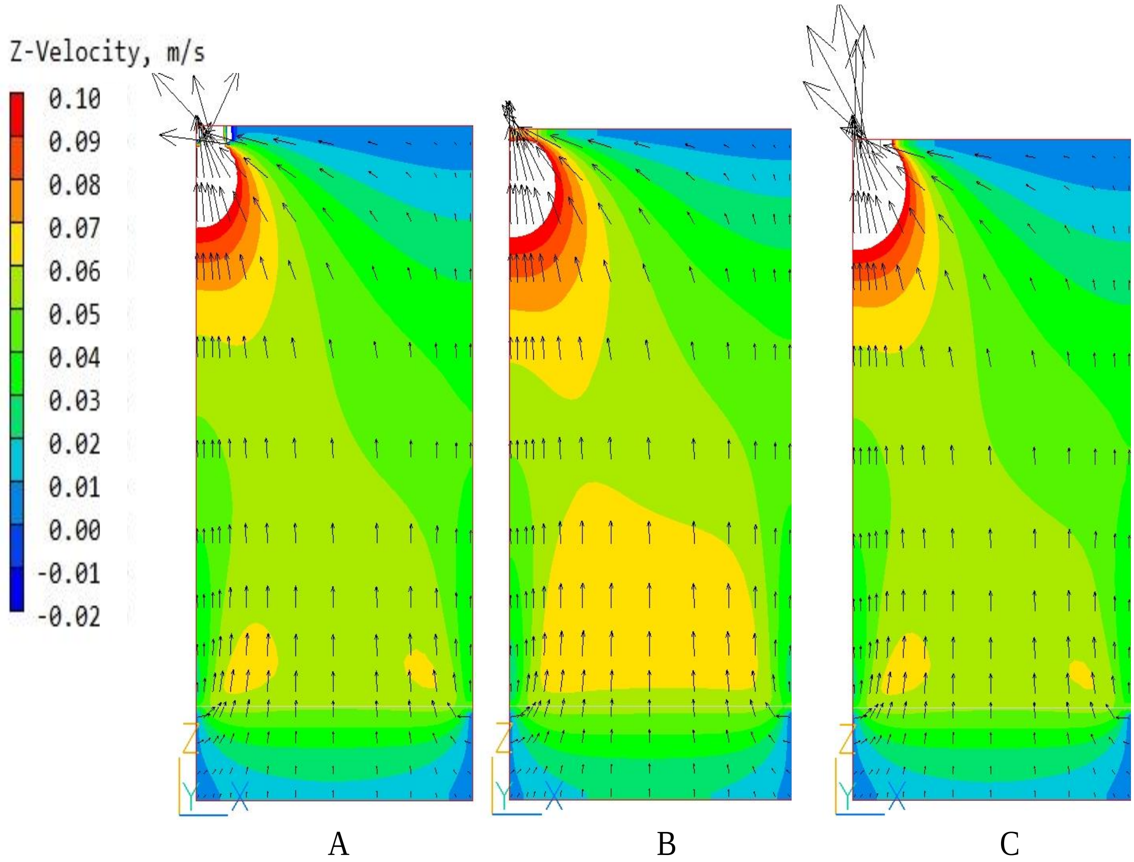

Figure 3.6 Airflow distribution simulation of the chamber in y-direction (A, B, and C) for z-velocity.

3.2.3 Results of validation

The accuracy of the simulation model was evaluated by RMSE and MAPE. The value of RMSE and MAPE were calculated for cross section from 1 A, B, C to 6 A, B, C. Absolute value was used in the simulation results as well as anemometer can only detect the absolute value.

As shown in Table 3.3, the accuracy of simulation results from x-velocity was compared with the measurement data. The MAPE results showed high percentage error from 1 A, B, C to 6 A, B, C were approximately 35 – 155%. Even though the measured data and simulation data have almost similar value. The initial value of measured data was so low and the minimum of range of anemometer only can detect until 0.01 m s^{-1}.

RMSE results showed the results for each cross section from 1 A, B, C to 6 A, B, C were 0.004-0.03 m s^{-1}. However, simulation results in this study may be reasonable because measurement and simulation results has a good agreement and the air velocity obtained both by measurement and simulation in the lower part of the real chamber was so small (order of 10^{-2} m s^{-1}).

Table 3.3 RMSE and MAPE results of air velocity from x-velocity.

Distance from top chamber (m)	Measured (m s^{-1})																	
	1			2			3			4			5			6		
	A	B	C	A	B	C	A	B	C	A	B	C	A	B	C	A	B	C
0.15	0.09	0.08	0.05	0.17	0.10	0.14	0.07	0.04	0.02	0.03	0.02	0.01	0.01	0.01	0.01	0.01	0.01	0.01
0.30	0.03	0.02	0.02	0.04	0.02	0.01	0.05	0.03	0.02	0.01	0.02	0.01	0.01	0.01	0.01	0.01	0.01	0.01
0.50	0.03	0.03	0.02	0.01	0.01		0.01	0.01	0.02		0.02	0.02			0.01			
0.80	0.01	0.01			0.01	0.01	0.01			0.02		0.02	0.01	0.01	0.01	0.01	0.01	0.01
1.10													0.01	0.01				

Distance from top chamber (m)	Simulation (m s^{-1})																	
	1			2			3			4			5			6		
	A	B	C	A	B	C	A	B	C	A	B	C	A	B	C	A	B	C
0.15	0.08	0.06	0.07	0.12	0.09	0.10	0.08	0.07	0.07	0.05	0.04	0.04	0.03	0.03	0.03	0.01	0.01	0.01
0.30	0.03	0.02	0.03	0.04	0.04	0.04	0.05	0.04	0.04	0.04	0.03	0.03	0.02	0.02	0.02	0.01	0.01	0.01
0.50	0.01	0.01	0.01	0.02	0.02		0.02	0.02	0.02		0.02	0.02			0.01			
0.80	0.00	0.00			0.01	0.01	0.01			0.01		0.01	0.01	0.01	0.01	0.00	0.00	0.00
1.10													0.00	0.00				

Distance from top chamber (m)	Percentage error (%)																	
	1			2			3			4			5			6		
	A	B	C	A	B	C	A	B	C	A	B	C	A	B	C	A	B	C
0.15	10.56	30.88	48.20	31.62	12.75	29.69	9.11	72.20	235.51	56.33	115.50	331.00	172.92	165.23	164.26	27.50	24.69	25.03
0.30	8.00	14.50	26.50	9.86	100.23	311.24	5.24	48.53	121.61	252.00	61.00	229.00	123.10	115.96	117.17	6.07	2.69	4.07
0.50	66.00	69.63	51.85	77.42	69.73		141.76	132.14	17.23		0.50	3.50			45.55			
0.80	66.30	67.60			40.06	37.85	9.09			53.45		54.95	39.38	42.40	40.39	76.71	80.80	77.65
1.10													76.96	72.65				
MAPE	37.71	45.65	42.18	39.63	55.69	126.26	41.30	84.29	124.78	120.59	59.00	154.61	103.09	99.06	91.84	36.76	36.06	35.58
RMSE	0.01	0.02	0.02	0.03	0.01	0.03	0.01	0.02	0.03	0.02	0.02	0.02	0.01	0.01	0.01	0.00	0.00	0.00

0.00 means < 0.005 m s^{-1}

As shown in Table 3.4, the accuracy of simulation results from z-velocity was compared with the measurement data. The MAPE results showed high percentage error from 1 A, B, C to 6 A, B, C were approximately 41-272 %. Even though the measured data and simulation data have almost similar value.

RMSE results showed the results for each cross section from 1 A, B, C to 6 A, B, C were 0.01-0.05 m s^{-1}. The CFD model's accuracy seemed sufficient to investigate the velocity because the difference between the measurement and simulation data in the same order of 10^{-2} m s^{-1}.

Table 3.4 RMSE and MAPE results of air velocity from z-velocity.

Distance from top chamber (m)	Measured ($m\ s^{-1}$) 1 A	1 B	1 C	2 A	2 B	2 C	3 A	3 B	3 C	4 A	4 B	4 C	5 A	5 B	5 C	6 A	6 B	6 C
0.15	0.19	0.13	0.13	0.15	0.05	0.05	0.08	0.03	0.02	0.03	0.02	0.01	0.03	0.02	0.01	0.02	0.02	0.02
0.30	0.17	0.1	0.13	0.16	0.05	0.04	0.07	0.03	0.02	0.03	0.02	0.01	0.03	0.02	0.02	0.02	0.02	0.02
0.50	0.13	0.06	0.07	0.12	0.02	0.02	0.05	0.02	0.02	0.02	0.02	0.01	0.03	0.02	0.01	0.03	0.01	0.01
0.80	0.05	0.03	0.03	0.02	0.02	0.01	0.01	0.02	0.02	0.02	0.03	0.01	0.02	0.03	0.02	0.02	0.02	0
1.10	0.01	0.01	0.01	0.02	0.02	0.02							0.02	0.01	0.02			

Distance from top chamber (m)	Simulation ($m\ s^{-1}$) 1 A	1 B	1 C	2 A	2 B	2 C	3 A	3 B	3 C	4 A	4 B	4 C	5 A	5 B	5 C	6 A	6 B	6 C
0.15	0.19	0.13	0.15	0.12	0.10	0.08	0.04	0.04	0.04	0.02	0.03	0.02	0.01	0.02	0.01	0.01	0.01	0.01
0.30	0.11	0.10	0.10	0.09	0.09	0.08	0.06	0.06	0.05	0.03	0.04	0.04	0.03	0.03	0.03	0.02	0.02	0.02
0.50	0.07	0.08	0.07	0.07	0.07	0.07	0.06	0.06	0.06	0.04	0.05	0.04	0.04	0.04	0.04	0.03	0.03	0.03
0.80	0.05	0.06	0.05	0.06	0.06	0.06	0.06	0.06	0.06	0.05	0.05	0.05	0.05	0.05	0.05	0.04	0.04	0.04
1.10	0.05	0.05	0.05	0.05	0.06	0.05							0.05	0.06	0.05			

Distance from top chamber (m)	Percentage error (%) 1 A	1 B	1 C	2 A	2 B	2 C	3 A	3 B	3 C	4 A	4 B	4 C	5 A	5 B	5 C	6 A	6 B	6 C
0.15	1.69	2.80	15.05	21.62	90.43	68.50	46.19	36.75	83.76	32.46	35.73	107.58	51.37	18.65	44.34	41.79	32.99	41.41
0.30	35.04	3.70	24.63	42.67	79.06	105.13	17.96	89.03	167.45	15.46	106.01	250.03	10.52	42.93	32.40	10.84	20.58	10.51
0.50	42.76	27.45	2.24	41.33	265.54	241.20	16.32	195.15	184.02	117.06	145.68	340.91	24.40	94.94	270.77	7.98	240.32	222.52
0.80	8.85	95.32	82.36	178.38	200.32	461.31	450.04	190.48	175.92	139.11	78.41	389.13	129.08	63.17	130.68	106.93	118.66	
1.10	371.00	415.67	375.97	153.45	182.27	157.18							154.22	469.50	156.55			
MAPE (%)	91.87	108.99	100.05	87.49	163.53	206.66	132.63	127.85	152.79	76.02	91.46	271.91	73.92	137.84	126.95	41.89	103.14	91.48
RMSE ($m\ s^{-1}$)	0.04	0.02	0.03	0.05	0.04	0.04	0.03	0.03	0.03	0.02	0.02	0.03	0.02	0.02	0.02	0.01	0.02	0.02

The simulations showed that the airflow did not distribute evenly inside the chamber, due to the fans placed only at the one top side of the chamber. This made the air actively move to the left towards the fans and may cause the stagnation area on the right side of the chamber. In case, the chamber with plant, there was possibility the optimum photosynthesis can only achieve on the left side of the plant canopy. To find out the details about the airflow distribution in the chamber, several simulations about it were carried out on the Chapter 4 and Chapter 5.

3.3 Model Validation for CO_2 (Chamber 2)

Model validation conducted to analyze detailed CO_2 distribution including the photosynthesis with numerical simulations inside of the chamber.

3.3.1 Model Settings

3.3.1.1 Computational domain

The chamber model replicated the bottom open chamber. A similar chamber has been used to investigate photosynthetic rate, related environmental factors (Shimomoto et al., 2020), and airflow uniformity (Nurmalisa et al., 2021). Chamber dimensions of length, width, and height were 1, 0.52, and 1.64 m, respectively (Figure 3.7). In the calculation of chamber simulation, the scale of the domain was small and consisted of one plant (actually, it represents two plants due to make simplifications of the calculation, one plant was made with the average height of plant) and one fan as outlet and inlet at the bottom part of the chamber. The CO_2 distribution model used in chamber simulation was the laminar flow model. In the calculation of chamber simulation, the scale of the domain was compact but sufficient to calculate canopy photosynthesis for the whole body of the tomato plant, and laminar flow shows good simulation results instead of turbulence flow. The mesh numbers in the computational domain had 5,940 cells inside the chamber (Figure 3.8). Chamber simulation has been conducted to investigate CO_2 distribution and photosynthesis, particularly net photosynthetic rate. The initial CO_2 concentration for the simulation was set at 450 ppm, which is same as the measured from the outlet of bottom chamber.

In this study, the inflow air including CO_2 enter to chamber from the bottom opening of chamber. The air including CO_2 will move until reach the outlet at the top of chamber. Inside of the chamber, the plant model was set up with considering of photosynthesis. Therefore, the amount of CO_2 may absorb by plant through photosynthesis.

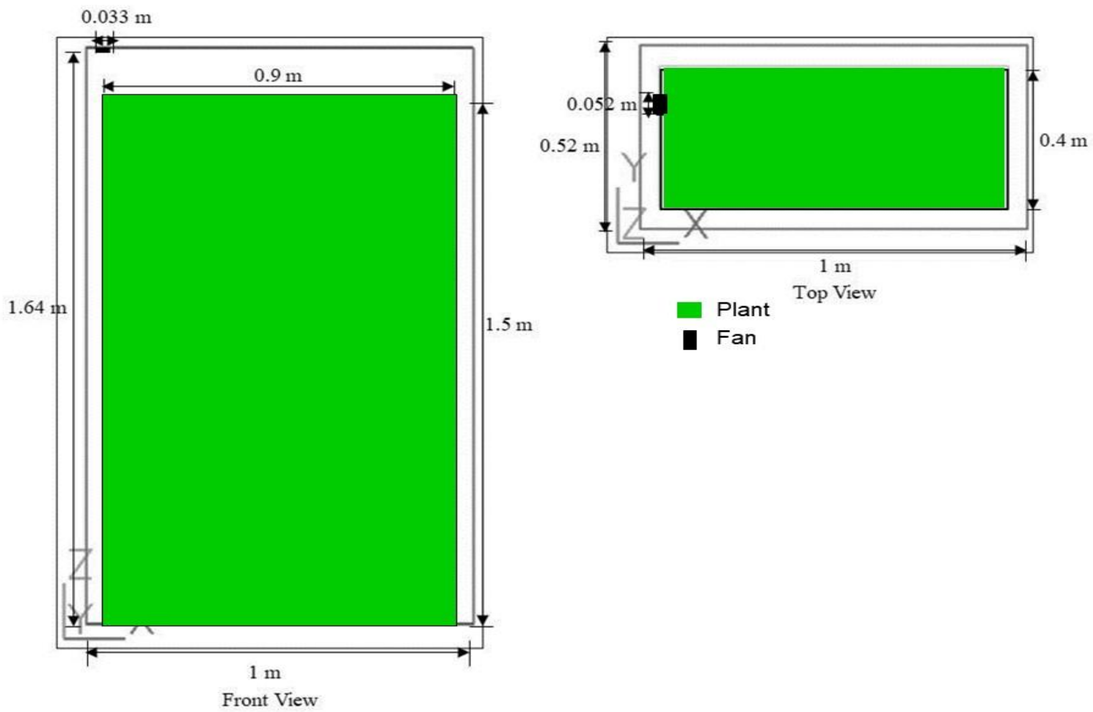

Figure 3.7 Chamber model: Fans are placed at the top left side of the chamber (▄). The rectangular shape inside of the chamber represent the plant.

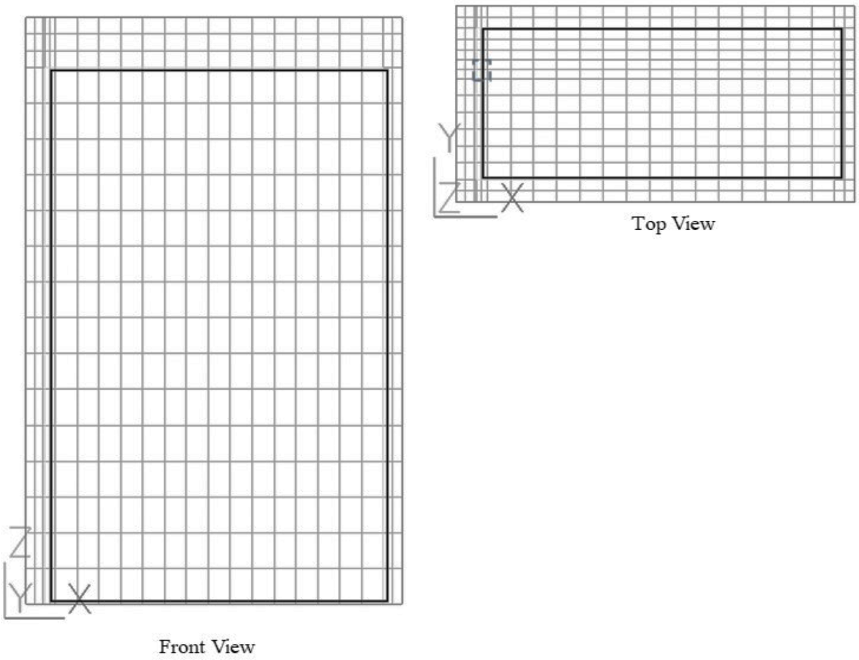

Figure 3.8 Meshing of chamber model: the dotted line represents fan ( ). The rectangular shapes inside of the chamber represent the plant.

Managing the meshing grid was quite challenging to get accurate simulation results. Hong et al. (2017) discussed that finer meshes might not improve the accuracy anymore, whereas coarser meshes might still give accurate results for some cases. Additionally, the numbers of mesh in the computational domain had 5,940 cells, which can gain stability of numerical computations inside the chamber. The meshing characters shown in Table 3.5.

.

Table 3.5 Meshing of computational domain for chamber 2.

Mesh	**Properties**
Number	5,940
Coordinate Type	Cartesian

3.3.1.2 Initial and boundary conditions

Equations for net photosynthesis were solved according using CFD (PHOENICS) with source terms placed in user defined functions (UDF) which energy, crop respiration, and carbon dioxide balance equations for the canopy inside the chamber were describe in APPENDIX, page A.2. The characteristics of the numerical procedure and input values for chamber 2 in Table 3.6.

Table 3.6 The characteristics of the numerical procedure and input values of chamber 2.

Parameter	**Symbol**	**Unit**	**Value**
CO_2 density	*C'*	g m^{-3}	1839
Conductance of CO_2	τ_c	m s^{-1}	12.168×10^{-4}
Crop respiration	*R'*	g h^{-1} m^{-2}	2.84×10^{-2}
Initial CO_2	-	ppm	450
Leaf area density	*LAD/α*	m^2_{leaf} m^{-3}_{row}	2.67
Leaf area index	*LAI*	m^2 m^{-2}	4
The light use efficiency of the plant canopy	α_c	g CO_2 J^{-1}	3.705×10^{-6}
The incident light flux PAR	J_o	W m^{-2}_{leaf}	380

3.3.2 Comparison of CO_2 concentration between measurement and simulation data

Carbon dioxide concentration measurement was conducted in the chamber with plant with the total measurement data were 9 values of CO_2 concentration as shown in Figure 3.9. Figures 3.10 shows cross section from bottom (left, middle, and right cross section) to the top (left, middle, and right cross section), compare the CO_2 concentration between measurement and simulation. CO_2 concentration from bottom to the top of canopy showed decreasing of CO_2 concentration. The CO_2 concentration at the bottom of canopy were almost constant. The CO_2 concentration in the middle of canopy were decreasing due to CO_2 absorption by photosynthesis. The CO_2 concentration at the left side (near to the fan) has lower values than right side (apart from the fan). The CO_2 concentration distribution according to the chamber measurement and simulation for each height were compared to evaluate numerical simulation properties. The simulation results of CO_2 concentration were plotted in cross-section from bottom (left, middle, and right cross section) to the top (left, middle, and right cross section) to compare between the measurement data and simulated CO_2 concentration inside the chamber. The simulation results at the bottom of canopy showed good agreement with the measurement results. In cross section middle and top of canopy showed simulation results were slightly overestimated.

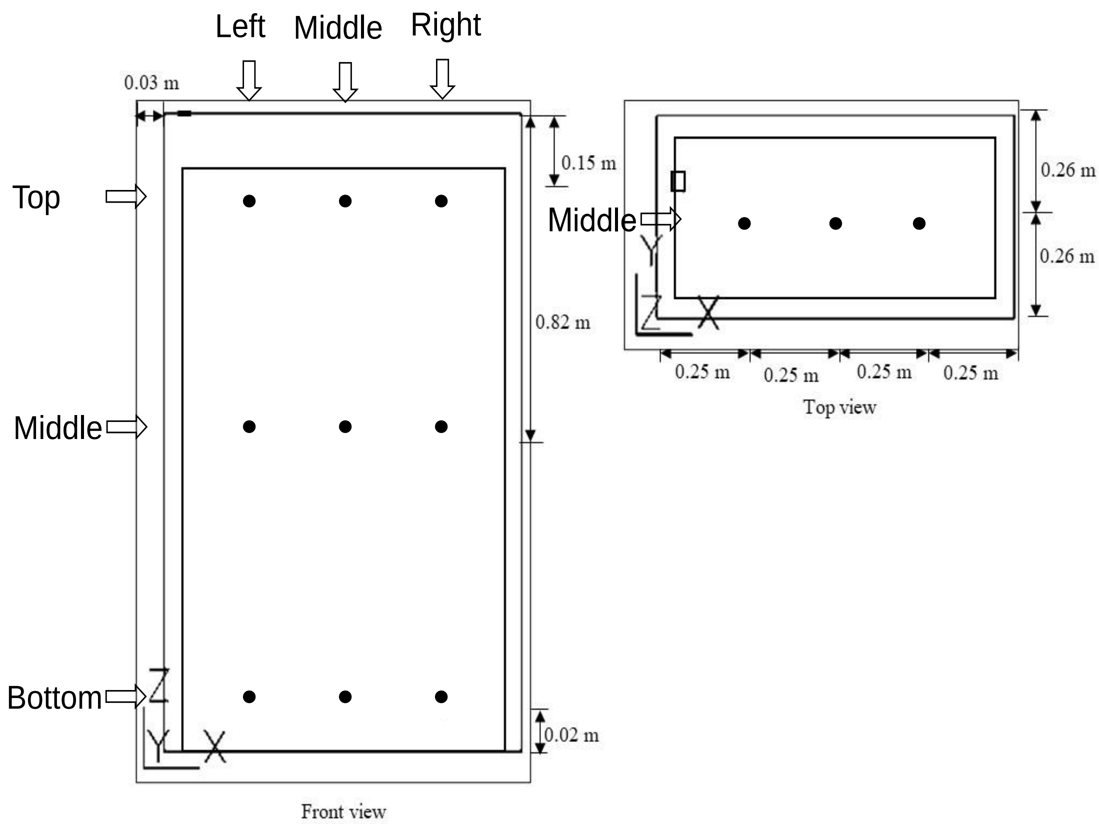

Figure 3.9 Points of CO_2 measurement for model validation: x-direction consist of 1 section (middle) and y-direction consist of 3 sections (left, middle, and right).

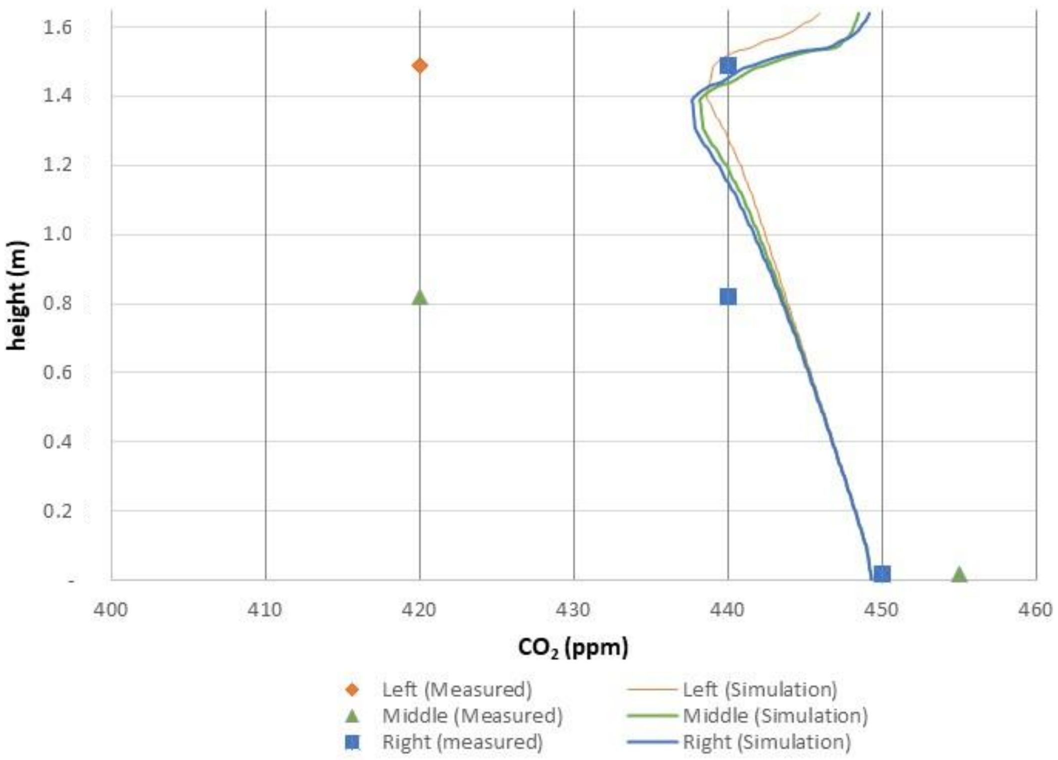

Figure 3.10 Measured and simulated data of CO_2 concentration inside the chamber.

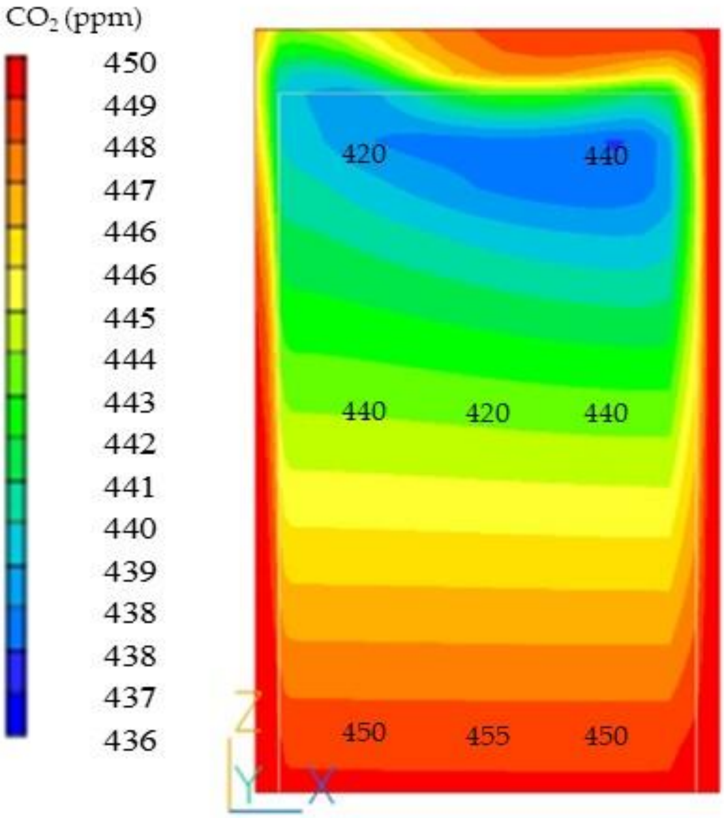

Figure 3.11 Carbon dioxide distribution simulation from middle cross section of the chamber: The values inside of the chamber shows the measurement value.

The simulation results showed that employing a tomato plant as a porous medium considered the photosynthetic process could reasonably predict CO_2 distribution. However, modeled tomato plant has been easy compared to the actual canopy of the tomato plant. That is, the dense leaves were considered homogenous for the entire plant. Thus, the CO_2 concentration shows a decrease inside the porous medium (corresponding to tomato plant), where the air, including $CO_{2,}$ may go through the canopy of the tomato plant; then, the CO_2 is absorbed by the process of photosynthesis (Figure 3.11).

3.3.3 Results of validation

The measured points of CO_2 concentration were compared with the simulated CO_2 distribution inside the chamber. The accuracy of the simulation model was evaluated by RMSE and MAPE. RMSE and MAPE were calculated for cross section from bottom (left, middle, and right cross section) to the top (left, middle, and right cross section).

As shown in Table 3.7, the accuracy of simulation results from left, middle, and right part were compared with the measurement data. The MAPE results showed low percentage error from left, middle, and right part were 1.85%, 3.43%, and 0.43%, respectively. The measured and simulation data have almost similar value.

RMSE showed the results for each cross section from left, middle, and right part were 11.20 ppm, 16.99 ppm, and 2.71 ppm, respectively. These results showed that the simulation was reasonable and can be used for greenhouse numerical simulation.

Table 3.7 Comparison of CO_2 concentration between measured and simulated data for model validation in chamber.

Canopy Layer	Measured			Simulation			Percentage error (%)		
	Left	Middle	Right	Left	Middle	Right	Left	Middle	Right
Top	420	–	440	439	442	442	4.53	–	0.36
Middle	440	420	440	444	443	443	0.84	5.59	0.76
Bottom	450	455	450	449	449	449	0.17	1.27	0.17

MAPE (%)	1.85	3.43	0.43
RMSE (ppm)	11.2	17.0	2.2

3.4 Model validation for CO_2 (greenhouse)

Model validation conducted to analyze detailed CO_2 distribution including the photosynthesis with numerical simulations inside of the greenhouse.

3.4.1 Model Settings

3.4.1.1 Computational domain

The computational model greenhouse has dimensions length of 12 m, width of 10 m, and height of 6 m. The greenhouse model has four circulating fans, four shelves of cultivating bed tomato, and four CO_2 perforated tubes on each shelf (Figure 3.12). Leakage paths were managed in the door area and tiny gaps across the greenhouse rib structure between the wall and the roof (Kuroyanagi, 2017b). Several turbulence models were tested to predict suitable turbulence models in the greenhouse (Kim et al., 2017; Flores-Velzquez et al., 2012). Natural ventilation greenhouse simulation was validated by performing the effect of mesh size and different turbulence models to determine the accuracy of CFD simulation (Hong et al., 2017). This study tested different turbulence models to simulate CO_2 distribution while considering CO_2 absorption in the photosynthesis process and found that the optimum convergence was achieved in the standard

$k-\varepsilon$ turbulence model. Accordingly, standard $k-\varepsilon$ turbulence model was applied in the greenhouse simulation. The numbers of mesh in the computational domain had 739,350 cells inside the greenhouse (Figure 3.13). The meshing characters shown in Table 3.8.

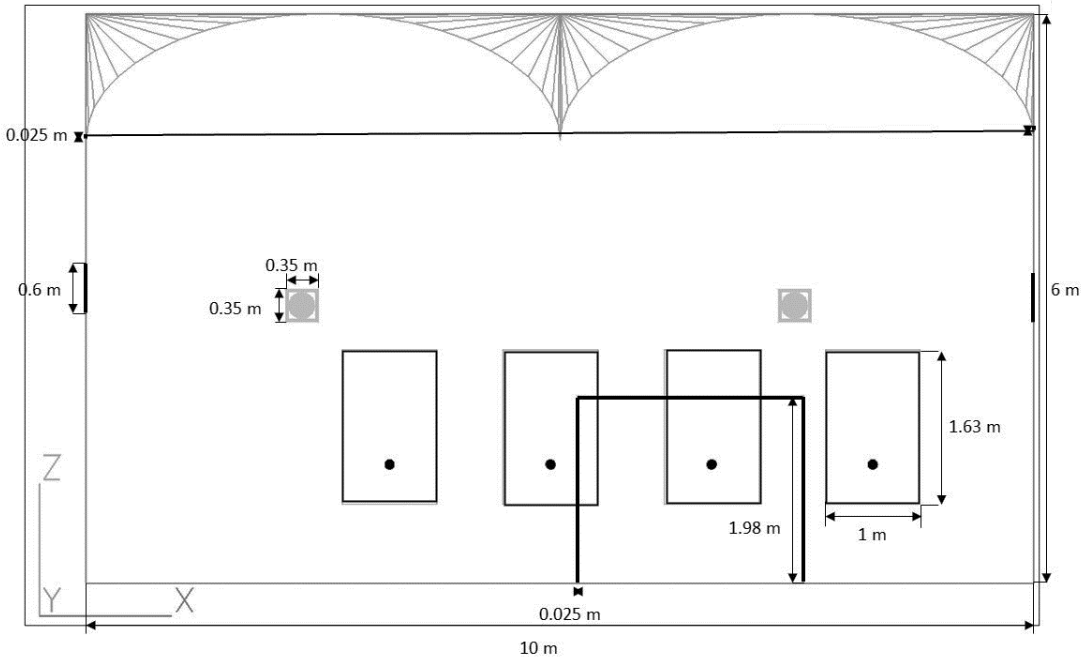

Figure 3.12 Greenhouse model: (the squares represent fan circulator, rectangular shapes represent the plants, the circles represent CO_2 perforated tube, and the thick lines and dots represent outlet).

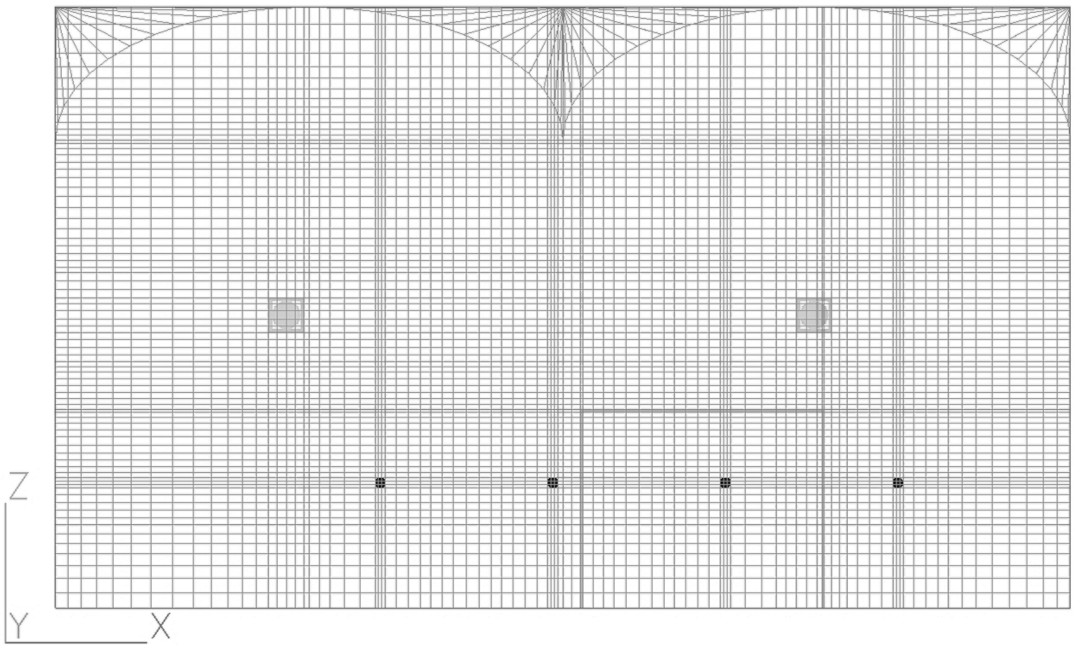

Figure 3.13 Meshing of greenhouse model: (the four rectangular shapes inside the chamber represent the plants, the circles represent CO_2 perforated tube, and the squares represent fans).

Table 3.8 Meshing of computational domain for greenhouse.

Mesh	**Properties**
Number	739,350
Coordinate Type	Cartesian

3.4.1.2 Initial and boundary conditions

Equations for net photosynthesis were solved according using CFD (PHOENICS) with source terms placed in user defined functions (UDF) which energy, crop respiration, and carbon dioxide balance equations for the canopy inside the greenhouse were describe in APPENDIX, page A.3. The characteristics of the numerical procedure and input values for greenhouse in Table 3.9.

Table 3.9 The characteristics of the numerical procedure and input values for greenhouse.

Parameter	**Symbol**	**Unit**	**Value**
CO_2 density	*C'*	g m^{-3}	1839
Conductance of CO_2	τ_c	m s^{-1}	12.168×10^{-4}
Crop respiration	*R'*	g h^{-1} m^{-2}	2.84×10^{-2}
Initial CO_2	-	ppm	450
Leaf area density	*LAD/α*	m^2_{leaf} m^{-3}_{row}	0.67
Leaf area index	*LAI*	m^2 m^{-2}	1.1
The light use efficiency of the plant canopy	α_c	g CO_2 J^{-1}	3.705×10^{-6}
The incident light flux PAR	J_o	W m^{-2}_{leaf}	355

3.4.2 Comparison of CO_2 concentration between measurement and simulation data

Carbon dioxide concentration measurement was conducted in the greenhouse with plant with the total measurement data points were 8 points of CO_2 concentration as shown in Figure 3.15. The measurement points for the comparison start from (1.2 m, 1.8 m, 2.4 m, and 4.2 m from the ground).

Figures 3.14 shows measurement points 3.4 m from north wall (1.2 m, 1.8 m, 2.4 m, and 4.2 m from the ground) and 3.4 m from south wall (1.2 m, 1.8 m, 2.4 m, and 4.2 m from the ground), compare the CO_2 concentration between measurement and simulation. CO_2 concentration measurement from bottom to the top of canopy showed decreasing of CO_2 concentration. The CO_2 concentration at the bottom of canopy (1.2 from the ground) were higher than other parts. The CO_2 concentration in the middle of canopy were decreasing due to CO_2 absorption by photosynthesis. The CO_2 concentration distribution according to the chamber measurement and simulation for each height were compared to evaluate numerical simulation properties.

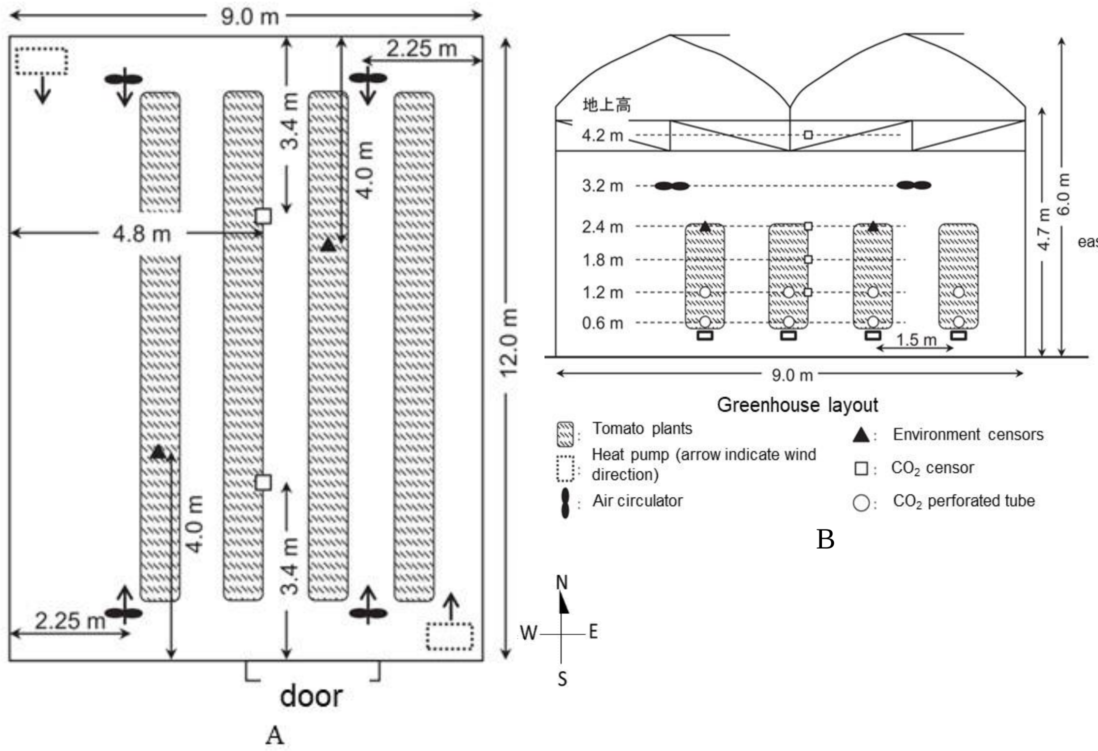

Figure 3.14 Points of CO_2 measurement for model validation: from north and south wall consist of 4 points (1.2 m, 1.8 m, 2.4 m, and 4.2 m from the ground) for each.

The simulation results of CO_2 concentration were plotted in 3.4 m from north wall (1.2 m, 1.8 m, 2.4 m, and 4.2 m from the ground) and 3.4 m from south wall (1.2 m, 1.8 m, 2.4 m, and 4.2 m from the ground) to compare between the measurement data and simulated CO_2 concentration inside the greenhouse (Figure 3.15). The simulation results at the bottom of canopy showed good agreement with the measurement results. In position of 3.4 m from north wall showed simulation results were overestimated. Whereas, in position of 3.4 m from south wall showed simulation results were slightly underestimated for height of 1.2 m and 2.4 m from the ground, while for height of 1.8 m and 4.2 m from the ground were overestimated. Simulation results showed the CO_2 concentration were slightly decrease inside the porous medium (corresponding to tomato plant), where the air, including $CO_{2,}$ may go through the canopy of the tomato plant; then, the CO_2 is absorbed by the process of photosynthesis (Figure 3.16).

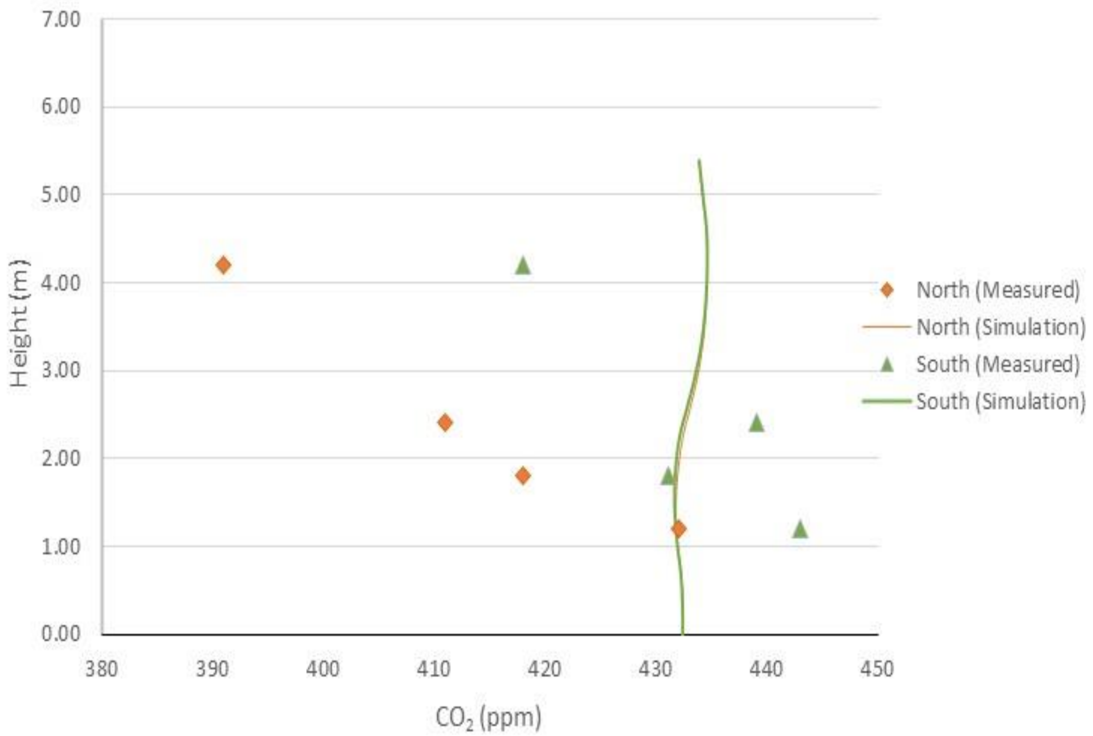

Figure 3.15 Measured and simulated data of CO_2 concentration inside the greenhouse.

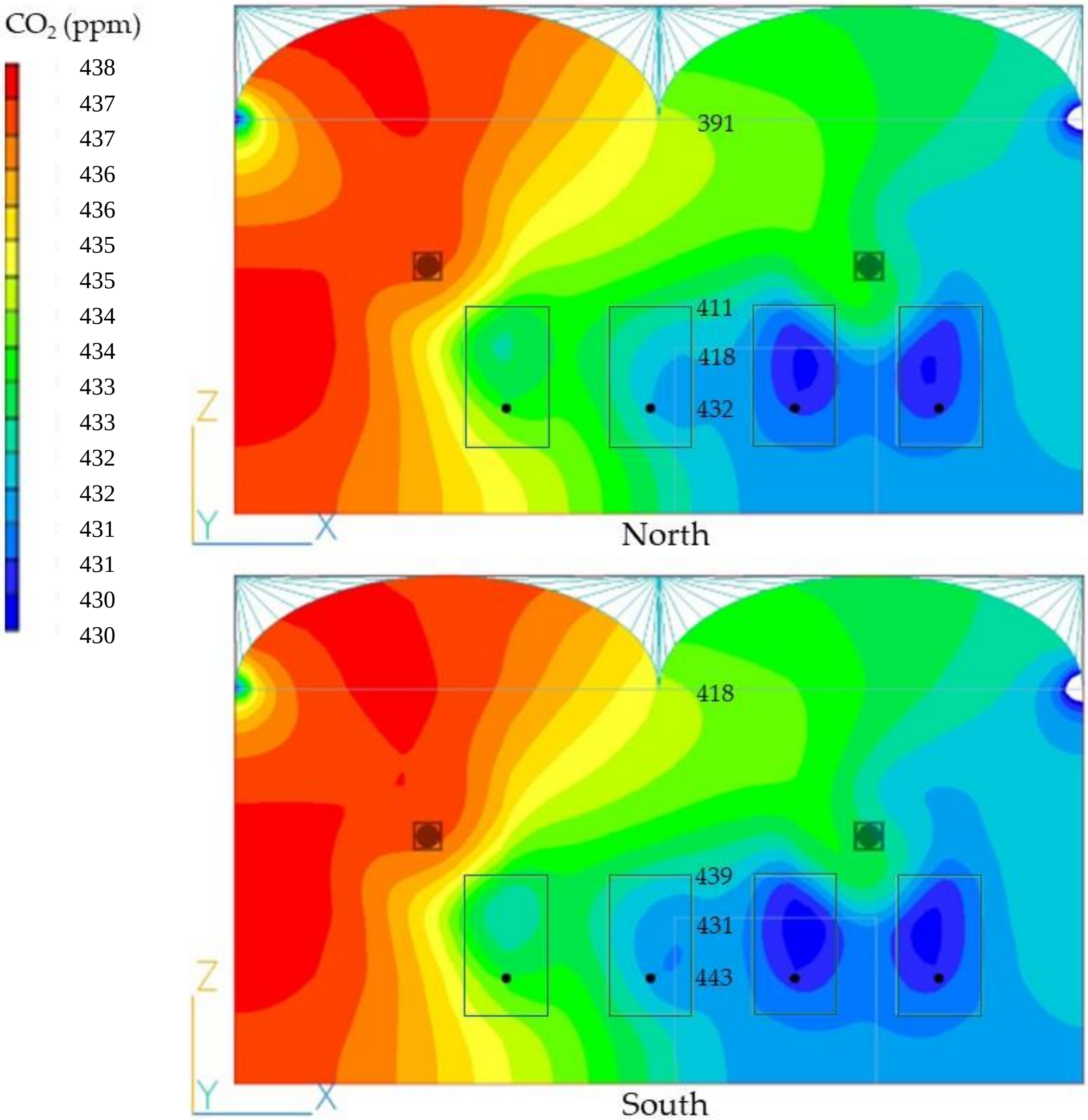

Figure 3.16 Carbon dioxide distribution inside the greenhouse considering CO_2 absorption through photosynthesis by plants (image taken at cross-section 3.4 m from north and south wall).

3.4.3 Results of validation

The greenhouse model validation was conducted according to the measurement data of Kumazaki et al. (2021), who studied influential positions of CO_2 supply in tomato plants inside the same greenhouse as the present study. The simulation results were compared with the measurement data of CO_2 concentration in the condition 20 min after 1 hour of CO_2 being supplied at the middle canopy (1.2 m above the ground, see Figure 3.16). The CO_2 gas emitted from perforated tube in vertical direction (z-velocity). The results of measurement data at 1.2 m from the ground has the highest CO_2 concentration, it probably because this position was the place where CO_2 gas was released. Beside of that the density of CO_2 gas is higher than the air density and make the amount of CO_2 concentration is higher at the bottom part. Furthermore, the initial simulation value of CO_2 concentration was assumed to be constant in every mesh inside the greenhouse, whereas the actual condition has various CO_2 concentrations.

In contrast, the simulation results at the bottom part showed the lowest CO_2 concentration, it was the results in the condition 20 min after 1 hour of CO_2 being supplied. The CO_2 distribution displayed the result was not symmetrical due to unsymmetrical properties position (such as plant row and CO_2 tube tend to the right side).

The measured points of CO_2 concentration were compared with the simulated CO_2 distribution inside the greenhouse. The accuracy of the simulation model was evaluated by RMSE and MAPE. RMSE and MAPE were calculated in position 3.4 m from north wall (1.2 m, 1.8 m, 2.4 m, and 4.2 m from the ground) and 3.4 m from south wall (1.2 m, 1.8 m, 2.4 m, and 4.2 m from the ground). As shown in Table 3.10, the accuracy of simulation results from north and south wall were compared with the measurement data. The MAPE results showed low percentage error from north and south wall were 4.95% and 2.04%, respectively.

RMSE showed the results for each cross section from north and south wall were 25.33 ppm and 10.57 ppm, respectively. However, the simulation results in this study may be reasonable to predict the CO_2 distribution considering CO_2 absorption through the process of photosynthesis of the plant inside the greenhouse.

Table 3.10 Comparison of CO_2 concentration between measured and simulated data for model validation in greenhouse.

Height (m)	Measured (ppm)		Simulation (ppm)		Percentage error (%)	
	North	South	North	South	North	South
4.2	391	418	435	435	11.15	3.96
2.4	411	439	433	432	5.28	1.53
1.8	418	431	432	432	3.34	0.14
1.2	432	443	432	432	0.03	2.55

MAPE (%)	4.95	2.04
RMSE (ppm)	25.33	10.57

Chapter 4 Effect of Different Arrangement Positions of Fans on Airflow Pattern (chamber 1)

4.1 Description

Three fans were placed at the top of the chamber as outflow with a few designated positions. The fan position was designed to investigate the airflow pattern and airspeed within the chamber. The net photosynthesis in the plant canopy was also calculated for each pattern. Pattern default position was in the default system, as set in the real chamber, with the fans placed on one side. Patterns middle and diagonal position placed the fans in the middle and diagonally. Setting chamber model for airflow study in CFD was stated in object management chamber model in APPENDIX, page A.4.

The variability of airflow inside the chamber and the plant canopy were analyzed with a coefficient of variation (CV), which is the ratio of the standard deviation to the mean value. CV is a useful statistic for comparing the degree of variation from one data series to another, even if the means are drastically different from one another.

4.2 Model Settings

4.2.1 Computational domain

The meshing of the modeled chamber without plant is shown in Figure 4.1 and chamber with plant is shown in Figure 4.2. A finer mesh was applied near the fans and walls compare to other parts. The meshing characters is shown in Table 4.1.

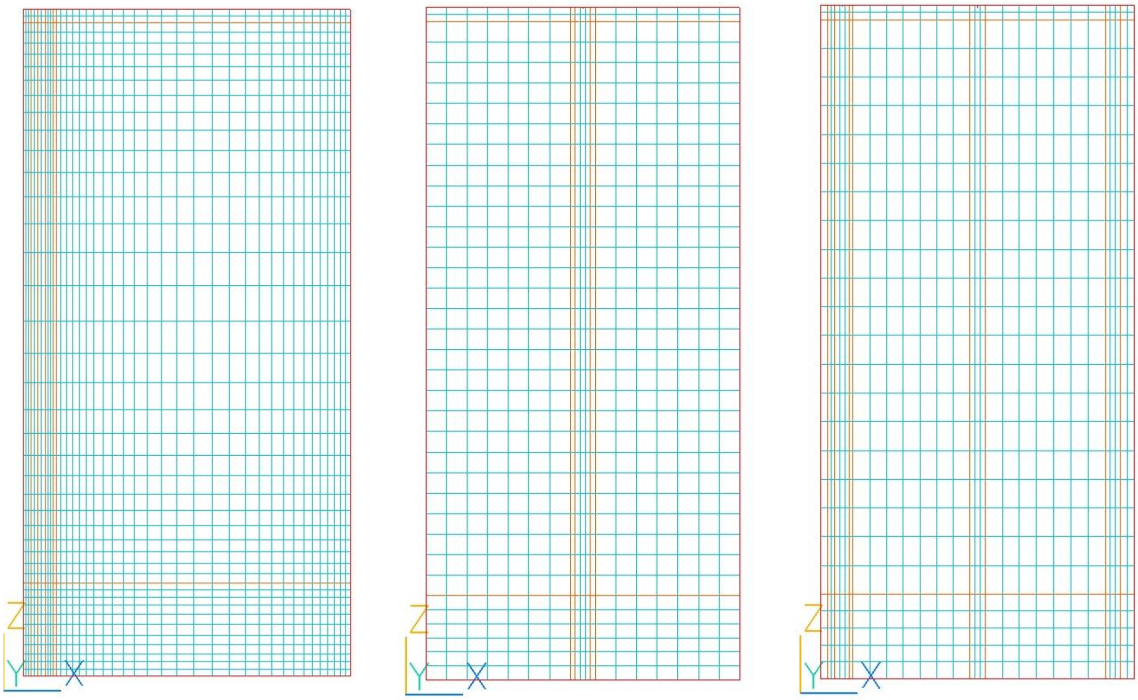

Default Middle Diagonal

Figure 4.1 Meshing of computational domain chamber without plant.

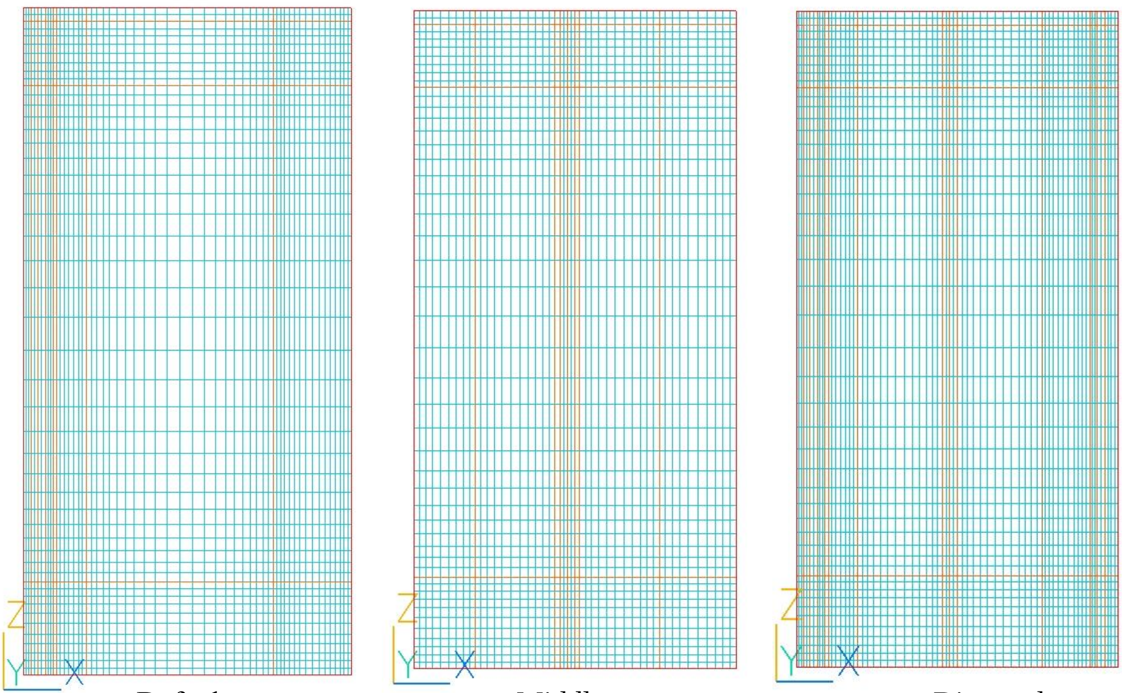

Default Middle Diagonal

Figure 4.2 Meshing of computational domain chamber with plant.

Table 4.1 Meshing characteristics of computational domain for chamber 1.

Mesh	Fans position					
	Chamber without plant			Chamber with plant		
	Default	Middle	Diagonal	Default	Middle	Diagonal
Number	110,880	19836	50,895	185,472	160176	231,744

4.2.2 Initial and boundary conditions

The Chen-Kim turbulence model developed by modifying the two-equation eddy-viscosity *k*-*ε* turbulence model was employed in the modeled chamber 1. The Chen-Kim model proposed a modification that improves the dynamic response of the *ε* equation by introducing an additional time scale (PHOENICS user manual). The *k*-*ε* based turbulence model including the realizable *k*-*ε* model has been well used to improve airflow uniformity for the design of air circulation system in a single cultivation shelf (Zhang et al., 2016). This model has been also used in studies related to ecological agriculture (Niam et al., 2019) and airflow in greenhouses (Molina-Aiz et al., 2017). The average of airflow rate from the three fans is approximately 0.009 $m^3 s^{-1}$, which is used in the simulation (Table 4.2). The chamber was modeled on the basis of the real chamber's dimensions. Chamber's length, width, and height were 1.05, 0.52, and 1.88 m, respectively (Figure 4.3).

Table 4.2 Boundary conditions for model validation chamber 1.

Parameter	Conditions
Air volume rate of the fans	0.009 $m^3 s^{-1}$
Bottom opening	Pressured fixed
Wall	No slip

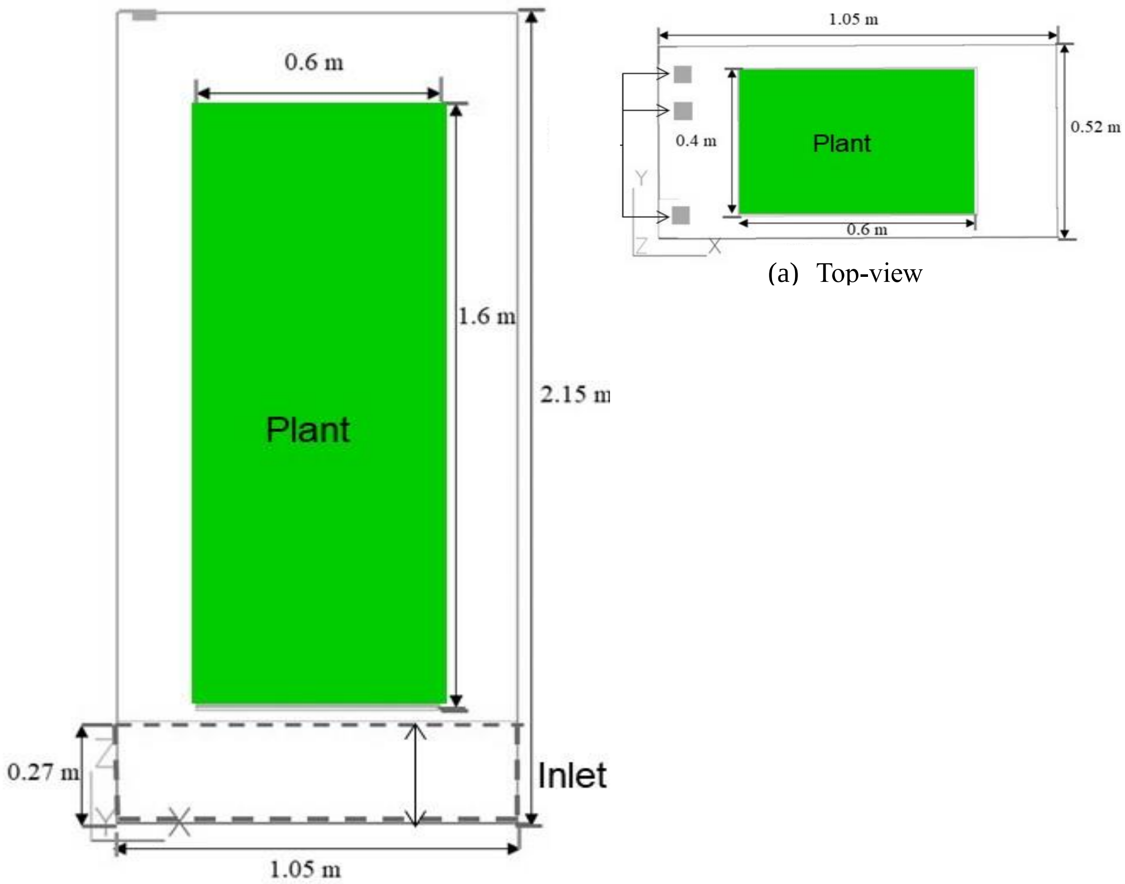

(b) Front-view

Figure 4.3 The structure of the plant: (a) front-view and (b) top-view.

4.2.3 Simulation Cases

4.2.3.1 Fans arrangement in chamber without plant

The simulation was made to know the airflow distribution inside the chamber without the plant as shown in Figure 4.4.

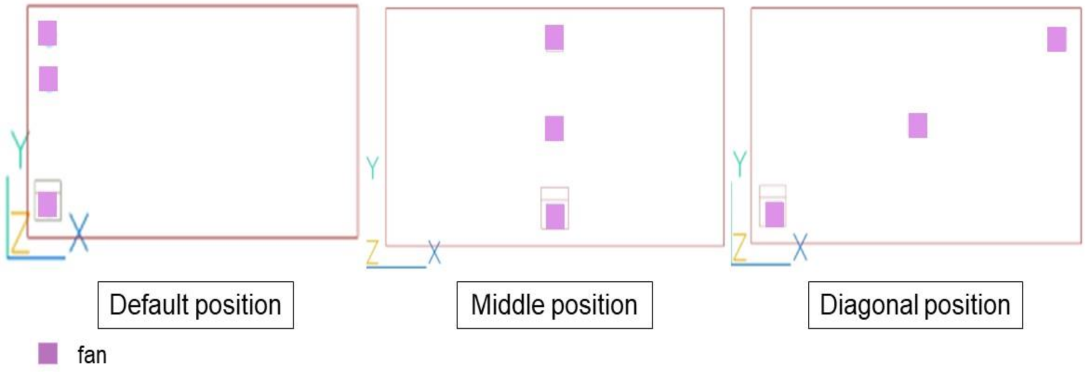

Figure 4.4 Arrangement position of fans in chamber without plant.

4.2.3.2 Fans arrangement in chamber with plant

The simulation was made to know the airflow distribution inside the chamber with the plant as shown in Figure 4.5.

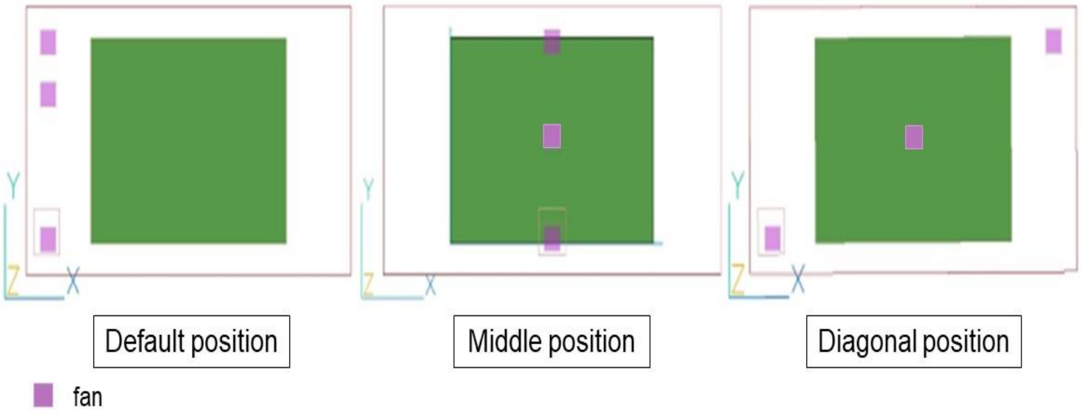

Figure 4.5 Arrangement position of fans in chamber with plant.

4.3 Results and discussions

4.3.1 Chamber without plant

Figure 4.6 shows the distribution of x-velocity (horizontal velocity) at different fan positions in chamber without plant. In the patterns, (a), (b), and (c), the average of air velocity in each pattern inside the chamber was 0.01 m s^{-1}.

As shown in Table 4.3, in the case of default position, the variability of air velocity has lowest value, 45.74 % at height of 1.9 m which showed a more even airflow distribution near to the fans. The variability of air velocity was 55.59 % at height of 1.08 in the middle cross section of the chamber. In the position near to the bottom opening, the variability of air velocity has the largest value, 74.80 %.

In the case of middle position, the variability of air velocity has lowest value, 46.19 % at height of 1.9 m which showed a more even airflow distribution at near to the fans. In the middle cross section of the chamber, the variability of air velocity has the largest value, 76.92%. The variability of air velocity was 68.25% at height of 0.27 m from the chamber's bottom (near to the bottom opening).

In the case of diagonal position, the variability of air velocity has lowest value, 67.27 % at height of 1.08 m which showed a more even airflow distribution in the middle cross section of the chamber. The variability of air velocity was 67.94% at height of 0.27 m from the chamber's bottom (near to the bottom opening). In the position near to the fans, the variability of air velocity has the largest value, 100.09%.

Table 4.3 The variability of air velocity (x-velocity) in different height for each of fan position.

Parameter	Fans Position Cases Default			Fans Position Cases Middle			Fans Position Cases Diagonal		
	Height from chamber bottom			Height from chamber bottom			Height from chamber bottom		
	1.9 m	1.08 m	0.27 m	1.9 m	1.08 m	0.27 m	1.9 m	1.08 m	0.27 m
SD ($m\ s^{-1}$)	0.017	0.001	0.004	0.007	0.000	0.003	0.006	0.000	0.003
Average ($m\ s^{-1}$)	0.036	0.003	0.005	0.014	0.000	0.004	0.006	0.000	0.004
CV (%)	45.74	55.59	74.80	46.19	76.92	68.25	100.09	67.27	67.94

0.000 means the air velocity < 0.0008 ($m\ s^{-1}$)

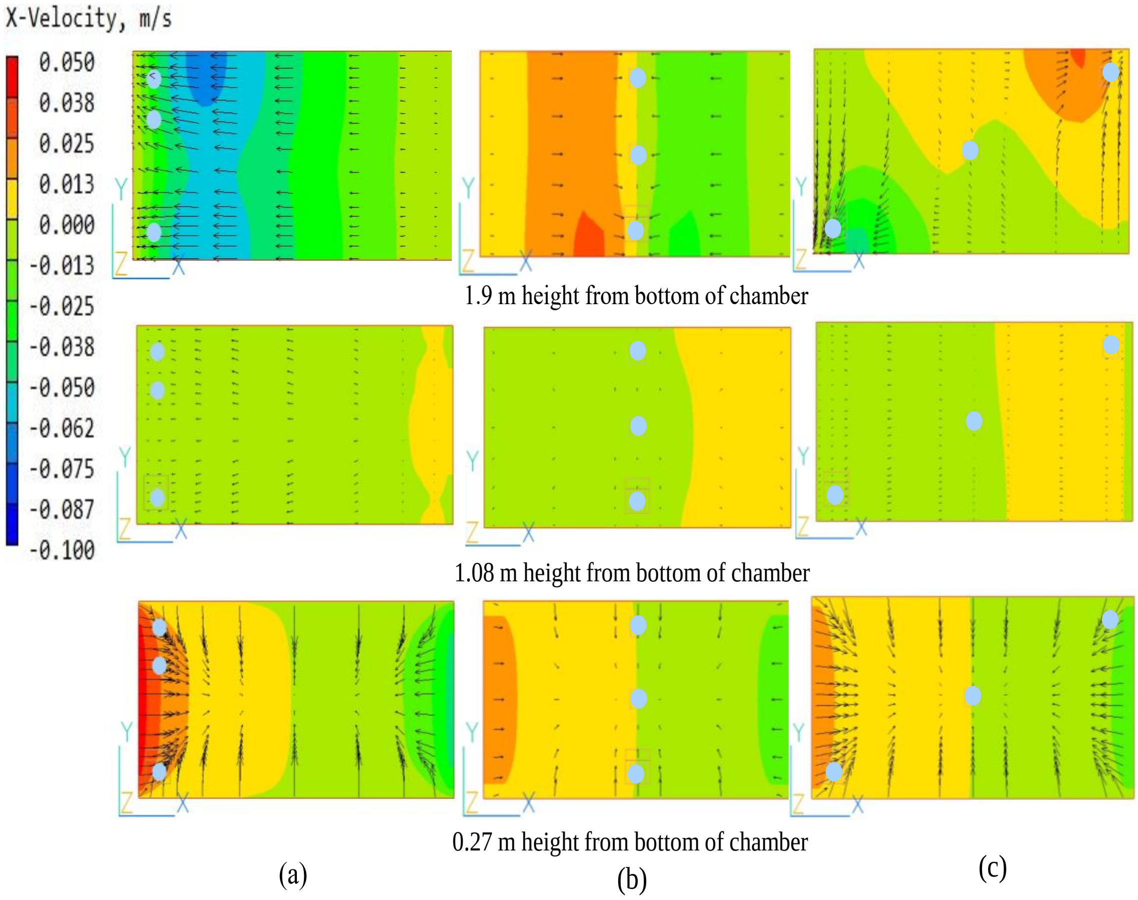

Figure 4.6 Airflow distribution simulation of x-velocity of the chamber without plant: (a) default, (b) middle, and (c) diagonal position of fans.

Figure 4.7 shows the distributions of z-velocity (vertical velocity) at different fan positions in chamber without plant. The airflow passed through the bottom opening as inlet and spread to inside of the chamber. In the patterns, (a), (b), and (c), the average of air velocity inside the chamber were 0.047 m s^{-1}, 0.054 m s^{-1}, and 0.051 m s^{-1}, respectively. In pattern (b), the variability of air velocity inside the chamber was quite high as the effect of all the fans was placing in the middle top of chamber. In pattern (c), the variability of air velocity inside the chamber has high variation may because influence of two fans position put on both side of the chamber wall. The simulation predicted the detail of the airflow distribution inside the chamber. As shown in Table 4.4, a better airflow distribution was observed in default position with coefficients of variation of 34.99 %, while the middle position and diagonally position have coefficients of variation of 79.48 % and 71.18 %, respectively.

Table 4.4 Summary the variability of air velocity (z-velocity) for each of fans position.

Parameter	Fans Position Cases		
	Default	Middle	Diagonal
SD (m s^{-1})	0.016	0.043	0.036
Average (m s^{-1})	0.047	0.054	0.051
CV (%)	34.99	79.48	71.18

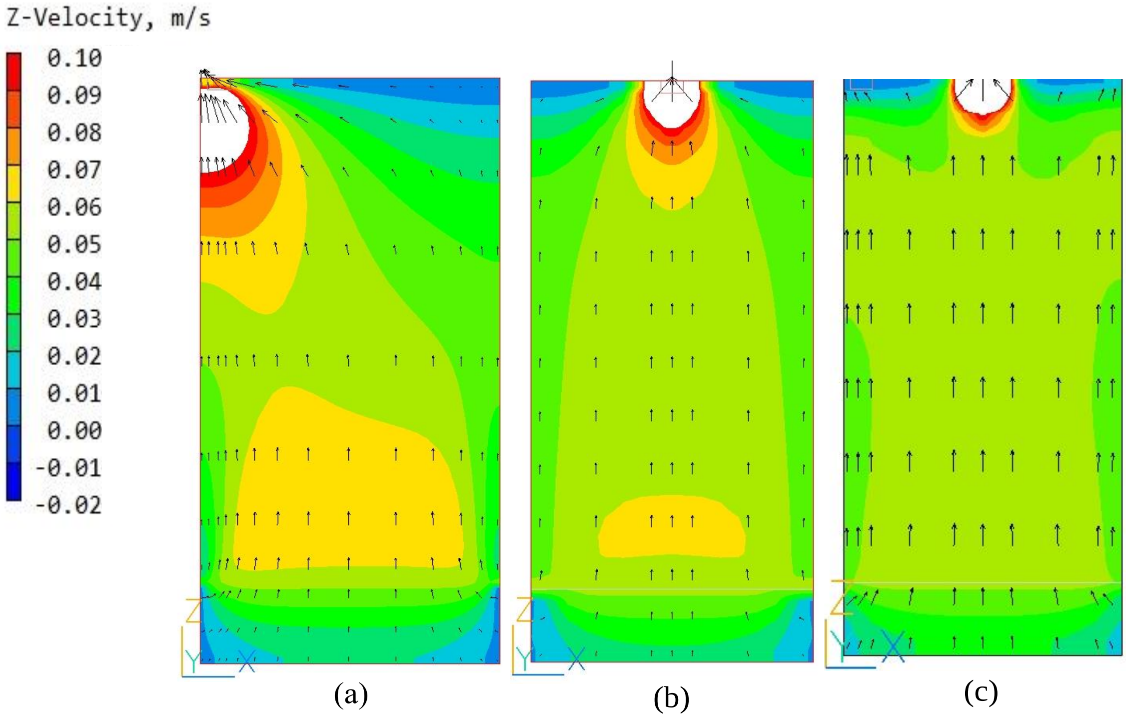

Figure 4.7 Airflow distribution simulation of z-velocity from middle cross section of the chamber without plant: (a) default, (b) middle, and (c) diagonal position of fans.

4.3.2 Chamber with plant

Figure 4.8 shows the distributions of x-velocity (horizontal velocity) at different fan positions in chamber with plant. In the patterns, (a), (b), and (c), the average of air velocity inside the chamber were 0.01m s^{-1}. As shown in Table 4.5, in default position, the variability of air velocity has lowest value, 37.69 % at height of 1.08m which showed a more even airflow distribution in the middle cross section of the chamber. The variability of air velocity was 44.26 % at height of 1.9m from the chamber's bottom in position near to the fans. In the position near to the bottom opening, the variability of air velocity has the largest value, 74.30%.

In middle position, the variability of air velocity has lowest value, 42.58 % at height of 1.9m which showed a more even airflow distribution at near to the fans. In the middle cross section of the chamber, the variability of air velocity has the largest value, 55.45 %. The variability of air velocity was 76.68 % at height of 0.27 m from the chamber's bottom (near to the bottom opening). In diagonal position, the variability of air velocity has lowest value, 60.32 % at height of 1.08 m which showed a more even airflow distribution in the middle cross section of the chamber. The variability of air velocity was 77.01 % at height of 0.27 m from the chamber's bottom (near to the bottom opening). In the position near to the fans, the variability of air velocity has the largest value, 95.48 %.

Table 4.5 The variability of air velocity (x-velocity) in different height for each of fans position.

Parameter	Fans Position Cases			Fans Position Cases			Fans Position Cases		
	Default			Middle			Diagonal		
	Height from chamber bottom			Height from chamber bottom			Height from chamber bottom		
	1.9 m	1.08 m	0.27 m	1.9 m	1.08 m	0.27 m	1.9 m	1.08 m	0.27 m
SD (m s^{-1})	0.016	0.001	0.003	0.007	0.000	0.003	0.005	0.000	0.003
Average (m s^{-1})	0.036	0.003	0.004	0.016	0.001	0.004	0.005	0.001	0.004
CV (%)	44.26	37.69	74.30	42.58	55.45	76.68	95.48	60.32	77.01

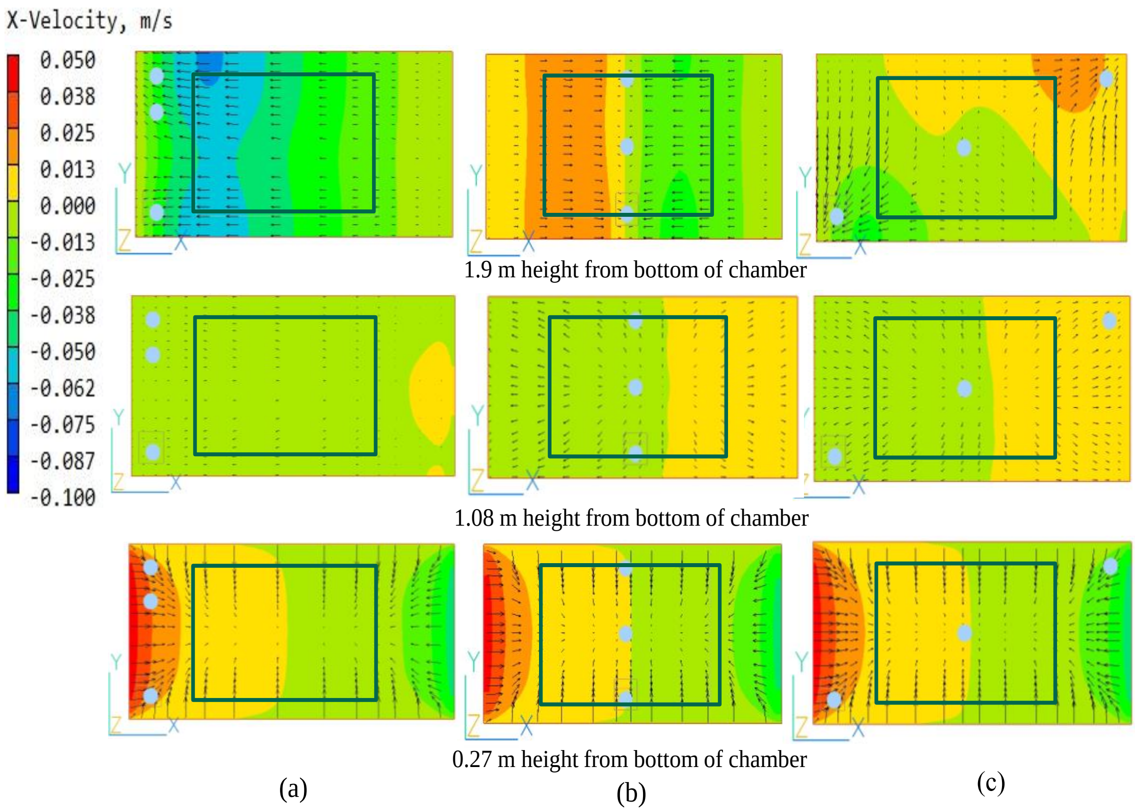

Figure 4.8 Airflow distribution simulation of x-velocity of the chamber with plant: (a) default, (b) middle, and (c) diagonal position of fans.

Figure 4.9 shows the distribution patterns of air velocity at different fan positions in chamber with plant. In the patterns, (a), (b), and (c), the average of air velocity inside the chamber were 0.046 m s^{-1}, 0.053 m s^{-1}, and 0.050 m s^{-1}, respectively. In pattern (b) and (c), the variability of air velocity inside the chamber has high variation of air velocity. As shown in Table 4.6, a better airflow distribution was observed in default position with coefficients of variation of 34.81 %, while the middle position and diagonally position have coefficients of variation of 84.83 % and 82.76 %, respectively in chamber. According to these results, adjusting fans position to middle and diagonal position did not give enough contribution to even the distribution of airflow in the entire chamber with plant.

The average of air velocity inside the plant were 0.053 m s^{-1}, 0.055 m s^{-1}, and 0.053 m s^{-1}, respectively. The variability of air velocity inside the plant in the patterns, (a), (b), and (c) were 14.76 % m s^{-1}, 9.27 % m s^{-1}, and 10.01 m s^{-1}, respectively. In pattern (a), the variability of air velocity inside the plant has lowest variation of air velocity. As shown in Table 4.6, a better airflow distribution was observed in middle position with coefficients of variation of 9.27 %, while the default position and diagonally position have coefficients of variation of 14.76 % and 10.01 %, respectively.

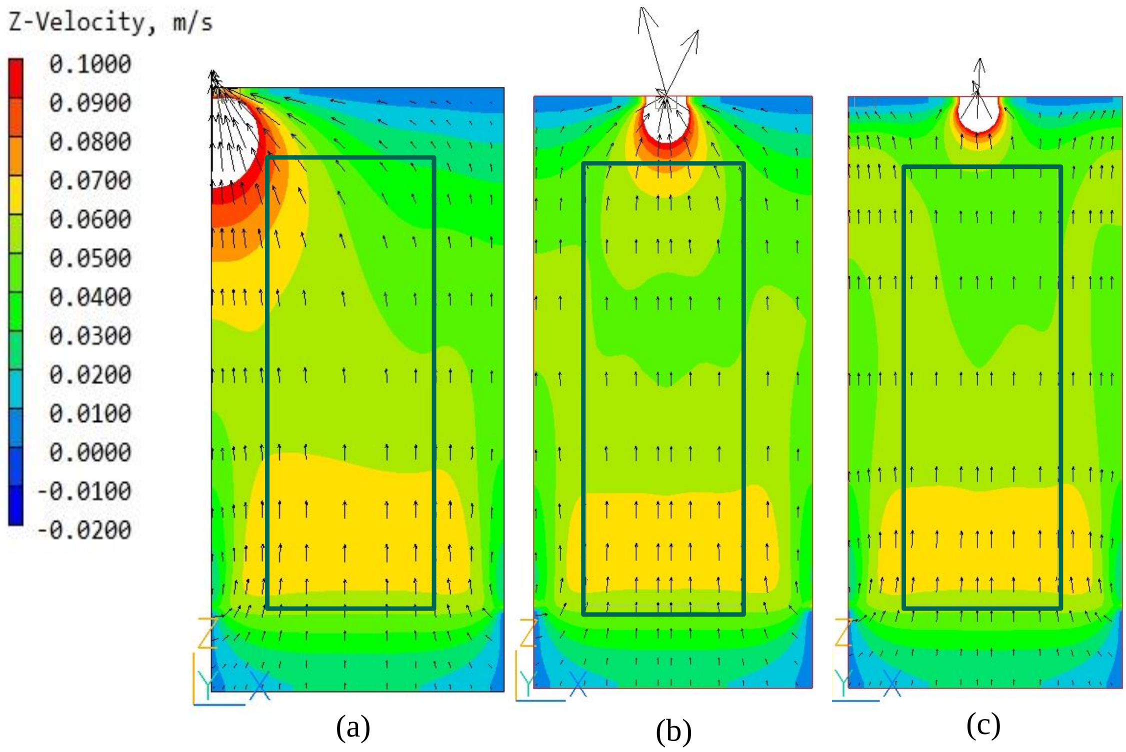

Figure 4.9 Airflow distribution simulation of z-velocity from middle cross section of the chamber with plant: (a) default, (b) middle, and (c) diagonal position of fans.

Table 4.6 Summary the variability of air velocity (z-velocity) for each of fans positions.

Parameter	Cases					
	Fan Positions					
	Default		Middle		Diagonal	
	Chamber	Plant	Chamber	Plant	Chamber	Plant
SD (m s^{-1})	0.016	0.008	0.045	0.005	0.041	0.005
Average (m s^{-1})	0.046	0.053	0.053	0.055	0.050	0.053
CV (%)	34.81	14.76	84.83	9.27	82.76	10.01

4.4 Conclusions

Case of chamber without plant, according to horizontal velocity (x-velocity) results, adjusting fans position to the middle has slightly different variability of air velocity with default position at the top part of chamber (1.9 m from chamber's bottom). Whereas the others simulation results of middle position (in the middle of the chamber and the near to the opening bottom) and diagonal position have high variability of air velocity. Based on vertical velocity (z-velocity) results, adjusting fans position to middle and diagonal position did not give enough contribution to even the distribution of airflow in the entire chamber.

Case of chamber with plant, according to horizontal velocity (x-velocity) results, adjusting fans position to the middle gave contribution to even the distribution of airflow at the top of the plant. Even though the others simulation results of middle position (in the middle of the chamber and the near to the opening bottom) and diagonal position have high variability of air velocity. Based on vertical velocity (z-velocity) results, adjusting fans position to middle and diagonal position give contribution to even the distribution of airflow inside the plant. Similar to Okayama et. al., 2008, that the airflow from one side of a cultivation room cannot provide a uniform air current between the near side and the far side of a plant canopy.

Chapter 5 Effect of Different Size of Transparent Plate on Airflow Pattern (chamber 1)

5.1 Description

Transparent plate was placed at the top of the chamber with a few different sizes. The transparent plate was designed to investigate the airflow pattern and airspeed within the chamber. The net photosynthesis in the plant canopy was also calculated for each model. Model default position was in the default system, as set in the real chamber, with no plate. Setting chamber model for airflow study in CFD was stated in object management chamber model in APPENDIX, page A.4. The variability of airflow inside the chamber and the plant canopy were analyzed with a coefficient of variation (CV), which is the ratio of the standard deviation to the mean value.

5.2 Model settings

5.2.1 Computational domain

The meshing of the modeled chamber without plant is shown in Figure 5.1 and that of chamber with plant is shown in Figure 5.2. A finer mesh was applied near the fans and walls. The meshing characters is shown in Table 5.1.

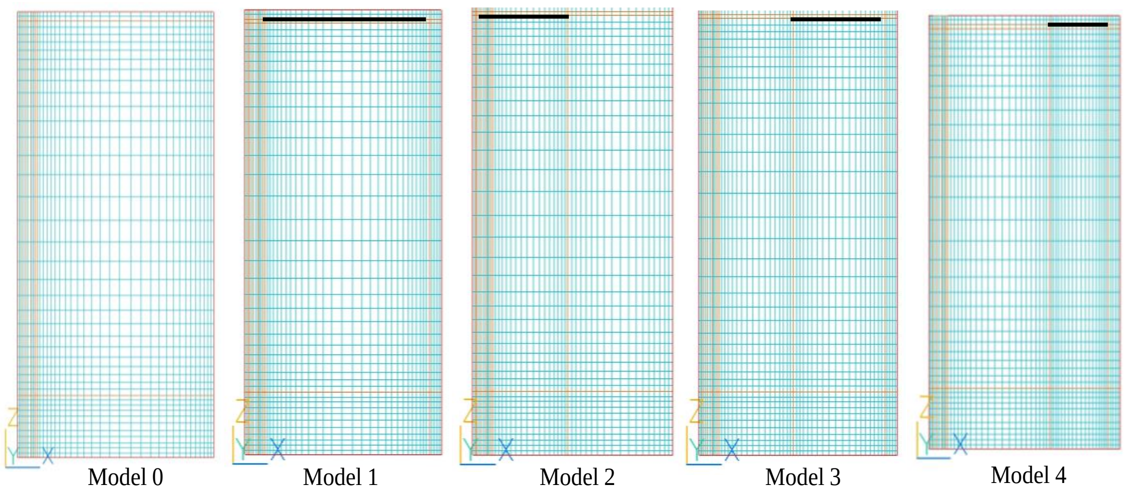

Figure 5.1 Meshing of computational domain chamber without plant.

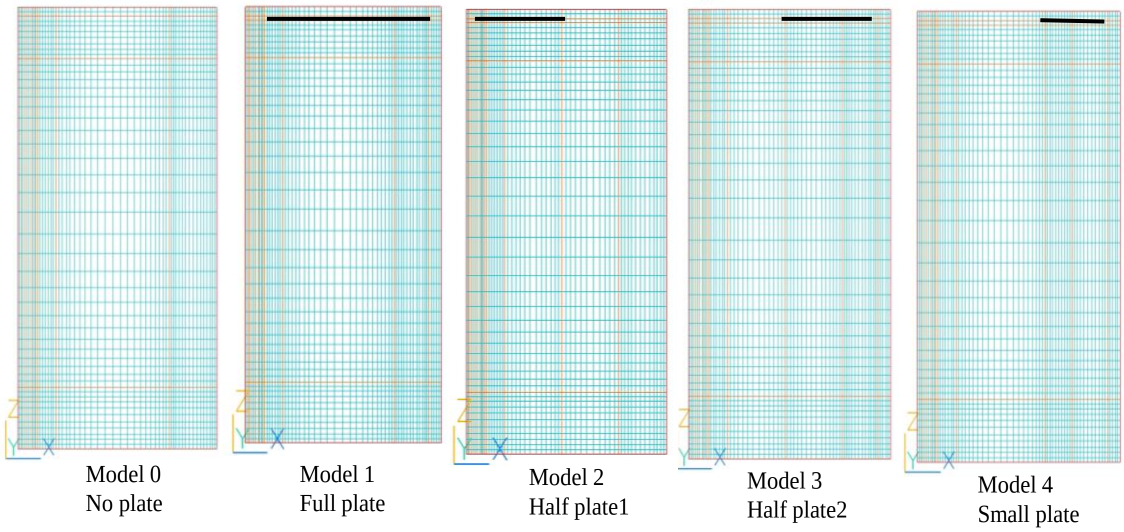

Figure 5.2 Meshing of computational domain chamber with plant.

Table 5.1 Meshing characteristics of computational domain for chamber 1.

Mesh	**Fans position**				
	Chamber without plant				
	No plate	Full plate	Half plate1	Half plate2	Small plate
Number	110,880	127,710	132,526	147,576	158,928
Mesh	**Chamber with plant**				
	No plate	Full plate	Half plate1	Half plate2	Small plate
Number	185,472	198,240	187,440	218,112	218,112

5.2.2 Initial and boundary conditions

The Chen-Kim turbulence model was used in simulation case of different size of plate in chamber without and with plant. The boundary condition is shown in Table 5.2.

Table 5.2 Boundary conditions for model validation chamber 1.

Parameter	**Conditions**
Air volume rate of the fans	0.009 $m^3\ s^{-1}$
Bottom opening	Pressured fixed
Wall	No slip

5.2.3 Simulation cases

5.2.3.1 Transparent plate arrangement in chamber with and without plant

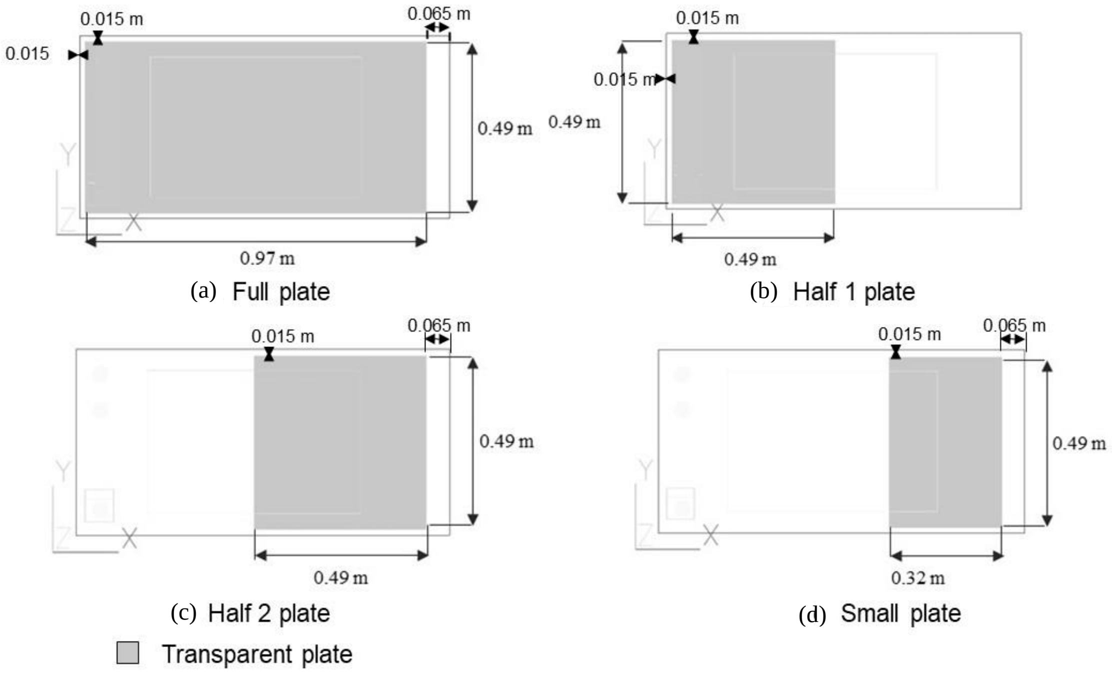

Figure 5.3 Model simulations with different plate size (a) full plate, (b) half left side, (c) half right side, (d) small plate (Top – view).

Figure 5.3 illustrated the size and position of transparent plates. Various sizes of transparent plates installed at 0.065 m just below the ceiling of the chamber to uniform the airflow was introduced and then evaluated the effect of the transparent plates on the uniformity of airflow in the chamber. The transparent plates were assumed to be smooth and had a length of 0.49 m with different widths: 0.97 m (full plate, Fig. 5.3a), 0.49 m (half plate, Fig. 5.3b, c), and 0.32 m (small plate, Fig. 5.3d).

Five simulation cases were assumed and compared in this study: Model 0 – control case (no plate); Model 1 – full plate; Model 2 – plate covering the left half; Model 3 –plate covering the right half; Model 4 – small plate covering the right third (Figure 5.3), where the transparent plate in a vertical position (same as in a front-view position as shown in Figure 5.4). The numbers of mesh in the computational domain for each case model 0 – model 4 had around 180-220 thousand cells. Finer meshes were applied near the fans and walls. The ceiling of the chamber was assumed to be smooth.

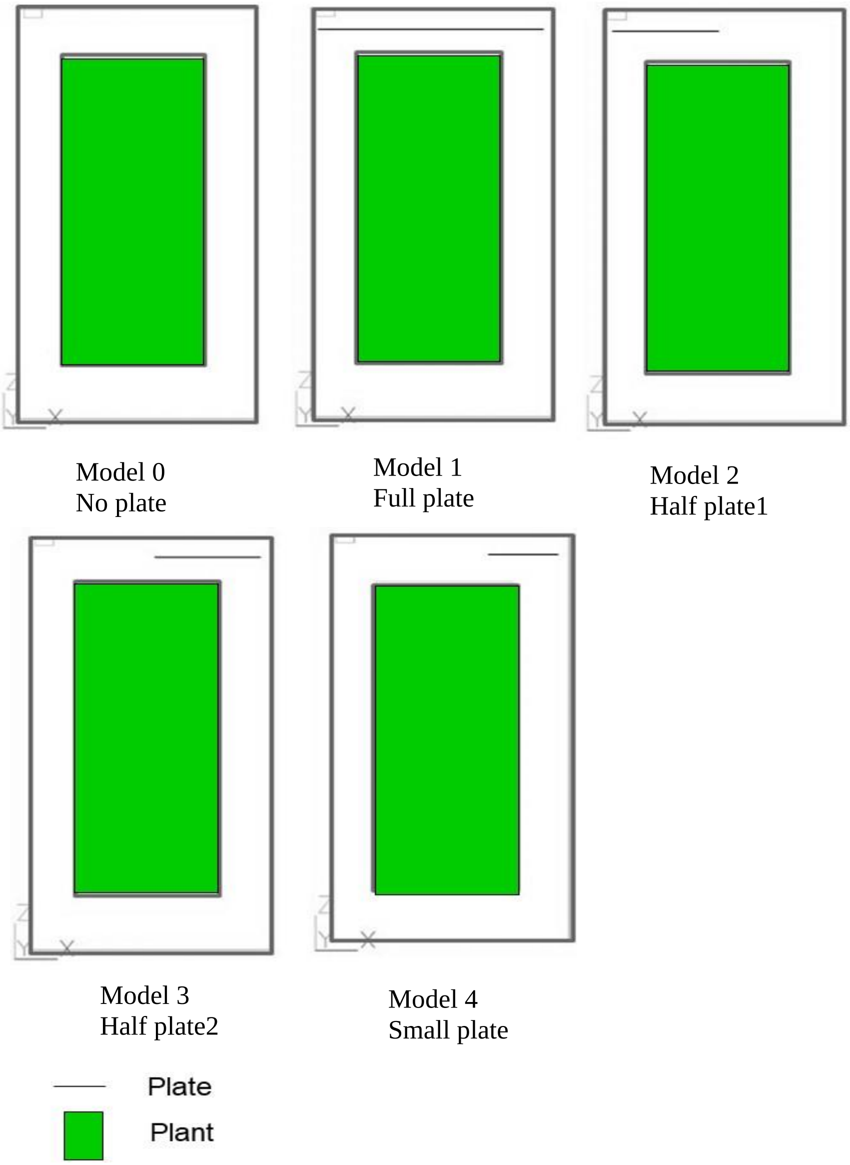

Figure 5.4 Model for airflow uniformity system: Model 0: control case (no plate), Model 1: full plate, Model 2: half plate placed near the fans, Model 3: half plate placed opposite with the fans, Model 4: small plate placed opposite with the fans.

5.3 Results and discussions

5.3.1 Chamber without plant

Figure 5.5 shows the distribution patterns of x-velocity (horizontal velocity) at different size transparent plate in chamber without plant. In the Model 0, Model 3, and Model 4, the average of air velocity was 0.01 m s^{-1}, while in Model 1 and Model 2 was 0.02 m s^{-1} inside the chamber. As shown in Table 5.3, in Model 0, the variability of air velocity has lowest value, 45.74 % at height of 1.9 m from chamber's bottom which showed a more even airflow distribution in position near to the fans. The variability of air velocity was 55.59 % at height of 1.08 in the middle cross section of the chamber. In the position near to the bottom opening, the variability of air velocity has the largest value, 74.80%.

In Model 1, the variability of air velocity has lowest value, 46.19 % at height of 1.9 m from chamber’s bottom which showed a more even airflow distribution at near to the fans. In the middle cross section of the chamber, the variability of air velocity was 51.81 %. The highest variability of air velocity was 76.13 % at height of 0.27 m from the chamber’s bottom (near to the bottom opening).

In Model 2, the variability of air velocity has lowest value, 16.97 % at height of 1.9 m from chamber’s bottom which showed a more even airflow distribution at near to the fans. The variability of air velocity was 71.97 % at height of 1.08 in the middle cross section of the chamber. The highest variability of air velocity was 74.04 % at height of 0.27 m from the chamber’s bottom (near to the bottom opening).

In Model 3, the variability of air velocity has lowest value, 36.71 % at height of 1.08 m in the middle cross section of the chamber. The variability of air velocity was 49.66 % at height of 1.9 m from chamber’s bottom at near to the fans. The highest variability of air velocity was 73.23 % at height of 0.27 m from the chamber’s bottom (near to the bottom opening).

In Model 4, the variability of air velocity has lowest value, 36.74 % at height of 1.08 m in the middle cross section of the chamber. The variability of air velocity was 46.90 % at height of 1.9 m from chamber’s bottom at near to the fans. The highest variability of air velocity was 73.62 % at height of 0.27 m from the chamber’s bottom (near to the bottom opening).

Table 5.3 The variability of air velocity (x-velocity) in different height for each model of different size of transparent plate.

Parameter	Model Transparent Plate								
	Default (No plate)			Full plate			Half plate1		
	Height from chamber bottom			Height from chamber bottom			Height from chamber bottom		
	1.9 m	1.08 m	0.27 m	1.9 m	1.08 m	0.27 m	1.9 m	1.08 m	0.27 m
SD ($m\ s^{-1}$)	0.017	0.001	0.004	0.004	0.000	0.003	0.003	0.001	0.003
Average ($m\ s^{-1}$)	0.036	0.003	0.005	0.010	0.001	0.004	0.016	0.001	0.004
CV (%)	45.74	55.59	74.80	46.01	51.81	76.13	16.97	71.97	74.04

Parameter	Model Transparent Plate					
	Half plate2			Small plate		
	Height from chamber bottom			Height from chamber bottom		
	1.9 m	1.08 m	0.27 m	1.9 m	1.08 m	0.27 m
SD ($m\ s^{-1}$)	0.018	0.001	0.003	0.017	0.001	0.003
Average ($m\ s^{-1}$)	0.036	0.003	0.004	0.036	0.003	0.004
CV (%)	49.66	36.71	73.23	46.90	36.74	73.62

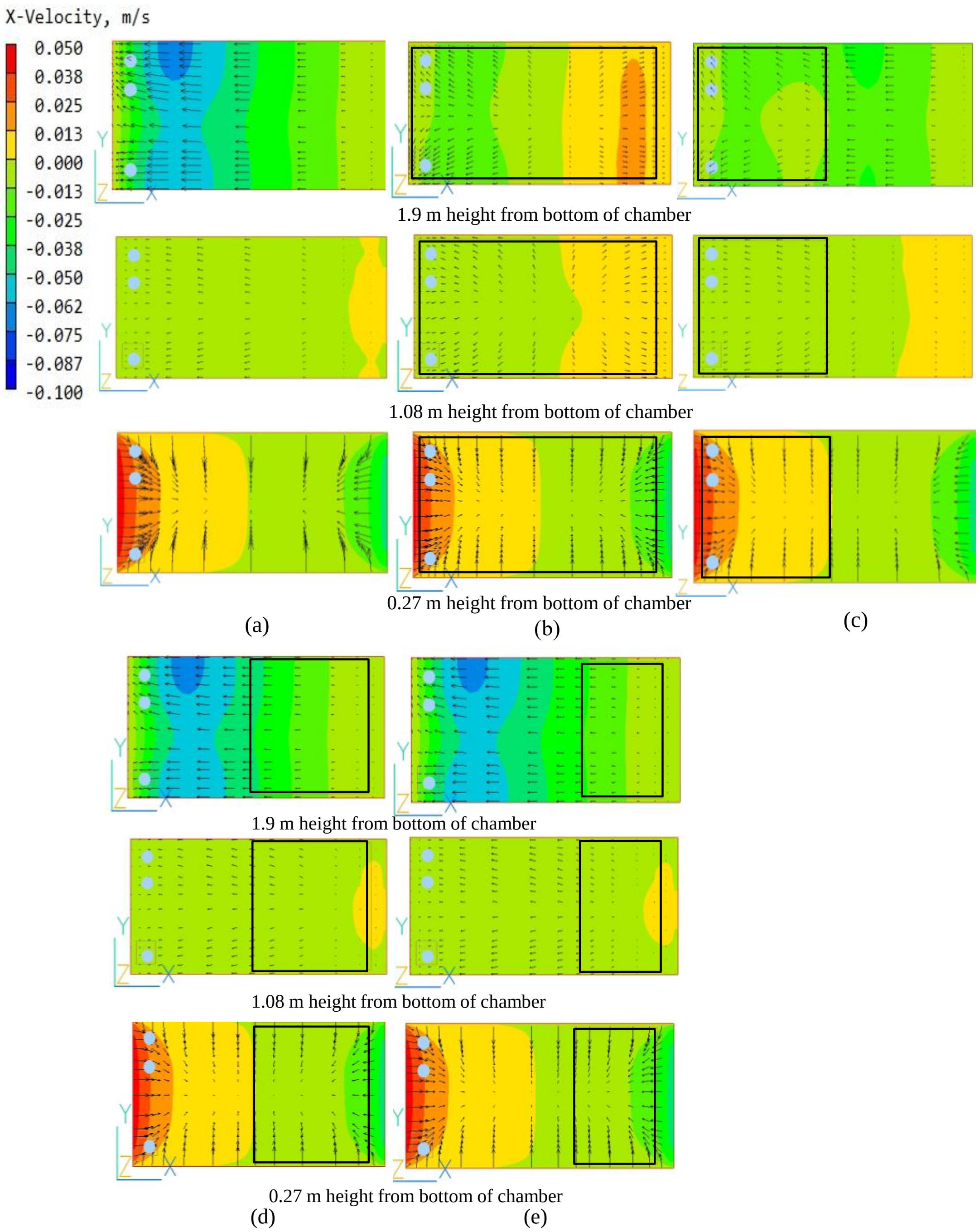

Figure 5.5 Airflow distribution simulation of x-velocity of the chamber without plant: (a) default (Model 0), (b) full plate (Model 1), (c) half plate1 (Model 2), (d) half plate2 (Model 3), and (c) small plate (Model 4).

Figure 5.6 showed the airflow distributions of z-velocity in vertical cross-sections of for each simulation case mentioned previously. Note that vertical cross-sections (Figure 5.6) are at the center of the chamber and positive and negative values in the legend indicate airflow velocity upward and downward directions, respectively. Table 5.4 shows no significant differences in average air velocity appeared in each model chamber (difference of air velocity is less than 0.1 m s^{-1} in absolute value).

The high variability of air velocity was found in Model 2 and Model 3. The highest variability of air velocity was observed in Model 2 with coefficients of variation of 41.27 %, following with Model 3, Model 4, Model 0, and Model 1 have coefficients of variation of 36.57 % and 35.97 %, 34.99 %, and 29.48 %, respectively. As shown in Table 5.4, a better vertical airflow distribution was observed in Model 1 with coefficients of variation of 29.48 %. Even though for every model showed not significant different for vertical airflow distribution in the middle of the chamber.

Similar results can be also seen in the vertical cross-sections shown in Figure 5.6, that is, the uneven distribution of airflow around the upper right of the chamber disappeared in Model 1, while Model 2, Model 3, and Model 4 show that the transparent plate does not contribute to even the airflow.

On the other hand, since the variability of air velocities in the middle of the chamber is a similar level in all cases (33.08 %, 33.35 %, 41.61 %, 34.98 %, and 34.13 % for Models 0 to 4), the transparent plate installed just below the ceiling of the chamber induces no significant improvement contribution to vertical airflow distribution of the center of the plant canopy (Table 5.5).

Table 5.4 Summary the variability of air velocity (z-velocity) for each model of different size of transparent plate without plant.

Parameter	Model Transparent Plate				
	Default	Full plate	Half plate1	Half plate2	Small plate
SD (m s^{-1})	0.016	0.014	0.021	0.017	0.017
Average (m s^{-1})	0.047	0.047	0.051	0.047	0.047
CV (%)	34.99	29.48	41.27	36.57	35.97

Table 5.5 The variability of air velocity (z-velocity) for each model transparent plate in the middle of chamber without plant.

Parameter	Model Transparent Plate				
	Default	Full plate	Half plate1	Half plate2	Small plate
	In the middle of chamber				
SD (m s^{-1})	0.017	0.017	0.023	0.018	0.017
Average (m s^{-1})	0.051	0.050	0.054	0.050	0.051
CV (%)	33.08	33.35	41.61	34.98	34.13

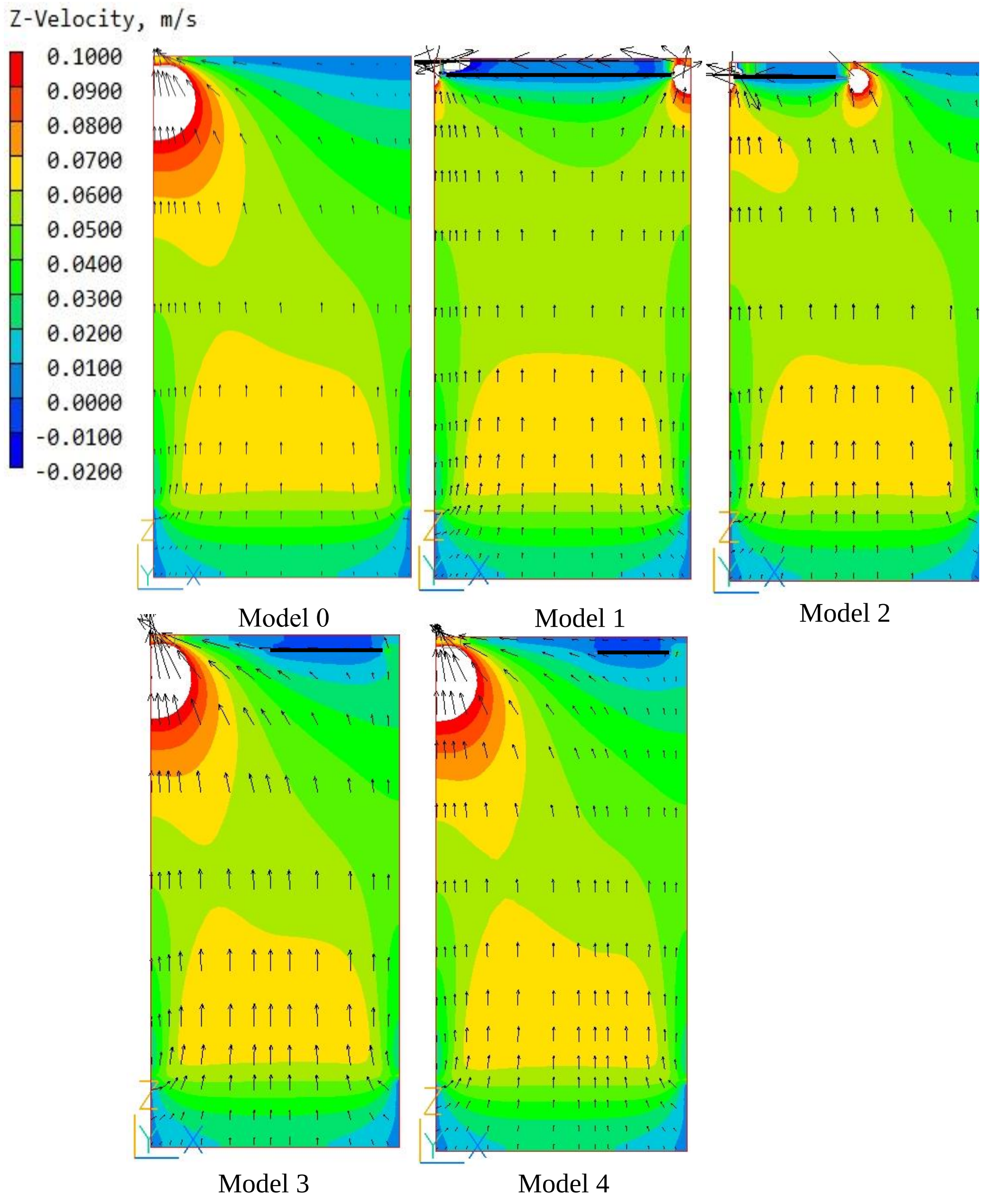

Figure 5.6 Airflow distribution in different size of transparent plates (Front-view).

5.3.2 Chamber with plant

Figure 5.7 showed the distribution patterns of x-velocity (horizontal velocity) at different size transparent plate in chamber without plant. All simulation Model have average of air velocity of 0.01 m s^{-1}, except Model 1 was 0.02 m s^{-1} inside the chamber.

As shown in Table 5.6, in Model 0, the variability of air velocity has lowest value, 37.69 % at height of 1.08 in the middle cross section of the chamber showed a more even airflow distribution in position near to the fans. The variability of air velocity was 44.26 % at height of 1.9 m from chamber's bottom (at the top surface of the plant). In the position near to the bottom opening, the variability of air velocity has the largest value, 74.30%.

In Model 1, the variability of air velocity has lowest value, 45.67 % at height of 1.9 m from chamber's bottom which showed a more even airflow distribution at near to the fans. In the middle cross section of the chamber, the variability of air velocity was 46.85 %. The highest variability of air velocity was 76.85 % at height of 0.27 m from the chamber's bottom (near to the bottom opening).

In Model 2, the variability of air velocity has lowest value, 19.29 % at height of 1.9 m from chamber's bottom which showed a more even airflow distribution at near to the fans. The variability of air velocity was 75.95 % at height of 1.08 in the middle cross section of the chamber. The highest variability of air velocity was 75.56 % at height of 0.27 m from the chamber's bottom (near to the bottom opening).

In Model 3, the variability of air velocity has lowest value, 37.64 % at height of 1.08 m in the middle cross section of the chamber. The variability of air velocity was 46.90 % at height of 1.9 m from chamber's bottom at near to the fans. The highest variability of air velocity was 74.06 % at height of 0.27 m from the chamber's bottom (near to the bottom opening).

In Model 4, the variability of air velocity has lowest value, 40.15 % at height of 1.08 m in the middle cross section of the chamber. The variability of air velocity was 44.09 % at height of 1.9 m from chamber's bottom at near to the fans. The highest variability of air velocity was 74.53 % at height of 0.27 m from the chamber's bottom (near to the bottom opening).

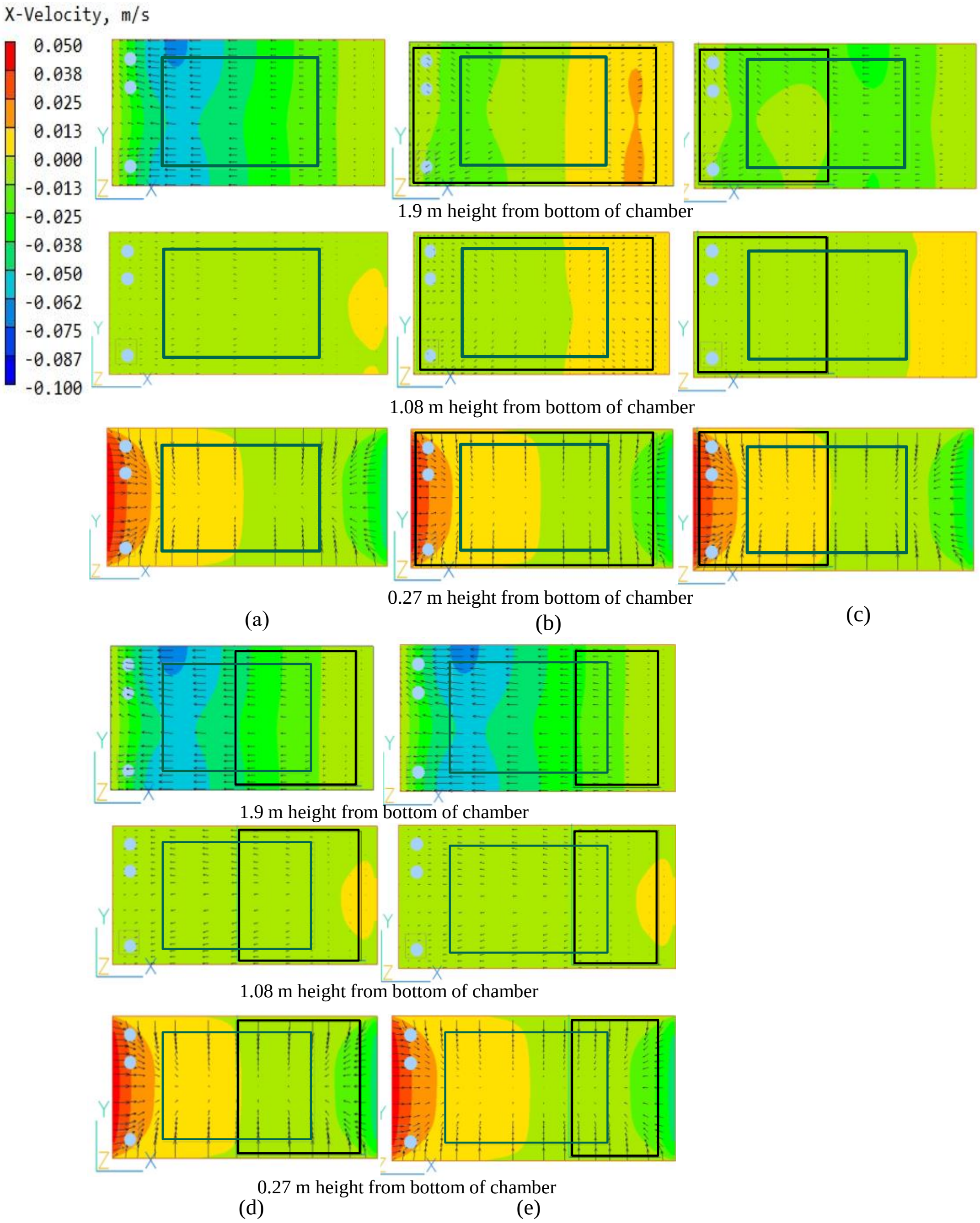

Figure 5.7 Airflow distribution simulation of x-velocity of the chamber with plant: (a) default (Model 0), (b) full plate (Model 1), (c) half plate1 (Model 2), (d) half plate2 (Model 3), and (e) small plate (Model 4).

Table 5.6 The variability of air velocity (x-velocity) in different height for each.

Parameter	Model Transparent Plate								
	Default (No Plate) Height from chamber bottom			Full plate Height from chamber bottom			Half plate1 Height from chamber bottom		
	1.9 m	1.08 m	0.27 m	1.9 m	1.08 m	0.27 m	1.9 m	1.08 m	0.27 m
SD ($m\ s^{-1}$)	0.016	0.001	0.003	0.004	0.000	0.003	0.003	0.001	0.003
Average ($m\ s^{-1}$)	0.036	0.003	0.004	0.009	0.001	0.004	0.016	0.001	0.004
CV (%)	44.26	37.69	74.30	45.67	46.85	76.85	19.29	75.95	75.56

Parameter	Model Transparent Plate					
	Half plate2 Height from chamber bottom			Small plate Height from chamber bottom		
	1.9 m	1.08 m	0.27 m	1.9 m	1.08 m	0.27 m
SD ($m\ s^{-1}$)	0.017	0.001	0.003	0.016	0.001	0.003
Average ($m\ s^{-1}$)	0.036	0.003	0.004	0.036	0.003	0.004
CV (%)	46.90	37.64	74.06	44.09	40.15	74.53

Figures 5.8 vertical cross-sections of the distributions of air velocity for each simulation case. As can be seen in figures, no significant differences in average air velocity in each chamber (difference of air velocity is less than 0.1 m s^{-1} in absolute value).

On the other hand, the effect of the transparent plate on airflow distribution especially in the upper part of the chamber was significant other than Model 3 and 4. Focusing on the airflow distribution in the plant canopy (illustrated as a rectangular in the chamber), Model 1 and 2 (the full-plate and the plate covering the left half) may be able to even airflow distribution than the other cases. Figure 5.8 shows the uneven distribution of airflow around the upper right of the plant canopy disappeared in Model 1 and 2, while Model 3 and Model 4 show that the transparent plate does not contribute to even the airflow in the plant canopy.

The quantitative evaluation of these results using CV is shown in Table 5.7 is that 10.8% for the middle of the plant and 50.9% for the top surface of the plant in Model 0, while 11.0% and 9.1% in Model 1. The large difference in CV between Model 0 (50.9% for no plate) and Model 1 (9.1% for the full plate) may be due to the suppression of the airflow turbulence in Model 1. This result suggests that a transparent plate may be effective to even the airflow at the top of the plant canopy. This effect also clearly can be seen in the half plate cases (Model 2 and Model 3 in Table 3) that the value of CV is 12.2% and 45.5% for the top surface of the plant canopy.

In Model 3 (half plate on the right side) and Model 4 (one-third of the size of the full plate on the right side), the position of the plate has almost no effect, the CV of each model is similar to 50.9% (Model 0), 45.5% (Model 3) and 44.0% (Model 4). On the other hand, since the variability of air velocity in the middle of the plant canopy is a similar level in all cases (10.8%, 11.2%, 8.1%, 13.3%, and 13.4% for Models 1 to 4), the transparent plate installed just below the ceiling of the chamber induces no significant improvement contribution to uniformity of the center of the plant canopy.

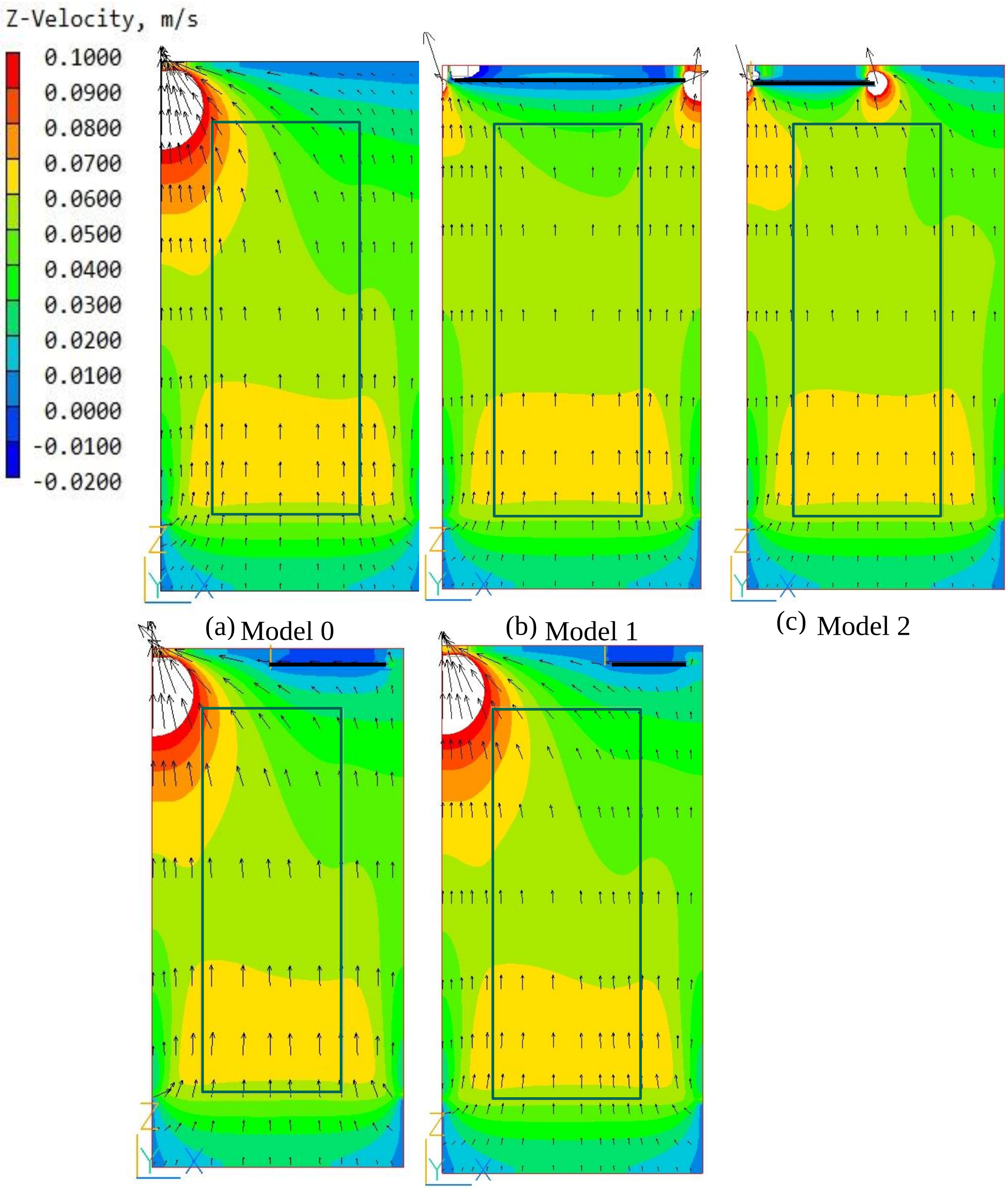

Figure 5.8 Vertical Airflow distribution (z-velocity) with transparent plates (Front-view).

Table 5.7 Summary the variability of air velocity (z-velocity) for each model of different size of transparent plate with plant.

Parameter	Default		Full plate		Half plate 1		Half plate 2		Small plate	
	In the middle of plant	Top surface of Plant	In the middle of plant	Top surface of Plant	In the middle of plant	Top surface of Plant	In the middle of plant	Top surface of Plant	In the middle of plant	Top surface of Plant
SD (m s^{-1})	0.01	0.02	0.01	0.00	0.00	0.01	0.01	0.02	0.01	0.02
Average (m s^{-1})	0.08	0.05	0.06	0.04	0.06	0.05	0.06	0.04	0.06	0.04
CV	10.8	50.9	11.2	9.1	8.1	12.2	13.3	45.5	13.4	44.0

5.4 Conclusions

Case of chamber without plant, according to horizontal velocity (x-velocity) results, the effect of the transparent plate Model 2 (half plate1) was significant to even the distribution of airflow at the top of part of the chamber (1.9 m from chamber's bottom). While model 3 and Model 4 showed a more evenly airflow distribution in the middle of the chamber. Whereas the others simulation results of variability of air velocity showed unsignificant different compared to Model 0 (default).

On the other hand, since the variability of air velocities in the middle of the chamber is a similar level in all cases (33.1 %, 33.4 %, 41.6 %, 35.0 %, and 34.1 % for Models 0 to 4), the transparent plate installed just below the ceiling of the chamber induces no significant improvement to vertical airflow distribution of the center of the plant canopy.

In the case of chamber with plant, according to horizontal velocity (x-velocity) results, the effect of the transparent plate Model 2 (half plate1) was significant to even the distribution of airflow at the top of part of the chamber (1.9 m from chamber's bottom). Whereas the others simulation results of variability of air velocity showed unsignificant different compared to Model 0 (default).

On the other hand, since the variability of air velocity in the middle of the plant canopy is a similar level in all cases (10.8%, 11.2%, 8.1%, 13.3%, and 13.4% for Models 1 to 4), the transparent plate installed just below the ceiling of the chamber induces no significant improvement to uniformity of the center of the plant canopy.

Chapter 6 Simulation Cases of CO_2 Distribution on Various Environmental Conditions in Greenhouse

6.1 Description

A few simulations of greenhouse were conducted to know the effect of various environmental conditions to the CO_2 distribution inside of the greenhouse. The variability of CO_2 concentration inside the chamber and the plant canopy were analyzed with a coefficient of variation (CV), which is the ratio of the standard deviation to the mean value. The uniformity of CO_2 distribution inside the greenhouse for scenario cases open and closed side ventilation, the weather (rainy and sunny days), and different outside wind speed (0 m s^{-1}, 3 m s^{-1}, and 6 m s^{-1}) were analyzed with a coefficient of variation (CV). The 7,070 points of CO_2 concentration were taken to measure the uniformity inside the greenhouse and 8,484 points of CO_2 concentration for plants.

6.2 Model Settings

6.2.1 Computational domain

The computational model greenhouse for all the cases has dimensions length of 12 m, width of 10 m, and height of 6 m. The greenhouse model has four circulating fans, four shelves of cultivating bed tomato, and four CO_2 perforated tubes on each shelf. Accordingly, standard $k - \varepsilon$ turbulence model was applied in the greenhouse simulation. The meshings of the modeled greenhouse in the case of open and closed side ventilation are shown in Figure 6.1. Those of greenhouse in the case of sunny and rainy day are shown in Figure 6.2, and greenhouse in different outside wind speeds at the side ventilation are shown in Figure 6.3. The meshing characters are shown in Table 6.1.

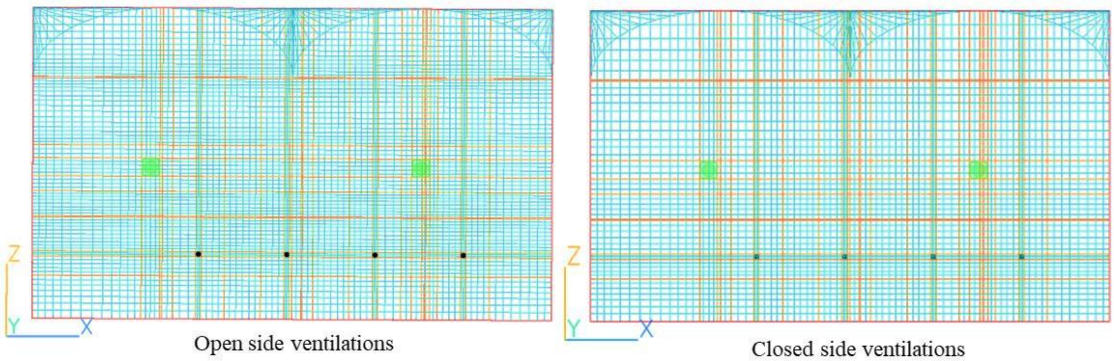

Figure 6.1 Meshing of computational domain greenhouse in the case of open and closed side ventilation.

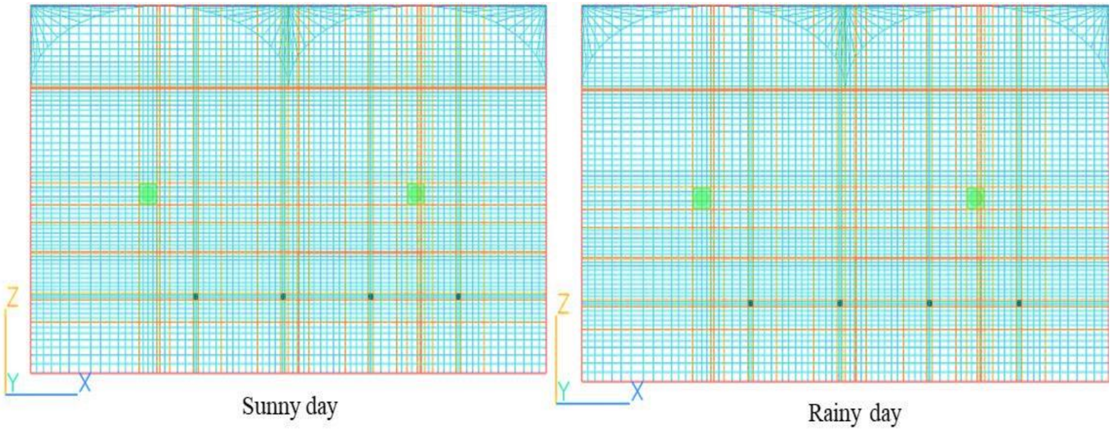

Figure 6.2 Meshing of computational domain greenhouse in sunny and rainy day.`

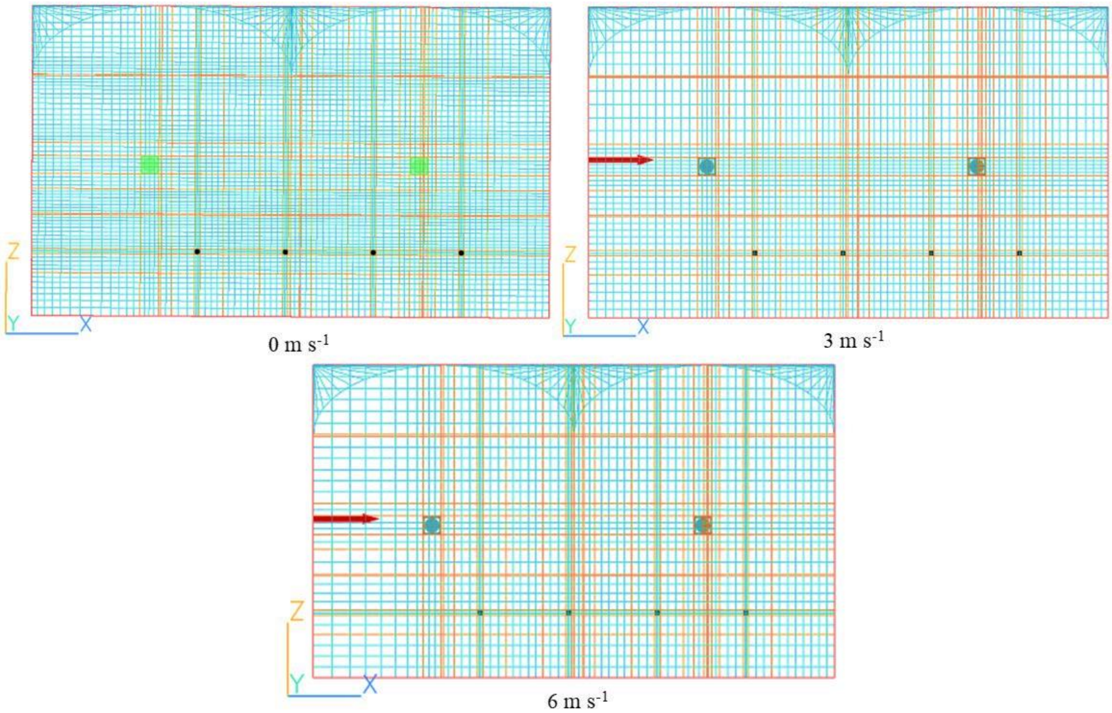

Figure 6.3 Meshing of computational domain greenhouse in different outside wind speed.

Table 6.1 Meshing characteristics of computational domain for greenhouse simulation cases.

Mesh	**Greenhouse simulation cases**					
	Side ventilation				**Weather**	
	Open			Closed	Sunny	Rainy
	0 m s^{-1}	3 m s^{-1}	6 m s^{-1}			
Number	759,066	415,096	313,760	502,758	749,208	749,208

6.2.2 Initial and boundary conditions

The characteristics of the numerical procedure and input values for greenhouse simulation cases in Table 3.9, except the incident light flux PAR for rainy day was 95 W m^{-2}.

6.2.3 Simulation cases

6.2.3.1 Effect of side ventilation condition (open and close)

Simulation predicts the effect of side ventilation to the CO_2 distribution inside of the greenhouse in condition open and close (Figure 6.4).

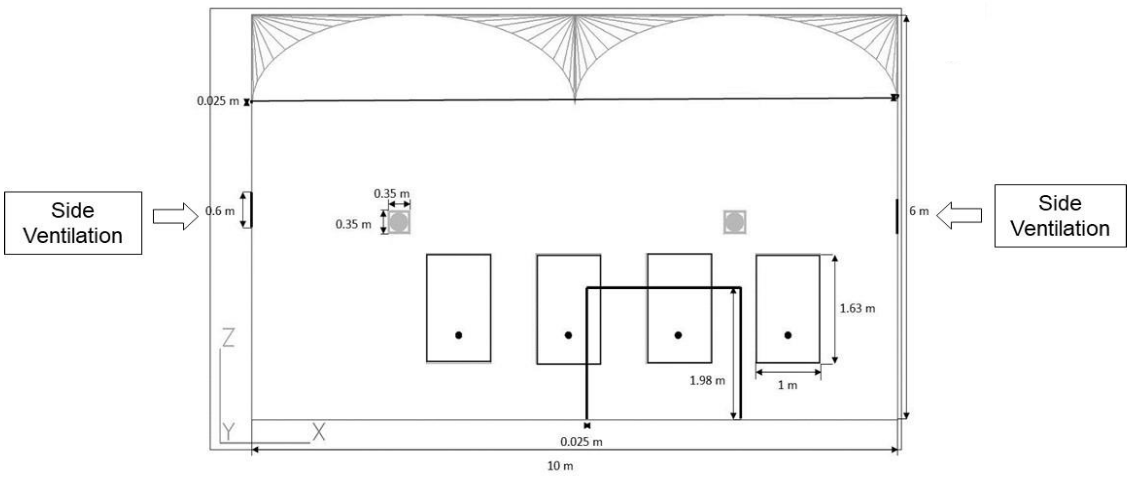

Figure 6.4 Imaging of greenhouse simulation for effect of side ventilation (open and close).

6.2.3.2 Effect of different weather (sunny and rainy day)

Simulation predicts the effect of different weather to the CO_2 distribution inside of the greenhouse in condition sunny and rainy day (Figure 6.5).

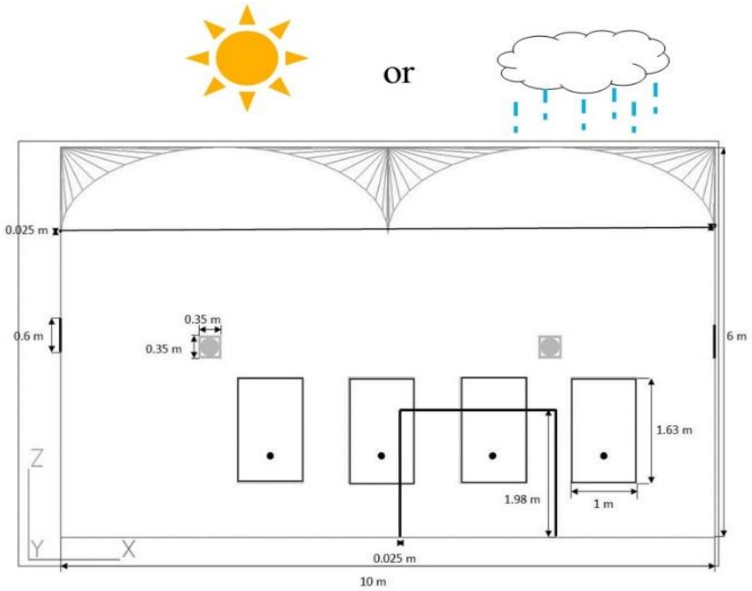

Figure 6.5 Imaging of greenhouse simulation for effect different weather (sunny and rainy day).

6.2.3.3 Effect of different outside wind speed at the side ventilation (0 m s^{-1}, 3 m s^{-1}, and 6 m s^{-1})

Simulation predicts the effect of different outside wind speed to the CO_2 distribution inside of the greenhouse in condition open and close (Figure 6.6).

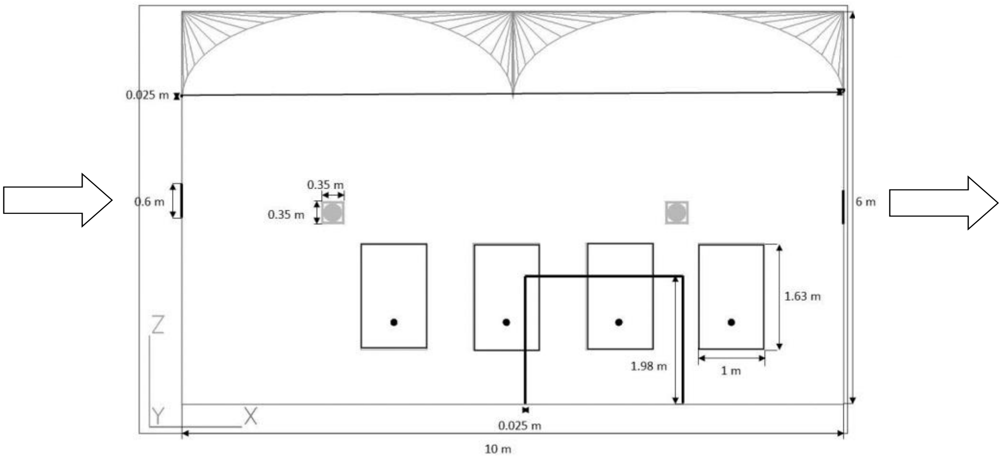

Figure 6.6 Imaging of greenhouse simulation for effect of different outside air velocity at the side ventilation (0, 3 and 6 m s^{-1}).

6.3 Results and discussions

6.3.1 Carbon dioxide distribution with open and closed side ventilation inside the greenhouse

Figure 6.7 shows the simulation of CO_2 distribution inside the greenhouse when 1160 ppm CO_2 concentration was supplied through perforated tubes inside the plants. The appearance of CO_2 emissions from the perforated tube was confirmed with the degradation colors inside of the plants. CO_2 distribution in case open and closed (Figure 6.7) side vents were showed a slight difference in CO_2 concentration. When the sidewall was opened (ventilated), the inflow wind from outside the greenhouse was continually updated to match the current wind velocity in each mesh (PHOENICS user manual). The CO_2 concentration outside of the greenhouse (400 ppm) was lower than the initial CO_2 concentration inside the greenhouse (450 ppm), which may cause the CO_2 concentration near the ventilated wall to be lower. Furthermore, the position of the plants in the greenhouse was asymmetry (tend to the right side).

The effects of open side vents on CO_2 distribution were slightly significant, especially near the wall. The case of closed side vents showed slightly more even CO_2 inside the greenhouse than the case of open side vents. Although the side vents are closed, air circulators supported moving large volumes of air to provide airflow distribution. The quantitative evaluation of these results using CV shown in Table 6.2 was 18.2% for the open and 15.6% for the closed side vents case for the whole greenhouse. However, focusing on the even distribution of CO_2 inside the plant, open (8.8%) and closed (8.7%) side vents induced almost no significant improvement at the plant canopy: because no initial wind velocity was considered at both side vents in our case. Therefore, virtually no air exchange occurred between outside and inside the greenhouse.

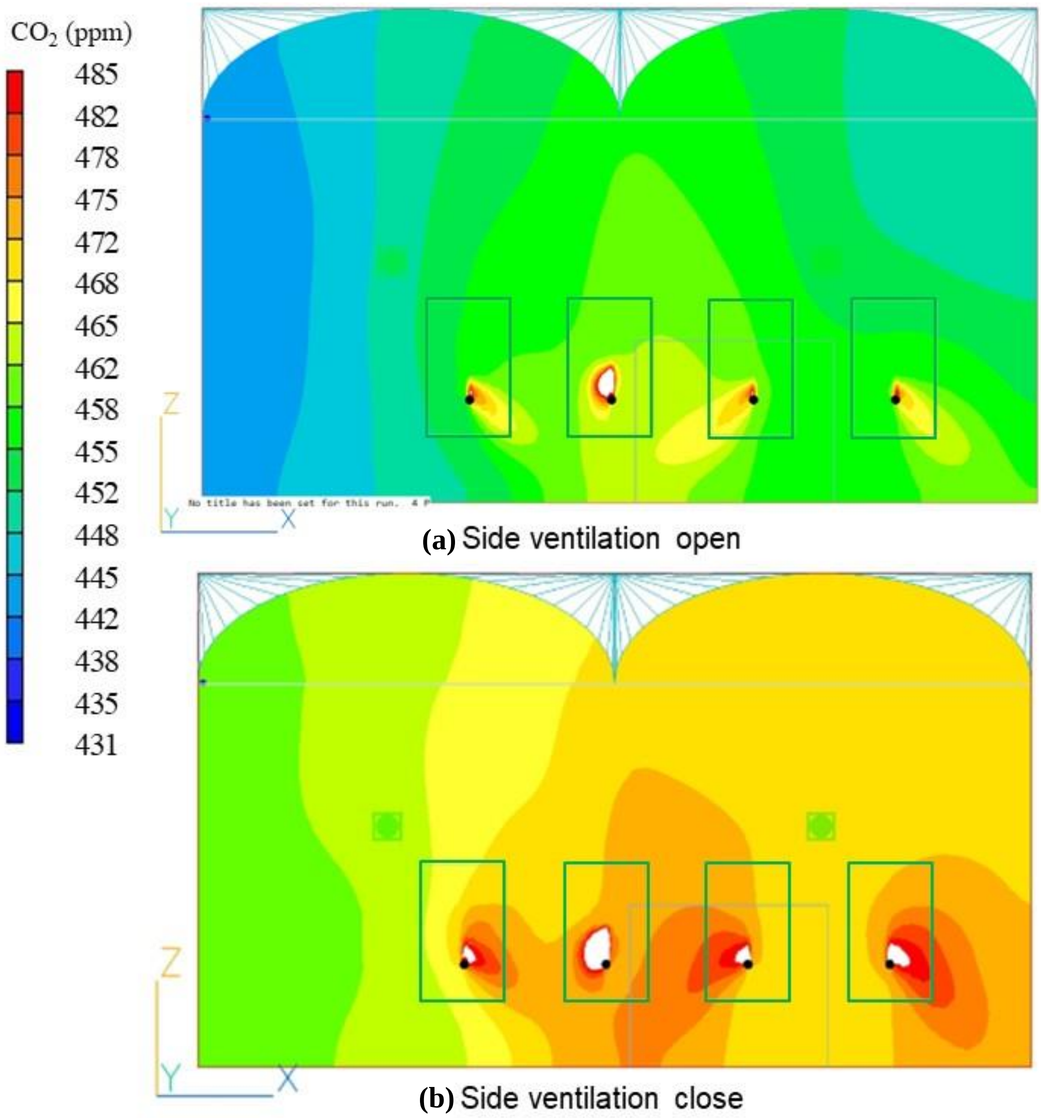

Figure 6.7 Carbon dioxide distribution inside of the greenhouse: (a) the side ventilations open and (b) closed (image taken at cross-section section 6 m from south wall).

Table 6.2 Coefficient of variations of CO_2 concentration in the case of open and closed side ventilation.

Parameter	**Greenhouse**		**Plants**	
	Side Vent		Side Vent	
	Open	Closed	Open	Closed
SD (ppm)	80	71	41	41
Mean (ppm)	438	457	464	476
CV (%)	18.2	15.6	8.8	8.7

6.3.2 Carbon dioxide distribution with sunny and rainy day inside the greenhouse

Simulations under treatment of 1000 ppm of CO_2 concentration, that had been done in the previous study (Nederhoof and Vegter, 1994b; Kim et al., 2015) were conducted on a rainy day condition with PAR of 95 W m^{-2} (Romdhonah et al., 2021) and sunny day condition with PAR of 355 W m^{-2} (based on NEDO solar radiation database). CO_2 distribution in case sunny day and rainy day were showed a slight difference in CO_2 concentration (Figure 6.8). The effects of solar radiation on CO_2 distribution were slightly significant. The case of rainy day showed a slightly more even of CO_2 distribution inside the greenhouse than the case of sunny day. The quantitative evaluation of these results using CV shown in Table 6.3 was 18.1% for the sunny day and 15.6% for the rainy day case for the whole greenhouse. However, focusing on the variability of CO_2 concentration inside the plant, sunny day (8.1%) and rainy day (8.7%) induced almost no significant contribution to even the variability of CO_2 concentration in the plant canopy.

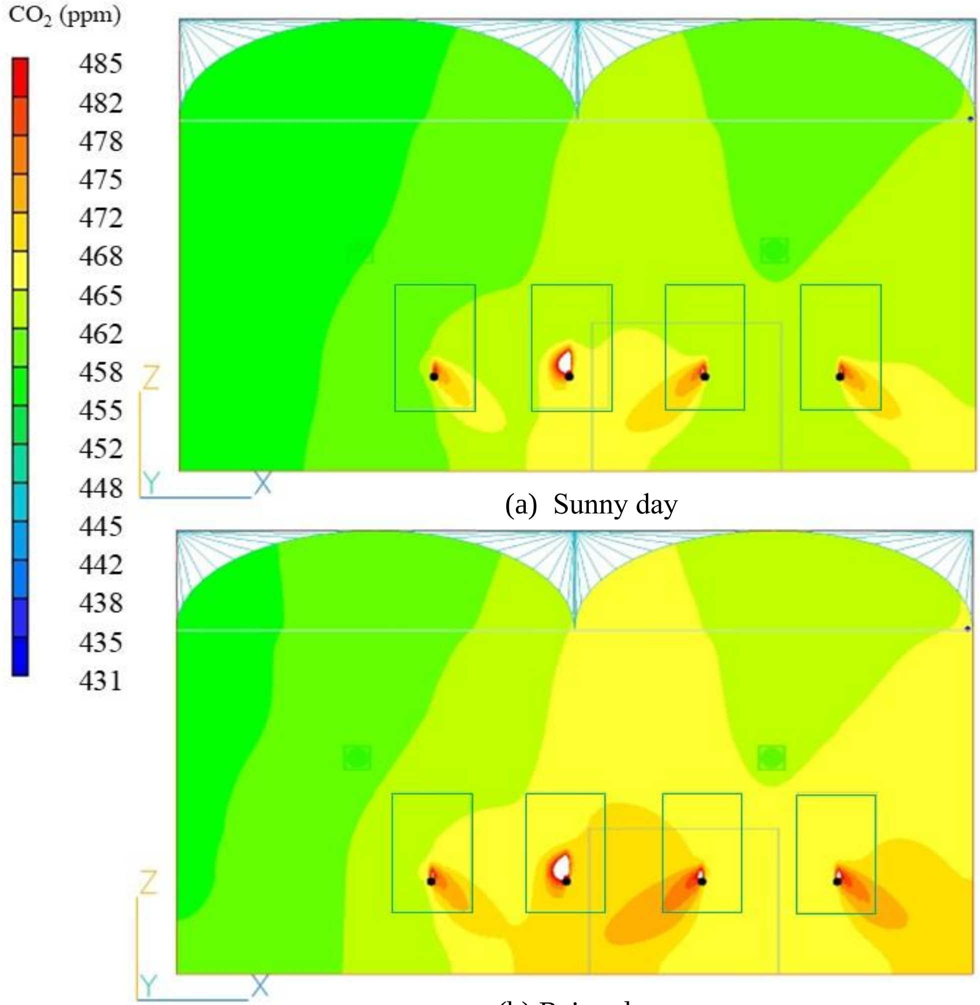

Figure 6.8 Carbon dioxide distribution inside of the greenhouse in the case of (a) the sunny and (b) rainy days.

Table 6.3 Coefficient of variations of CO_2 concentration in the case of sunny and rainy days.

Parameter	Greenhouse		Plants	
	Weather			
	Sunny	Rainy	Sunny	Rainy
SD (ppm)	81	71	38	41
Average (ppm	446	457	467	476
CV (%)	18.1	15.6	8.1	8.7

Figure 6.9 shows the net photosynthesis estimations of the greenhouse model under treatment of 1000 ppm of CO_2 enrichment on a rainy day and sunny day. The simulation results on a rainy day and sunny day determined the average of net photosynthesis were 3.82 and 9.69 µmol m^{-3} s^{-1}, respectively. The value of net photosynthesis results seemed reasonable according to the study of Nederhoof and Vegter (1994b) and Xu et al. (2014).

The PAR possibly compensated the CO_2 absorption through the photosynthesis process to be low at low light (rainy day) and was higher at high light (sunny day). Nevertheless, the different canopy layers such as the top layer (64%), middle layer (28%), and bottom layer (8%) were not assigned to the net photosynthesis as mentioned in the study by Reichrath et al. (2000) because in this simulation the dense of leaves were assumed to be homogenous for the whole plant. Thus, the net photosynthesis results were almost constant for the entire plant. However, according to the simulation results, this model may be appropriate to estimate the net photosynthesis average.

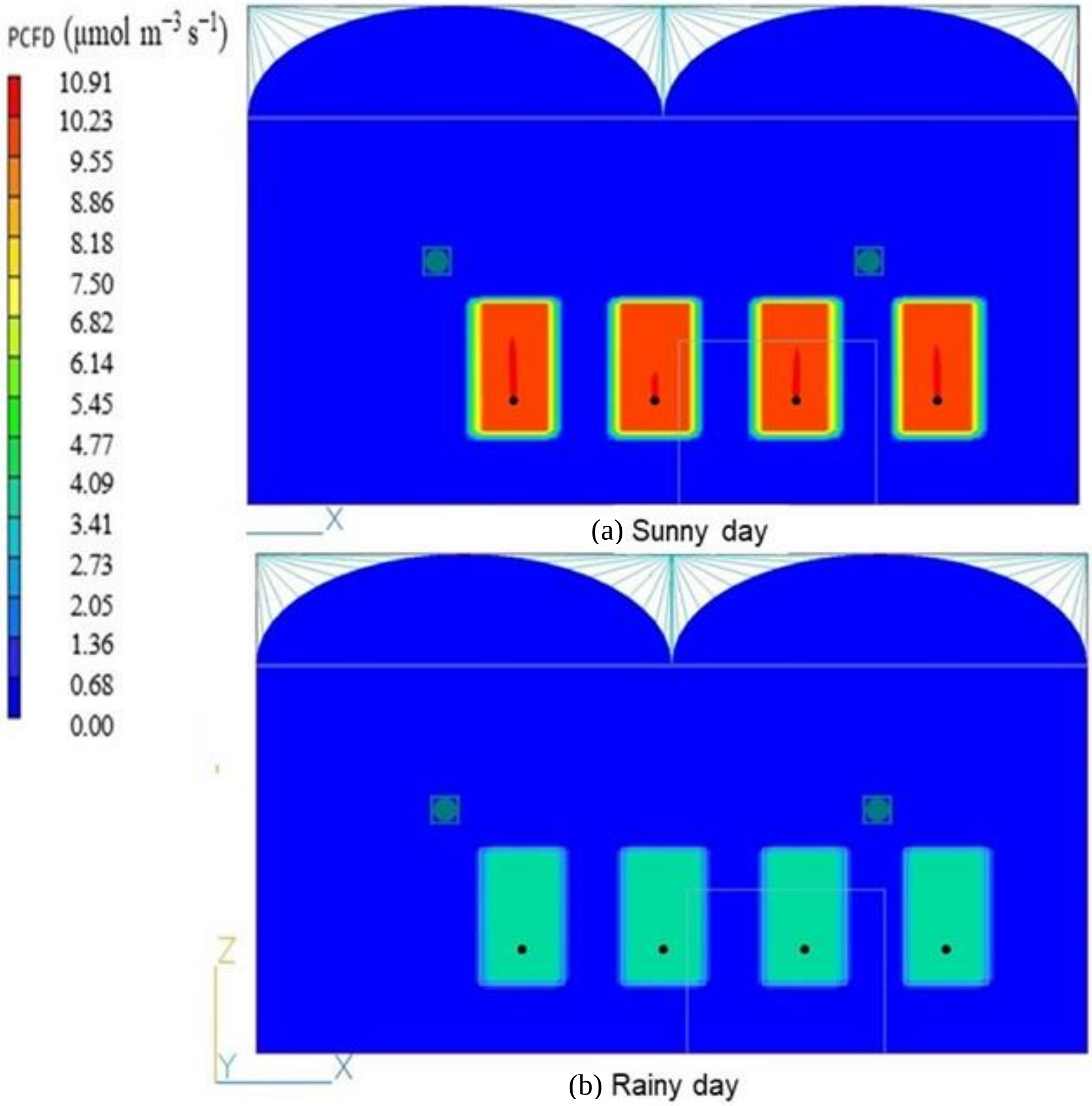

Figure 6.9 Net photosynthetic inside the greenhouse: 1000 ppm of CO_2 enrichment cases on rainy (a) and sunny days (b).

6.3.3 Carbon dioxide distribution with different outside wind speed at the side ventilation (0 m s^{-1}, 3 m s^{-1}, and 6 m s^{-1})

Figure 6.10 showed the simulation of CO_2 distribution inside the greenhouse when 1160 ppm of CO_2 concentration was supplied through perforated tubes inside the plants. The appearance of CO_2 emissions from the perforated tube was confirmed with the degradation colors inside of the plants. CO_2 distributions in 0 m s^{-1}, 3 m s^{-1}, and 6 m s^{-1} of outside wind speed at side vents were showed significant difference in the greenhouse. Note that CO_2 concentration inside/outside of the greenhouse was also set as 450 and 400 ppm, respectively.

The effects of 0 m s^{-1} outside wind speed showed a higher average of CO_2 concentration (438 ppm) than others outside wind speed as shown in Table 6.4. In case of 3 m s^{-1} outside wind speed showed a lower CO_2 concentration at the top part (above of air circulator) than bottom part (below of air circulator) of the greenhouse (see Figure 6.10 for 3m s^{-1}) with average of CO_2 concentration was 403 ppm. In case of 6 m s^{-1} outside wind speed showed a more even CO_2 distribution inside of the greenhouse and has the lowest average of CO_2 concentration (391 ppm). The quantitative evaluation of these results using CV is shown in Table 6.4. In the cases of 0 m s^{-1} and 3 m s^{-1} outside wind speed have similar CV, 18.2% and 18.6%, respectively for the whole greenhouse. In contrast, 6 m s^{-1} outside wind speed showed the lowest variability of CO_2 concentration inside the greenhouse (16.9%). Focusing on the even distribution of CO_2 inside the plant, case of 3 m s^{-1} (6.3%), and case of 6 m s^{-1} (7.9 %) outside wind speed showed significant improvement to even the CO_2 distribution inside the plant canopy compared to case of 0 m s^{-1} (8.8%) outside wind speed.

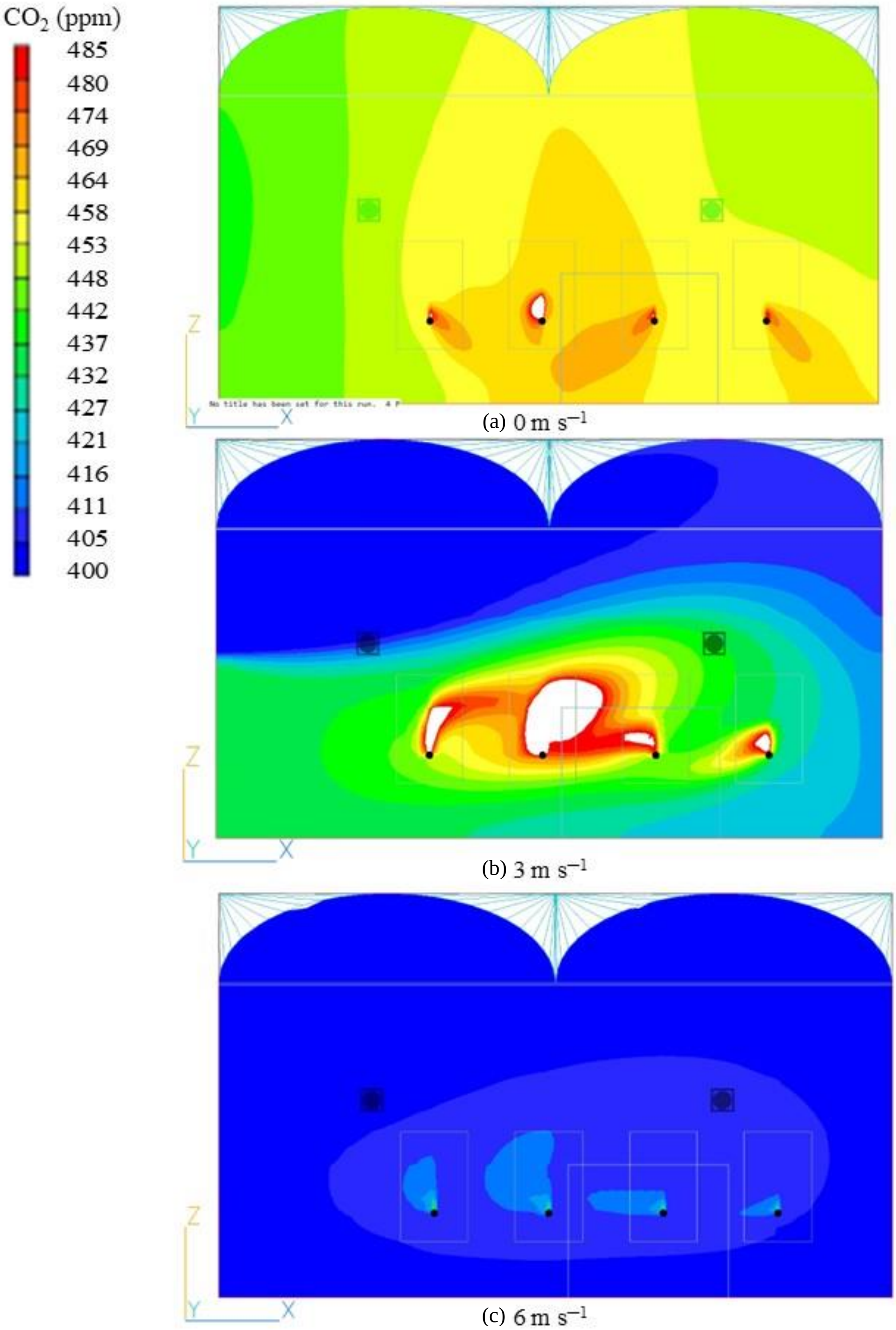

Figure 6.10 Carbon dioxide distribution inside of the greenhouse in case different outside windspeed: 0 m s^{-1}, (b) 3 m s^{-1}, and (c) 6 m s^{-1}.

Table 6.4 Coefficient of variations of CO_2 concentration in the case different outside wind speed.

Parameter	Greenhouse			Plants		
	Outside wind speed					
	0 m s^{-1}	3 m s^{-1}	6 m s^{-1}	0 m s^{-1}	3 m s^{-1}	6 m s^{-1}
SD (ppm)	80	75	66	41	28	32
Mean (ppm)	438	403	391	464	448	405
CV (%)	18.2	18.6	16.9	8.8	6.3	7.9

6.4 Conclusions

A few simulations of greenhouse were conducted to know the effect of various environmental conditions to the CO_2 distribution inside of the greenhouse while considering photosynthesis. In the case open dan closed side ventilation showed a slight difference of CO_2 distribution inside of the greenhouse. Focusing on the even distribution of CO_2 inside the plant, open (8.8%) and closed (8.7%) side vents induced almost no significant improvement contribution to uniformity of the plant canopy: because no initial wind velocity was considered at both side vents in our case.

In the case sunny and rainy day showed a slight difference of CO_2 concentration. The case of rainy day showed a slightly more even of CO_2 distribution inside the greenhouse than the case of sunny day. The variability of CO_2 concentration inside the plant between a rainy and a sunny day determined practically no significant difference. Moreover, these simulations showed no significant relation between PAR to even CO_2 distribution inside the plants.

Every case of different outside wind speed showed significant different of CO_2 distribution inside the greenhouse. In the case, 6 m s^{-1} outside wind speed showed the lowest average CO_2 concentration and a more even CO_2 distribution compared to 0 m s^{-1} and 3 m s^{-1} outside wind speed inside of the greenhouse. Focusing on the even distribution of CO_2 inside the plant, case of 3 m s^{-1} and case of 6 m s^{-1} outside wind speed showed significant improvement contribution to even the CO_2 distribution inside the plant canopy compared to case of 0 m s^{-1} outside wind speed. However, in the case of 6 m s^{-1} outside wind speed showed CO_2 enrichment inside plant canopy was not effective to keep high CO_2 concentration since the high volume of outside CO_2 concentration (400 ppm) will dominate the CO_2 concentration inside the greenhouse.

Chapter 7 Conclusions

Model validation conducted by comparing measurement and simulation data to know the spatial distribution of airflow and CO_2 inside the chamber and greenhouse. The accuracy of the simulation model was evaluated by RMSE and MAPE. The MAPE of horizontal velocity results showed high percentage error from 1 A, B, C to 6 A, B, C were approximately 35 – 155% and MAPE of vertical velocity results showed high percentage error from 1 A, B, C to 6 A, B, C were approximately 41-272 %. Even though the measured data and simulation data have almost similar value. RMSE of horizontal velocity results showed the results for each cross section from 1 A, B, C to 6 A, B, C were 0.004-0.03 m s^{-1} and RMSE of vertical velocity results showed the results for each cross section from 1 A, B, C to 6 A, B, C were 0.01-0.05 m s^{-1}. However, simulation results in this study may be reasonable because measurement and simulation results has a good agreement and the air velocity obtained both by measurement and simulation in the lower part of the real chamber was so small (order of 10^{-2} m s^{-1}). The simulations showed that the airflow did not distribute evenly inside the chamber, due to the fans placed only at the one top side of the chamber. This made the air actively move to the left towards the fans and may cause the stagnation area on the right side of the chamber. In case, the chamber with plant, there was possibility the optimum photosynthesis can only achieve on the left side of the plant canopy.

Model validation for CO_2 distribution inside chamber has a low percentage error of MAPE results from left, middle, and right part were 1.85%, 3.43%, and 0.43%, respectively. The measured and simulation data have almost similar value. RMSE showed the results for each cross section from left, middle, and right part were 11.20 ppm, 16.99 ppm, and 2.71 ppm, respectively. These results showed that the simulation was reasonable and can be used for greenhouse numerical simulation.

The measured points of CO_2 concentration were compared with the simulated CO_2 distribution inside the greenhouse. The MAPE results showed low percentage error from north and south wall were 4.95% and 2.04%, respectively. RMSE showed the results for each cross section from north and south wall were 25.33 ppm and 10.57 ppm, respectively. However, the simulation results in this study may be reasonable to predict the CO_2 distribution considering CO_2 absorption through the process of photosynthesis of the plant inside the greenhouse.

Predictive numerical simulation of airflow distribution in canopy plants could provide a suitable environment for plant growth. After model validation, airflow patterns and variability of air velocity were evaluated in the cases of different fan arrangements. The obtained results showed that a more even airflow distribution was observed in the middle position and diagonally position of fans at the top of chamber with CV of vertical velocity were 9.3% and 10%, respectively.

Moreover, the arrangement of the fan positions to the middle and diagonally can be significant help to produce even air velocity distribution inside the plant.

A numerical simulation was performed to predict the distribution the airflow in a new chamber. After model validation, multiple sizes of transparent plates were applied just below the top of the chamber to investigate the effect of the plates on airflow distribution. The simulation's results showed a diminishing stagnant area at the higher part of the plant, reaching a more even airflow distribution, with CV of vertical velocity were 9.1% (full plate), 12.2% (half plate placed near the fans), 50.9% (without a plate), 45.5% (half plate placed on the opposite side of the fans), and 44.0% (small plate placed opposite with the fans). From simulation results, mounting a full-size transparent plate and a half-size one near the fans can significantly help to produce even air velocity distribution at the plant canopy and enabled to contribute diminishing the stagnant area generated upper right of the plant.

The detail CO_2 distribution predicted by a computational fluid dynamics model considering CO_2 absorption by photosynthesis in a greenhouse in various environmental conditions. Cases with open and closed side vents showed that closed side vents have slightly more even of CO_2 concentration than those with open side vents inside the greenhouse. By contrast, the variability of CO_2 inside the plant, open (8.8%) and closed (8.7%) side vents, induced almost no significant improvement. Additionally, cases of a rainy- and sunny-day model showed that photosynthetically active radiation possibly compensated CO_2 absorption through photosynthesis to be low at low light (rainy day) and higher at high light (sunny day). Nonetheless, the variability of CO_2 concentration inside the plant between rainy and sunny days determined almost no significant difference.

Each case of different outside wind speed showed significant different of CO_2 distribution inside the greenhouse. Focusing on the even distribution of CO_2 inside the plant, case of 3 $m\ s^{-1}$ and case of 6 $m\ s^{-1}$ outside wind speed showed significant improvement contribution to even the CO_2 distribution inside the plant canopy compared to case of 0 $m\ s^{-1}$ outside wind speed. However, in the case of 6 $m\ s^{-1}$ outside wind speed showed CO_2 enrichment inside plant canopy was not effective to keep high CO_2 concentration since the high volume of outside CO_2 concentration (400 ppm) will dominate the CO_2 concentration inside the greenhouse. Thus, this research showed characteristics of CO_2 distribution, assessing photosynthesis and CO_2 that leads to the efficiency of CO_2 enrichment in the greenhouse.

References

Ali, H. B., Bournet, P.E., Cannavo, P., Chantoiseau, E., 2018, Development of a CFD crop submodel for simulating microclimate and transpiration of ornamental plants grown in a greenhouse under water restriction, Comput. Electron. Agric., 149, 26–40, https://doi.org/10.1016/j.compag.2017.06.021

Benni, S., Tassinari, P., Bonora, F., Barbaresi, A., Torreggiani, D., 2016, Efficacy of greenhouse natural ventilation: Environmental monitoring and CFD simulations of a study case, Energy Build., 125, 276–286, https://doi.org/10.1016/j.enbuild.2016.05.014

Boulard, T., Roy, J.C., Pouillard, J.B., Fatnassi, H., Grisey, A., 2017, Modelling of micrometeorology, canopy transpiration and photosynthesis in a closed greenhouse using computational fluid dynamics, Biosyst. Eng., 158, 110–133, https://doi.org/10.1016/ j.biosystemseng.2017.04.001

Boulard, T., Wang, S., 2002, Experimental and numerical studies on the heterogeneity of crop transpiration in a plastic tunnel, Comput. Electron. Agric., 34, 173–190, https://doi.org/10.1016 /S0168-1699(01)00186-7

Burkart, S., Manderscheid, R., Weigel, H.J., 2007, Design and performance of a portable gas exchange chamber system for CO2- and H2O-flux measurements in crop canopies, Environ. Exp. Bot. 61, 25–34, https://doi.org/10.1016/j.envexpbot.2007.02.007

Campen, J.B., 2005, Greenhouse design applying CFD for Indonesian conditions, Acta Hortic. 691, 419–424, https://doi.org/10.17660/ActaHortic.2005.691.50

Dugas, W.A., Reicosky, D.C., Kiniry, J.R., 1997, Chamber and micrometeorological measurements of CO2 and H2O fluxes for three C4 grasses, Agric. For. Meteorol., 83, 113–133, https://doi.org/10.1016/S0168-1923(96)02346-5

Fang, H., Li, K., Wu, G., Cheng, R., Zhang, Y., Yang, Q., 2020, A CFD analysis on improving lettuce canopy airflow distribution in a plant factory considering the crop resistance and LEDs heat dissipation, Biosyst. Eng. 200, 1–12, https://doi.org/10.1016/j.biosystemseng. 2020.08.017

Flores-Velzquez, J., la Torre-Gea, G. De, Rico-Garca, E., L., I., Rojano-Aguilar, A., 2012, Advances in Computational Fluid Dynamics Applied to the Greenhouse Environment, Appl. Comput. Fluid Dyn., https://doi.org/10.5772/26477

Furukawa, A., 1975, Influence of Air Flow Rates on Photosynthesis and Respiration of Poplar

Leaves under Various Environmental Conditions, Environ. Control Biol., 13, 77–85, https://doi.org/10.2525/ecb1963.13.77

Gruda, N., 2005, Impact of environmental factors on product quality of greenhouse vegetables for fresh consumption, CRC. Crit. Rev. Plant Sci., 24, 227–247, https://doi.org/10.1080/07352680591008628

Hamerlynck, E.P., McAllister, C.A., Knapp, A.K., Ham, J.M., Owensby, C.E., 1997, Photosynthetic gas exchange and water relation responses of three tallgrass prairie species to elevated carbon dioxide and moderate drought, Int. J. Plant Sci., 158, 608–616, https://doi.org/10.1086/297474

Hong, S.W., Exadaktylos, V., Lee, I.B., Amon, T., Youssef, A., Norton, T., Berckmans, D., 2017, Validation of an open source CFD code to simulate natural ventilation for agricultural buildings, Comput. Electron. Agric., 138, 80–91, https://doi.org/10.1016/j.compag.2017.03.022

Katsoulas, N., Baille, A., Kittas, C., 2007, Leaf boundary layer conductance in ventilated greenhouses: An experimental approach, Agric. For. Meteorol., 144, 180–192, https://doi.org/10.1016/j.agrformet.2007.03.003

Kichah, A., Bournet, P.E., Migeon, C., Boulard, T., 2012, Measurement and CFD simulation of microclimate characteristics and transpiration of an Impatiens pot plant crop in a greenhouse, Biosyst. Eng., 112, 22–34, https://doi.org/10.1016/j.biosystemseng.2012.01.012

Kim, C.H., Kim, M.H., Choi, E.G., Jin, B.O., Baek, G.Y., Yoon, Y.C., Kim, H.T., 2013, Co2 distribution due to thermal buoyancy in the greenhouse, IFAC Proceedings Volumes (IFAC-PapersOnline), IFAC, https://doi.org/10.3182/20130327-3-jp-3017.00015

Kim, Hee Tae, Kim, C.H., Choi, E.G., Jin, B.O., Yoon, Y.C., Kim, Hyeon Tae, 2015, The effect of thermal conditions on CO2 distribution in a greenhouse, Trop. Agric. Res., 26, 714, https://doi.org/10.4038/tar.v26i4.8134

Kim, R. woo, Lee, I. bok, Kwon, K. seok, 2017, Evaluation of wind pressure acting on multi-span greenhouses using CFD technique, Part 1: Development of the CFD model, Biosyst. Eng. 164, 235–256, https://doi.org/10.1016/j.biosystemseng.2017.09.008

Kimura, K., Yasutake, D., Miyoshi, Y., Yamanami, A., Daiou, K., Ueno, H., Kitano, M., 2016, Leaf boundary layer conductance in a tomato canopy under the convective effect of circulating fans in a greenhouse heated by an air duct heater, Environ. Control Biol., 54, 171–176, https://doi.org/10.2525/ecb.54.171

Kitaya, Y., Shibuya, T., Yoshida, M., Kiyota, M., 2004, Effects of air velocity on photosynthesis of plant canopies under elevated CO2 levels in a plant culture system, Adv. Sp. Res., 34, 1466–1469, https://doi.org/10.1016/j.asr.2003.08.031

Kitaya, Y., Tsuruyama, J., Shibuya, T., Yoshida, M., Kiyota, M., 2003, Effects of air current speed on gas exchange in plant leaves and plant canopies, Adv. Sp. Res, 31, 177–182, https://doi.org/10.1016/S0273-1177(02)00747-0

Kumazaki, T., Ikeuchi, Y., Tokairin, T. 2021, Relationship between positions of CO2 supply in a canopy of tomato grown by high-wire system and distribution of CO2 concentration in a greenhouse (in Japanese), Climate in Biospher,. 21, 54-59, https://doi.org/10.2480/cib.J-21-064

Kuroyanagi, T., 2017, Prediction of leakage rate of a greenhouse using computational fluid dynamics, Acta Hortic, 1170, 87–94, https://doi.org/10.17660/ActaHortic.2017.1170.9

Kuroyanagi, Takeshi, 2017, Investigating air leakage and wind pressure coefficients of single-span plastic greenhouses using computational fluid dynamics, Biosyst. Eng., 163, 15–27, https://doi.org/10.1016/j.biosystemseng.2017.08.004

Kuroyanagi, T., Yasuba, K. ichiro, Higashide, T., Iwasaki, Y., Takaichi, M., 2014, Efficiency of carbon dioxide enrichment in an unventilated greenhouse, Biosyst. Eng., 119, 58–68, https://doi.org/10.1016/j.biosystemseng.2014.01.007

Leadley, P.W., Drake, B.G., 1993, Open top chambers for exposing plant canopies to elevated CO2 concentration and for measuring net gas exchange, Vegetatio, 104–105, 3–15, https://doi.org/10.1007/BF00048141

Li, Y., Ding, Y., Li, D., Miao, Z., 2018, Automatic carbon dioxide enrichment strategies in the greenhouse: A review, Biosyst. Eng., 171, 101–119, https://doi.org/10.1016/ j.biosystemseng. 2018.04.018

Majdoubi, H., Boulard, T., Fatnassi, H., Bouirden, L., 2009, Airflow and microclimate patterns in a one-hectare Canary type greenhouse: An experimental and CFD assisted study, Agric. For. Meteorol, 149, 1050–1062, https://doi.org/10.1016/j.agrformet.2009.01.002

Molina-Aiz, F.D., Norton, T., López, A., Reyes-Rosas, A., Moreno, M.A., Marín, P., Espinoza, K., Valera, D.L., 2017, Using computational fluid dynamics to analyse the CO2 transfer in naturally ventilated greenhouses, Acta Hortic., 1182, 283–292, https://doi.org/10.17660/ ActaHortic.2017.1182.34

Nederhoff, E. M., Vegter, J. G. 1994a, Canopy photosynthesis of tomato, cucumber, and sweet pepper in greenhouses: measurements compared to models, Ann. Bot., 73, 421-427, https://doi.org/10.1006/anbo.1994.1044

Nederhoff, E. M., Vegter, J. G. 1994b, Photosynthesis of stands of tomato, cucumber, and sweet pepper measured in greenhouses under various CO2 concentrations, Ann. Bot., 73, 353-361, https://doi.org/10.1006/anbo.1994.1052

Niam, A.G., Muharam, T.R., Widodo, S., Solahudin, M., Sucahyo, L., 2019, CFD simulation approach in determining air conditioners position in the mini plant factory for shallot seed production, AIP Conf. Proc., 2062, https://doi.org/10.1063/1.5086564

Nurmalisa, M., Tokairin, T., Takayama, K., Inoue, T., 2021, Numerical simulation of detailed airflow distribution in newly developed photosynthesis chamber, IOP Conf. Ser. Earth Environ. Sci., 623, 2–8, https://doi.org/10.1088/1755-1315/623/1/012095

Okayama, T., Okamura, K., Park, J.E., Ushada, M., Murase, H., 2008, A simulation for precision airflow control using multi-fan in a plant factory, Environ. Control Biol., 46, 183–194, https://doi.org/10.2525/ecb.46.183

Papakonstantinou, K.A., Kiranoudis, C.T., Markatos, N.C., 2000, Numerical simulation of air flow field in single-sided ventilated buildings, Energy Build., 33, 41–48, https://doi.org/10.1016/S0378-7788(00)00063-3

PHOENICS user manual. 2022, Turbulence Model, CHAM, London, pp 7

Reichrath, S., Ferioli, F., Davies, T. W. 2000, A simple computational fluid dynamics (CFD) model of a tomato glasshouse, Acta Hortic., 534, 197-202, https://doi.org/10.17660/ActaHortic.2000.534.22

Romdhonah, Y., Fujiuchi, N., Shimomoto, K., Takahashi, N., Nishina, H., Takayama, K., 2021, Averaging techniques in processing the high time-resolution photosynthesis data of cherry tomato plants for model development, Environ. Control Biol., 59, 107–115, https://doi.org/10.2525/ecb.59.107

Romdhonah, Y., Suhardiyanto, H., Erizal, E., Saptomo, S., 2015, Analisis Ventilasi Alamiah Pada Greenhouse Tipe Standard Peak Menggunakan Computational Fluid Dynamics (in Indonesian) - Natural ventilation analysis of standard peak greenhouse using computational fluid dynamics, J. Ilm. Rekayasa Pertan. and Biosist., 3, 170–178

Roy, J.C., Boulard, T., Kittas, C., Wang, S., 2002, Convective and ventilation transfers in greenhouses, part 1: The greenhouse considered as a perfectly stirred tank, Biosyst. Eng., 83, 1–20, https://doi.org/10.1006/bioe.2002.0107

Roy, J.C., Pouillard, J.B., Boulard, T., Fatnassi, H., Grisey, A., 2014, Experimental and CFD results on the CO2 distribution in a semi closed greenhouse, Acta Hortic., 1037, 993–1000, https://doi.org/10.17660/ActaHortic.2014.1037.131

Rubanga, D.P., Hatanaka, K., Shimada, S., 2019, Development of a simplified smart agriculture system for small-scale greenhouse farming, Sensors Mater., 31, 831–843, https://doi.org/10.18494/SAM.2019.2154

Saberian, A., Sajadiye, S.M., 2019, The effect of dynamic solar heat load on the greenhouse microclimate using CFD simulation, Renew. Energy 138, 722–737, https://doi.org/10.1016/j.renene.2019.01.108

Santolini, E., Pulvirenti, B., Benni, S., Barbaresi, L., Torreggiani, D., Tassinari, P., 2018, Numerical study of wind-driven natural ventilation in a greenhouse with screens, Comput. Electron. Agric, 149, 41–53, https://doi.org/10.1016/j.compag.2017.09.027

Shibuya, T., Tsuruyama, J., Kitaya, Y., Kiyota, M., 2006, Enhancement of photosynthesis and growth of tomato seedlings by forced ventilation within the canopy, Sci. Hortic., (Amsterdam). 109, 218–222, https://doi.org/10.1016/j.scienta.2006.04.009

Shimomoto, K., Takayama, K., Takahashi, N., Nishina, H., Inaba, K., Isoyama, Y., Oh, S.C., 2020, Real-time monitoring of photosynthesis and transpiration of a fully-grown tomato plant in greenhouse, Environ. Control Biol., 58, 65–70, https://doi.org/10.2525/ECB.58.65

Spalding, D.B., Markatos, N.G., 1982, The Mathematical Basis of PHOENICS, Phoenics Lect. Notes, CHAM Ltd

Stathopoulou, O.I., Assimakopoulos, V.D., 2008, Numerical study of the indoor environmental conditions of a large athletic hall using the CFD code PHOENICS, Environ. Model. Assess., 13, 449–458, https://doi.org/10.1007/s10666-007-9107-5

Wang, X.W., Luo, J.Y., Li, X.P., 2013, CFD based study of heterogeneous microclimate in a typical chinese greenhouse in central China, J. Integr. Agric., 12, 914–923, https://doi.org/10.1016/S2095-3119(13)60309-3

Xu, S., Zhu, X., Li, C., Ye, Q., 2014, Effects of CO2 enrichment on photosynthesis and growth in Gerbera jamesonii, Sci. Hortic., (Amsterdam), 177, 77–84, https://doi.org/10.1016/j.scienta.2014.07.022

Zhang, Y., Kacira, M., An, L., 2016, A CFD study on improving air flow uniformity in indoor plant factory system, Biosyst. Eng., 147, 193–205, https://doi.org/10.1016/j.biosystemseng.

2016.04.012

Zhang, Y., Wei, Z., Xu, J., Wang, H., Zhu, H., Lv, H., 2021, Numerical simulation and application of micro-nano bubble releaser for irrigation, Mater. Express, 11, 1007–1015, https://doi.org/10.1166/mex.2021.1997

Zhang, Y., Yasutake, D., Hidaka, K., Kitano, M., Okayasu, T., 2020, CFD analysis for evaluating and optimizing spatial distribution of CO2 concentration in a strawberry greenhouse under different CO2 enrichment methods, Comput. Electron. Agric., 179, 105811, https://doi.org/10.1016/j.compag.2020.105811

Appendix

A-1 Flow chart of CFD simulation

Equations with boundary conditions were solved using CFD with the flow management simulation as show in below:

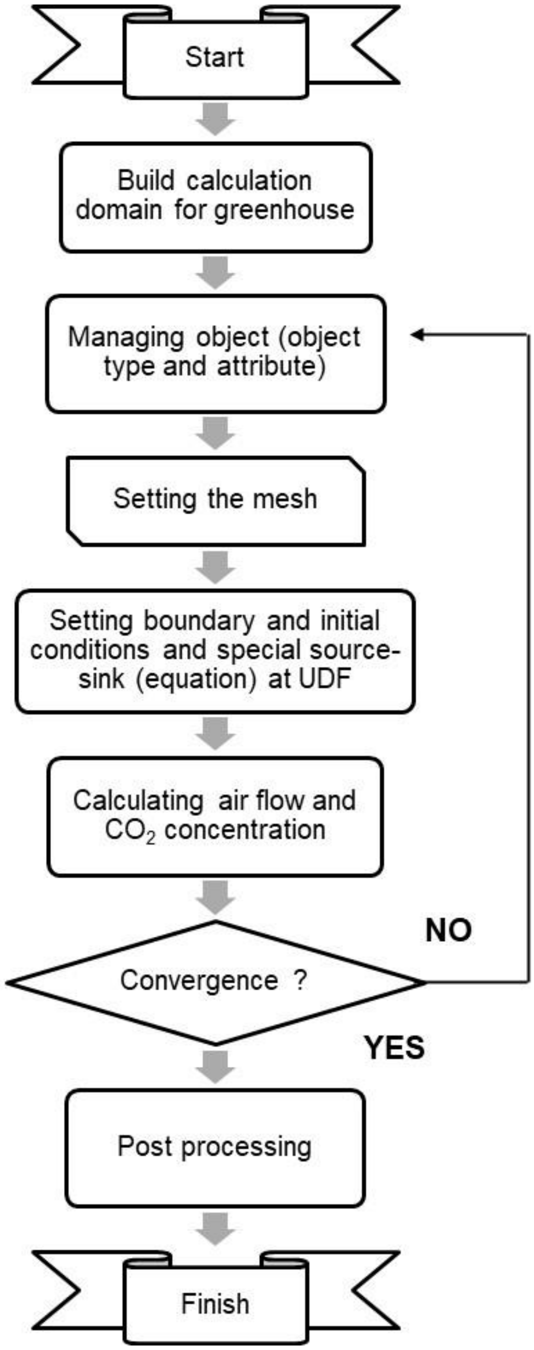

The flow chart of CFD simulation (Romdhonah et al., 2015) with modification. Note: UDF means User Defined File.

A-2 Source term for CO_2 absorption in chamber 2

Source terms placed in user defined functions (UDF) which energy, crop respiration, and carbon dioxide balance equations for the canopy inside the chamber 2.

```
Group 13. Boundary & Special Sources
   This patch is attached to object SNK
 PATCH(CANOPY, VOLUME, -1, 0, 0, 0, 0, 0, 1, 240)

 EGWF = T
 ************************************************************
  Echo save-block settings for Group 13
  save13begin

  *****************************************************
  *** LAD=LAI/CanopyHeight                         *
  *** Canopy height is 1.5m, LAI=4 given at Foliage *
(STORED LAI at CANOPY is 4)
(STORED LAD at CANOPY is 2.67)
  *****************************************************

  *** Light use efficiency [gCO2/J]
(STORED ac at CANOPY is 3.705E-6)

  *** Incident light flux PAR at the top of canopy [W/m^2leaf]
(STORED j0 at CANOPY is 379.998)

  *** Conductance of CO2 [m/s]
(STORED tc at CANOPY is 12.168E-4)

  *** Density of CO2 [g/m^3]
(STORED Cc is 1839)

  *** Canopy photosynthesis rate [gCO2/h/m^2ground area]
(STORED Pcg at CANOPY is ((ac*j0*tc*3600*(CO2*Cc))/((ac*j0)+(tc*(CO2*Cc)))))
```

*** Crop resipiration [g/h/m^2]
(STORED Resp at CANOPY is 2.845E-2)

*** Volumetric net photosynthesis [kg/s/m^3row]
(STORED PCFD at CANOPY is (((LAD/(LAI*1000*3600))*(Pcg-Resp))))
*(STORED PCFD at CANOPY is (LAD/(LAI*1000*3600))*2.95)

(source of CO_2 at CANOPY is -1.0*PCFD)
save13end

Object model for CO_2 distribution inside chamber 2.

Object Model	Object name	Type	Geometry
Fan	OUT	Outlet	cube12t
Tomato Plant	SNK	User Defined	box
	Plant	Foliage	foliage
Inflow air	Inlet	Inlet	cube3t

A-3 Source term for CO_2 absorption in greenhouse

Source terms placed in user defined functions (UDF) which energy, crop respiration, and carbon dioxide balance equations for the canopy inside the greenhouse.

Group 13. Boundary & Special Sources

```
   This patch is attached to object FOLI1_1
 PATCH(TOMAT1, VOLUME, -1, 0, 0, 0, 0, 0, 1, 20)

   This patch is attached to object FOLI2_2
 PATCH(TOMAT2, VOLUME, -1, 0, 0, 0, 0, 0, 1, 20)

   This patch is attached to object FOLI3_3
 PATCH(TOMAT3, VOLUME, -1, 0, 0, 0, 0, 0, 1, 20)

   This patch is attached to object FOLI4_4
 PATCH(TOMAT4, VOLUME, -1, 0, 0, 0, 0, 0, 1, 20)

 EGWF = T
 ************************************************************
  Echo save-block settings for Group 13
  save13begin

(STORED LAD at TOMAT1 is 0.675)
(STORED LAD at TOMAT2 is 0.675)
(STORED LAD at TOMAT3 is 0.675)
(STORED LAD at TOMAT4 is 0.675)

(STORED LAI at TOMAT1 is 1.1)
(STORED LAI at TOMAT2 is 1.1)
(STORED LAI at TOMAT3 is 1.1)
(STORED LAI at TOMAT4 is 1.1)

(STORED ac is 3.705E-6)
(STORED j0 is 355)
```

```
(STORED tc is 12.168E-4)
(STORED Cc is 1839)
(STORED Pcg at TOMAT1 is ((ac*j0*tc*3600*(CO2*Cc))/((ac*j0)+(tc*(CO2*Cc)))))
(STORED Pcg at TOMAT2 is ((ac*j0*tc*3600*(CO2*Cc))/((ac*j0)+(tc*(CO2*Cc)))))
(STORED Pcg at TOMAT3 is ((ac*j0*tc*3600*(CO2*Cc))/((ac*j0)+(tc*(CO2*Cc)))))
(STORED Pcg at TOMAT4 is ((ac*j0*tc*3600*(CO2*Cc))/((ac*j0)+(tc*(CO2*Cc)))))

(STORED Resp at TOMAT1 is 2.845E-2)
(STORED Resp at TOMAT2 is 2.845E-2)
(STORED Resp at TOMAT3 is 2.845E-2)
(STORED Resp at TOMAT4 is 2.845E-2)

(STORED PCFD at TOMAT1 is (((LAD/(LAI*1000*3600))*(Pcg-Resp))))
(STORED PCFD at TOMAT2 is (((LAD/(LAI*1000*3600))*(Pcg-Resp))))
(STORED PCFD at TOMAT3 is (((LAD/(LAI*1000*3600))*(Pcg-Resp))))
(STORED PCFD at TOMAT4 is (((LAD/(LAI*1000*3600))*(Pcg-Resp))))

(source of CO2 at TOMAT1 is -1.0*PCFD)
(source of CO2 at TOMAT2 is -1.0*PCFD)
(source of CO2 at TOMAT3 is -1.0*PCFD)
(source of CO2 at TOMAT4 is -1.0*PCFD)

  save13end
```

Object model for CO_2 distribution inside greenhouse.

Object Model	Object name	Type	Geometry
CO_2 Tube	DCT1-DCT4	Angled-In	Cylinder
	DCT1_1-DCT4_16	Blockage	Cylinder
Tomato plants	FOLI1	Foliage	Foliage
	FOLI1_1	User Defined	Foliage
Roof	ROOF1-ROOF4	Blockage	Hh1
Fan	FAN1-FAN4	Fan	Fan1
Leakage air	LEAKAGE1-LEAKAGE7	Outlet	Box

A-4 Object management for airflow study with effect different fans position and size plate.

Objects for airflow study inside chamber 1 with different fans position.

Object Model	Object name	Type	Geometry
Fan	IN1-IN3	Inlet	cube3t
Cover of Fan	Plat1-Plat5	Plate	Cube11
Inflow air	OUT-OUT5	Outlet	Cube12t
Plant	Plant	Foliage	Foliage
	SNK	User Defined	Box

Object model for airflow study inside chamber 1 with different size of plate.

Object Model	Object name	Type	Geometry
Fan	FAN1-Fan3	Fan	Cylpipe
Cover of Fan	Plat1-Plat5	Plate	Cube11
Inflow air	OUTL1-OUTL5	Outlet	Cube12t
Plant	Plant	Foliage	Foliage
Plate	Fullplate	plate	cube11